Supramolecular $Ga_4L_6^{12-}$ Cage Photosensitizes 1,3-Rearrangement of Encapsulated Guest via Photoinduced Electron Transfer

Derek M. Dalton, Scott R. Ellis, Eva M. Nichols, Richard A. Mathies, F. Dean Toste*, Robert G. Bergman*, and Kenneth N. Raymond*

Chemical Sciences Division, Lawrence Berkeley National Laboratory, and Department of Chemistry, University of California, Berkeley, California 94720, United States

Supporting Information

I. General Methods

Reaction solutions were magnetically stirred with the exception of those reactions performed in NMR tubes. Reactions were monitored using 0.25 mm pre−coated silica gel plates from Silicycle (TLGR10011B−323) containing a fluorescent indicator for visualization by UV light by thin layer chromatography. Various stains were used to visualize reaction products, including $KMnO_4$ and phosphomolybdic acid in ethanol. Flash chromatography was performed using MP Biomedicals SiliTech silica gel 32−63D.

Air sensitive materials were handled in an inert atmosphere N_2 glovebox. For moisture sensitive reactions, glassware was oven dried at 150 ºC overnight prior to use or flame dried under vacuum immediately before use and back filled with dry N_2 using a vacuum line manifold. NMR spectra were recorded at ambient temperature using either Bruker AV-600, AV-500, DRX-500 or AV-400 MHz spectrometers. ^{1}H NMR chemical shifts (δ) are reported in parts per million (ppm) downfield of TMS relative to residual protic solvent resonances (7.26 ppm for $CDCl_3$, 5.30 ppm for CD_2Cl_2, 3.31 ppm for CD_3OD, 4.80 for D_2O, 2.50 for DMSO−d_6). ^{13}C–NMR chemical shifts (δ) are reported in ppm relative to the carbon resonance of the deuterated solvent (77.23 ppm for $CDCl_3$, 53.84 for CD_2Cl_2, 49.00 for CD_3OD, 39.52 for DMSO−d_6).

GC/MS experiments were conducted on a Perkin Elmer Mass spectrometer. Both low− and high−resolution mass spectral data were obtained from the Micromass/Analytical Facility operated by the College of Chemistry, University of California, Berkeley. Infrared (IR) spectra were recorded on a as a Nujol mull or a thin film between NaCl plates. UV/Vis spectra were performed on a Hewlett Packard 8453 diode-array (deuterium/tungsten) spectrophotometer using quartz cuvettes. Fluorescence spectra were collected on a Varian Cary Eclipse fluorescence spectrophotometer at ambient temperature unless

otherwise indicated. Melting points for all $K_{12}Ga_4L_6$ complexes are not reported as decomposition occurs above 190 ºC. Photoreactions were conducted in a Rayonet photoreactor with a minimum of six UVB (280-315 nm) bulbs using N_2 degassed solvents under N_2 atmosphere in airtight pyrex (< 275 nm filter) glassware.

II. Materials

Diethyl ether, tetrahydrofuran and methylene chloride were dried and purified by passage through a column of activated alumina (type A2, 12 x 32, UOP LLC) under dry N_2. Degassed solvents were purged with dried N_2 for a minimum of 30 minutes prior to being stored in an N_2 atmosphere glove box. Unless noted, reagents were purchased from TCI, Acros, or Sigma Aldrich and used without further purification. Diethyl ether, tetrahydrofuran, pentane, hexanes, benzene, and toluene (Fisher) were passed through a column of activated alumina (type A2, size 12 x 32) under nitrogen pressure and purged with N_2 prior to use. $K_{12}Ga_4L_6$ host assemblies were prepared from N,N'-(1,5-diaminonaphthalene)bis-2,3-dihydroxybenzamide and $Ga(acac)_3$ as reported and stored in an N_2 atmosphere glove box prior to use.[1] Degassed solvents were purged with dried N_2 for a minimum of 30 minutes prior to being stored in an N_2 atmosphere glove box.

[1] Caulder, D. L.; Powers, R. E.; Parac, T. N.; Raymond, K. N. *Angew. Chem. Int. Ed.* **1998**, *37*, 1840-1843

III. UV/Vis Spectra and Determination of Molar Absorption Coefficient

$$\varepsilon = \frac{A(\lambda)}{cl}$$

Molar absorption coefficients (ε) for both $K_{12}Ga_4L_6$ **1** and **2b** were determined from a plot of absorbance versus concentration for a series of concentrations (Figure S1). A = absorbance (nm), c = concentration (M), l = path length (cm). For $K_{12}Ga_4L_6$: ε is 7.6 x 10^4 ± 0.3 $M^{-1}cm^{-1}$ at 330 nm when l = 1 cm. For **2b**: ε is low with an upper limit of 26 $M^{-1}cm^{-1}$ at 330 nm when l = 1 cm.

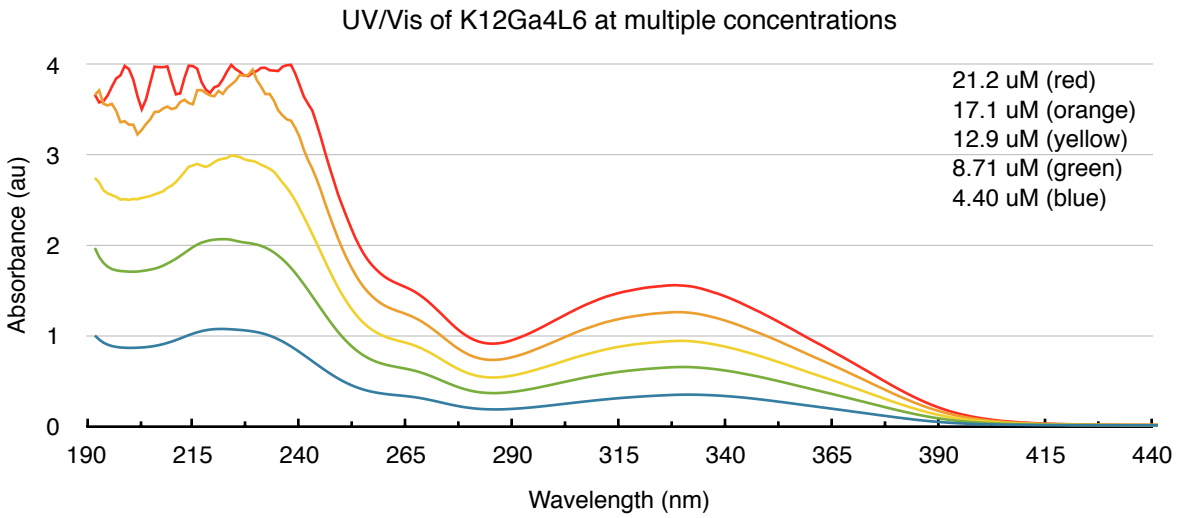

Figure S1. UV/Vis absorbance spectrum of $K_{12}Ga_4L_6$ at variable concentrations.

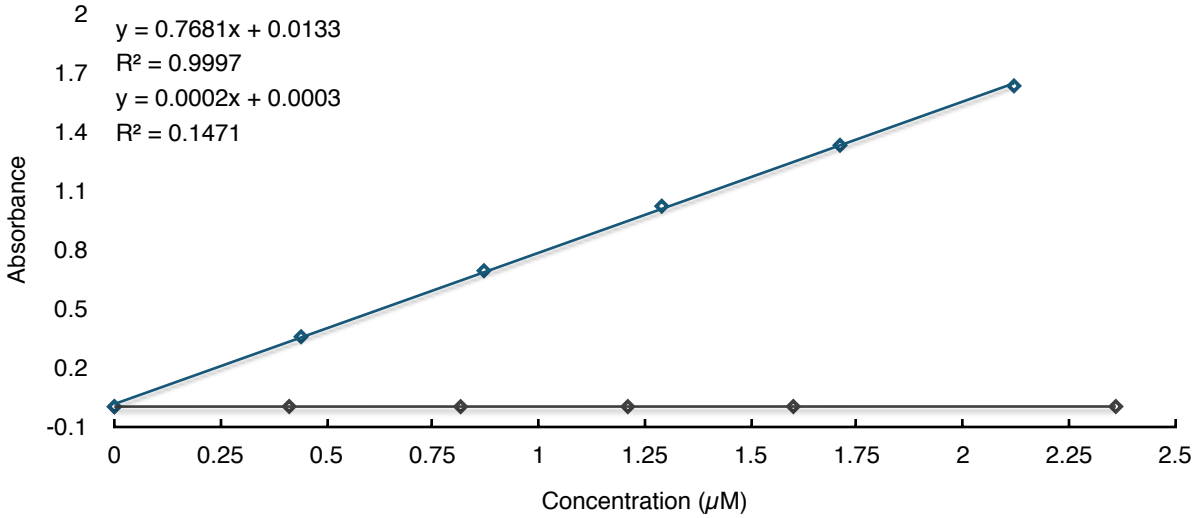

Figure S2. Molar absorption coefficient plots of solvent filled $K_{12}Ga_4L_6$ (blue) and **2b** (grey) at 330 nm. Concentrations are reported in μM.

Because the UV/Vis absorbance spectra were collected at concentrations much lower than the concentration that the 1,3-rearrangement takes place, we collected UV/Vis spectra for the cinnamyl ammonium at concentrations similar to that of the photorearrangement to determine whether the rearrangement was the result of direct absorbance of UV light or the result of energy transfer from the assembly. For **2b** under typical reaction conditions the concentration is 9.1 x 10^{-3} M. UV/Vis spectra were taken up to 2.1 x 10^{-4} M. Absorbance is not detected above 300 nm at the listed concentration (Figure S3). The UVA light source used emits from 315 - 400 nm. This provides evidence that the rearrangement is the result of photosensitization by the assembly.

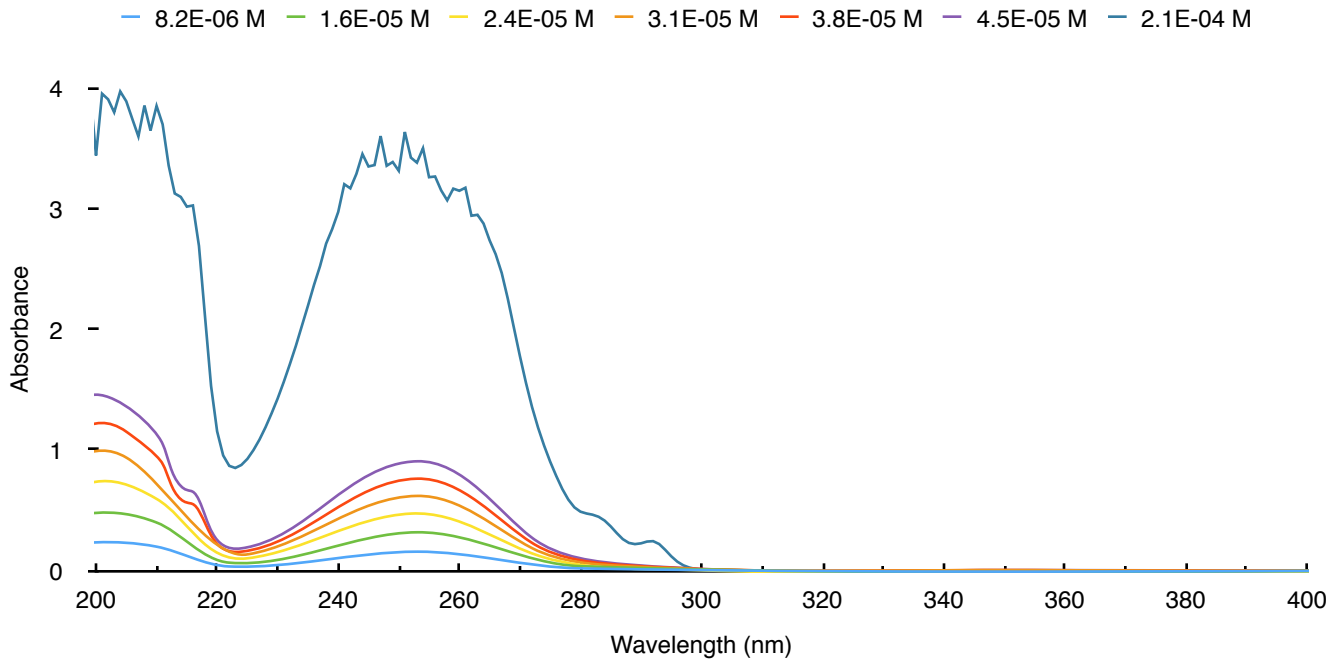

Figure S3. UV/Vis spectra of **2b** at a range of concentrations. Spectra show no absorbance by **2b** above 300 nm.

IV. Synthesis of Alkylcinnamyl Ammonium Salts

Dimethylcinnamyl amine **A1** was synthesized according to published procedures.[2]

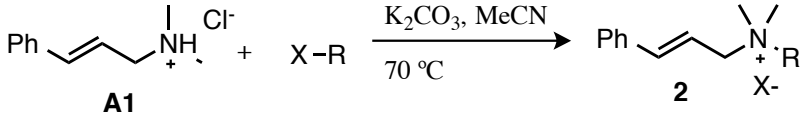

General procedure: To a round bottom flask or scintillation vial equipped with a magnetic stirbar was added **A1**•HCl (0.51 mmol, 1 equiv), alkyl halide (0.74 mmol, 1.5 equiv), K_2CO_3 (0.51 mmol, 1 equiv) and MeCN (1.0 ml, 0.5 M). The resultant heterogeneous mixture was heated to 70ºC with stirring for 10 hours. The reaction vessel was allowed to cool to room temperature and the mixture was diluted with DCM and filtered. Removal of solvent by rotary evaporation provides a residue that is dissolved in a minimal amount of DCM. To this solution an excess diethyl ether or hexanes is added until no change in opacity of the solution is seen. The mixture is then allowed to settle (~2-4 h) and the upper layer is decanted, providing crystalline solids or viscous oils in yields of 60-87%.

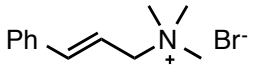

(E)-N,N,N-trimethyl-3-phenylprop-2-en-1-aminium bromide (**2b**)

The general procedure was modified for the synthesis of **2b**. To a scintillation vial equipped with a mechanical stirbar and charged with a solution of trimethylamine in EtOH (31-35% solution, 1.0 mmol, 2 equiv.) cooled to 0 ºC was added a solution of cinnamyl bromide (0.51 mmol, 1 equiv.) dissolved in acetone (1 ml). The solution was allowed to slowly warm to room temperature and stirred for 12 h. Addition of diethyl ether to this solution caused precipitation of a white solid that was collected by filtration (87%). ^{1}H-NMR (500 MHz; D_2O): δ 7.55 (d, J = 7.8 Hz, 2H), 7.45-7.38 (m, 3H), 6.93 (d, J = 15.7 Hz, 1H), 6.35 (dt, J = 15.6, 7.8 Hz, 1H), 3.99 (d, J = 7.7 Hz, 2H), 3.07 (s, 9H). ^{13}C NMR [126

[2] Fries, D. S., De Vries, J., Hazelhoff, B. & Horn, A. S. Synthesis and toxicity toward nigrostriatal dopamine neurons of 1-methyl-4-phenyl-1,2,3,6-tetrahydropyridine (MPTP) analogs. *J. Med. Chem.* **29,** 424–427 (1986).

MHz; D_2O (DMSO ref.)]: δ 144.5, 136.6, 131.1, 130.6, 128.8, 116.6, 69.7, 53.89. HRMS (ESI) *m/z* $[C_{12}H_{18}N]^+$ calculated 176.1434, found 176.1433.

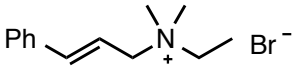

(E)-N-ethyl-N,N-dimethyl-3-phenylprop-2-en-1-aminium bromide (**2c**)

General procedure yielded an off white solid (81% yield). ^{1}H-NMR (500 MHz; D_2O): δ 7.55 (d, *J* = 7.6 Hz, 2H), 7.45-7.38 (m, 3H), 6.92 (d, *J* = 15.7 Hz, 1H), 6.31 (dt, *J* = 15.6, 7.8 Hz, 1H), 3.94 (d, *J* = 7.6 Hz, 2H), 3.31 (q, *J* = 7.3 Hz, 2H), 2.97 (s, 6H), 1.34 (t, *J* = 7.2 Hz, 3H). ^{13}C NMR [126 MHz; D_2O (DMSO ref.)]: δ 144.0, 136.7, 131.0, 130.7, 128.8, 116.5, 67.0, 60.9, 50.87, 50.84, 9.2. HRMS (ESI) *m/z* $[C_{13}H_{20}N]^+$ calculated 190.1590, found 190.1589.

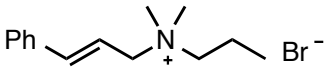

(E)-N,N-dimethyl-3-phenyl-N-propylprop-2-en-1-aminium bromide (**2d**)

General procedure yielded a yellow oil (68% yield). ^{1}H-NMR (500 MHz; D_2O): δ 7.55 (d, *J* = 7.3 Hz, 2H), 7.42 (t, *J* = 7.3 Hz, 3H), 6.90 (d, *J* = 15.7 Hz, 1H), 6.29 (dq, *J* = 15.1, 7.4 Hz, 1H), 3.93 (d, *J* = 6.5 Hz, 2H), 3.15 (dt, *J* = 7.7, 4.1 Hz, 2H), 2.97 (s, 6H), 1.78-1.73 (m, 2H), 0.94 (t, *J* = 7.3 Hz, 3H). ^{13}C NMR [126 MHz; D_2O (DMSO ref.)]: δ 144.0, 136.6, 131.0, 130.6, 128.8, 116.5, 67.5, 66.8, 51.4, 17.2, 11.6. HRMS (ESI) *m/z* $[C_{14}H_{22}N]^+$ calculated 204.1747, found 204.1745.

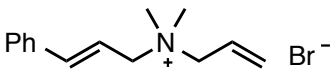

(E)-N-allyl-N,N-dimethyl-3-phenylprop-2-en-1-aminium bromide (**2a**)

General procedure yielded an off-white solid (61% yield). ^{1}H-NMR (500 MHz; D_2O): δ 7.56 (d, *J* = 7.5 Hz, 2H), 7.42 (dq, *J* = 12.9, 6.7 Hz, 3H), 6.93 (d, *J* = 15.8 Hz, 1H), 6.34 (dt, *J* = 15.6, 7.7 Hz, 1H), 6.03 (dtd, *J* = 16.5, 8.6, 7.9 Hz, 1H), 5.73 (d, *J* = 10.2 Hz, 1H), 5.68 (d, *J* = 16.9 Hz, 1H), 3.96 (d, *J* = 7.6 Hz,

2H), 3.86 (d, *J* = 7.4 Hz, 2H), 2.99 (s, 6H). ^{13}C NMR [126 MHz; D_2O(DMSO ref.)]: δ 144.3, 136.7, 131.1, 130.70, 130.66, 128.8, 126.0, 116.4, 67.54, 67.43, 50.99. HRMS (ESI) *m/z* $[C_{14}H_{20}N]^+$ calculated 202.1590, found 202.1589.

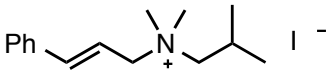

(E)-N-isobutyl-N,N-dimethyl-3-phenylprop-2-en-1-aminium iodide (**2e**)

General procedure yielded a viscous brown oil (63% yield). ^{1}H-NMR (500 MHz; DMSO-d_6): δ 7.48 (d, *J* = 7.5 Hz, 2H), 7.31 (dq, *J* = 15.2, 7.5 Hz, 3H), 6.88 (d, *J* = 15.7 Hz, 1H), 6.30 (dt, *J* = 15.5, 7.7 Hz, 1H), 3.97 (d, *J* = 7.5 Hz, 2H), 3.07 (d, *J* = 5.0 Hz, 2H), 2.94 (s, 6H), 2.15 (dquintet, *J* = 12.1, 6.1 Hz, 1H), 0.97 (d, *J* = 6.7 Hz, 6H). ^{13}C NMR (126 MHz; DMSO-d_6): δ 143.6, 136.2, 130.8, 130.4, 128.6, 116.5, 72.7, 67.9, 51.41, 24.4, 23.8. HRMS (ESI) *m/z* $[C_{15}H_{24}N]^+$ calculated 218.1903, found 218.1901.

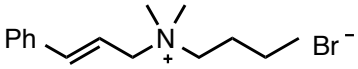

N-cinnamyl-N,N-dimethylbutan-1-aminium bromide (**2f**)

General procedure yielded a yellow oil (63% yield). ^{1}H-NMR (500 MHz; DMSO-d_6): δ 7.48 (d, *J* = 7.8 Hz, 2H), 7.34-7.27 (m, 3H), 6.88 (d, *J* = 15.7 Hz, 1H), 6.29 (dt, *J* = 15.6, 7.7 Hz, 1H), 3.93 (d, *J* = 7.6 Hz, 2H), 3.13 (dt, *J* = 7.8, 4.2 Hz, 2H), 2.91 (s, 6H), 1.66-1.60 (m, 2H), 1.23 (sextet, *J* = 7.3 Hz, 2H), 0.82 (t, *J* = 7.4 Hz, 3H). ^{13}C NMR (126 MHz; DMSO-d_6): δ 143.4, 136.3, 130.6, 130.4, 128.5, 116.5, 66.9, 64.7, 51.1, 25.0, 20.4, 14.5. HRMS (ESI) *m/z* $[C_{15}H_{24}N]^+$ calculated 218.1903, found 218.1901.

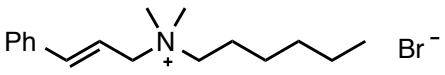

N-cinnamyl-N,N-dimethylhexan-1-aminium bromide (**2g**)

General procedure yielded a yellow oil (60% yield). ^{1}H-NMR (500 MHz; DMSO-d_6): δ 7.47 (d, *J* = 7.7 Hz, 2H), 7.34-7.26 (m, 3H), 6.87 (d, *J* = 15.7 Hz, 1H), 6.28 (dt, *J* = 15.5, 7.7 Hz, 1H), 3.94 (d, *J* = 7.5

Hz, 2H), 3.11 (dd, *J* = 10.1, 6.7 Hz, 2H), 2.92 (s, 6H), 1.63-1.63 (m, 2H), 1.18 (s, 6H), 0.73 (t, *J* = 6.5 Hz, 3H). ^{13}C NMR (126 MHz; DMSO-d_6): δ 143.3, 136.3, 130.7, 130.3, 128.5, 116.5, 66.8, 58.1, 51.2, 31.7, 26.5, 23.1, 22.9, 18.8. HRMS (ESI) *m/z* $[C_{17}H_{28}N]^+$ calculated 246.2216, found 246.2214.

V. Synthesis of Alkylphenylprop-2-enyl Ammonium Salts

Phenylpro-2-en-1-amonium chloride **A2**•HCl was synthesized according to published procedures.[3]

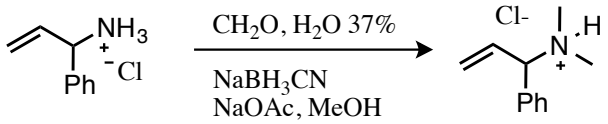

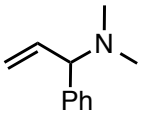

N,N-dimethyl-1-phenylprop-2-en-1-amine (**A3**)

To a scintillation vial equipped with a magnetic stirbar was added **A2**•HCl (2.5g, 14.74 mmol), NaOAc (1.5 g, 18.29 mmol), methanol (60 ml) and aqueous formaldehyde (4 ml, 37% w/v in H_2O). Solution was stirred 30 min and $NaCNBH_3$ (2.5 g, 39.78 mmol) was added. Stirring continued overnight. Reaction mixture was extracted with DCM (3x). Extracts dried with MgSO4, filtered through a plug of silica and rotavaped to yield **A3** as a yellow oil (1.6 g, 67%). Treatment of **A3** with a solution of HCl in ethyl acetate forms the **A3**•HCl salt as an off-white solid, which can be dissolved in DCM and recrystallized with dry EtOAc or Et_2O. NMR shifts are reported for the free amine.

^{1}H-NMR (400 MHz; $CDCl_3$): δ 7.34 (t, *J* = 4.5 Hz, 4H), 7.25 (dd, *J* = 8.2, 4.0 Hz, 1H), 5.99 (ddd, *J* = 17.1, 10.1, 8.8 Hz, 1H), 5.22 (dt, *J* = 17.1, 0.8 Hz, 1H), 5.10 (dd, *J* = 10.1, 1.5 Hz, 1H), 3.54 (d, *J* = 8.8 Hz, 1H), 2.21 (s, 6H). ^{13}C NMR (101 MHz; $CDCl_3$): δ 142.6, 140.5, 128.7, 128.0, 127.3, 116.3, 100.2, 76.3, 43.9. HRMS (ESI) *m/z* $[C_{11}H_{16}N]^+$ calculated 162.1277, found 162.1277.

---

[3] Schmidt, A. M. & Eilbracht, P. Synthesis of Pharmacologically Relevant Indoles with Amine Side Chains via Tandem Hydroformylation/Fischer Indole Synthesis. *J. Org. Chem.* **2005**, *70,* 5528–5535.

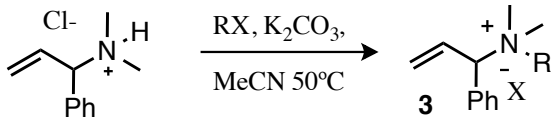

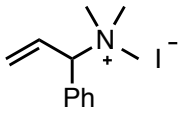

N,N,N-trimethyl-1-phenylprop-2-en-1-aminium iodide (**3b**)

General procedure for the alkylation of a secondary amine described previously yielded an off-white solid (91%). ^{1}H-NMR (500 MHz; CD_3OD): δ 7.67 (dd, *J* = 6.7, 2.7 Hz, 2H), 7.55 (dd, *J* = 5.0, 1.7 Hz, 3H), 6.71 (dt, *J* = 16.6, 10.1 Hz, 1H), 5.78 (d, *J* = 16.6 Hz, 1H), 5.72 (d, *J* = 10.2 Hz, 1H), 5.29 (d, *J* = 10.1 Hz, 1H), 3.10 (s, 9H). ^{13}C NMR (126 MHz; CD_3OD): δ 132.9, 132.11, 131.92, 130.51, 130.33, 127.4, 81.6, 51.78. HRMS (ESI) *m/z* $[C_{12}H_{18}N]^+$ calculated 176.1434, found 176.1433.

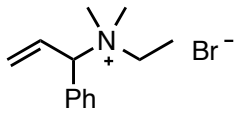

N-ethyl-N,N-dimethyl-1-phenylprop-2-en-1-aminium bromide (**3c**)

General procedure for the alkylation of a secondary amine described previously yielded an off-white solid (72%). ^{1}H-NMR (500 MHz; CD_3OD): δ 7.66 (dd, *J* = 6.6, 2.9 Hz, 2H), 7.53 (t, *J* = 3.3 Hz, 3H), 6.71 (dt, *J* = 16.7, 10.1 Hz, 1H), 5.76 (d, *J* = 16.7 Hz, 1H), 5.69 (d, *J* = 10.2 Hz, 1H), 5.27 (d, *J* = 10.1 Hz, 1H), 3.41 (q, *J* = 7.0 Hz, 2H), 3.03 (s, 3H), 2.96 (s, 3H), 1.42 (t, *J* = 7.2 Hz, 3H). ^{13}C NMR (126 MHz; CD_3OD): δ 132.8, 132.3, 131.8, 130.47, 130.37, 126.9, 80.6, 59.47, 59.45, 47.8, 8.5. HRMS (ESI) *m/z* $[C_{13}H_{20}N]^+$ calculated 190.1590, found 190.1589.

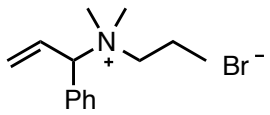

N,N-dimethyl-1-phenyl-N-propylprop-2-en-1-aminium bromide (**3d**)

General procedure for the alkylation of a secondary amine described previously yielded an off-white solid (67%). ^{1}H-NMR (500 MHz; CD_3OD): δ 7.64 (dd, *J* = 6.7, 2.9 Hz, 2H), 7.52 (dd, *J* = 4.9, 1.7 Hz, 3H), 6.71 (dt, *J* = 16.7, 10.2 Hz, 1H), 5.73 (d, *J* = 16.7 Hz, 1H), 5.68 (d, *J* = 10.2 Hz, 1H), 5.25 (d, *J* = 10.1 Hz, 1H), 3.28-3.18 (m, 2H), 3.03 (s, 3H), 2.97 (s, 3H), 1.93-1.81 (m, 2H), 0.97 (t, *J* = 7.3 Hz, 3H). ^{13}C NMR (126 MHz; CD_3OD): δ 132.8, 132.3, 131.9, 130.48, 130.40, 126.9, 80.8, 65.5, 17.0, 10.9. HRMS (ESI) *m/z* $[C_{14}H_{22}N]^+$ calculated 204.1747, found 204.1745.

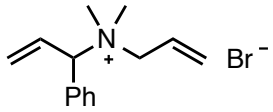

N-allyl-N,N-dimethyl-1-phenylprop-2-en-1-aminium bromide (**3a**)

General procedure for the alkylation of a secondary amine described previously yielded an off-white solid (70%). ^{1}H-NMR (500 MHz; CD_3OD): δ 7.72 (td, *J* = 3.2, 2.4 Hz, 2H), 7.54 (t, *J* = 3.2 Hz, 3H), 6.77 (dt, *J* = 16.6, 10.2 Hz, 1H), 6.19-6.10 (m, 1H), 5.80 (d, *J* = 16.6 Hz, 1H), 5.74-5.70 (m, 3H), 5.39 (d, *J* = 10.1 Hz, 1H), 4.01 (dd, *J* = 7.1, 4.9 Hz, 2H), 3.05 (s, 3H), 2.97 (s, 3H). ^{13}C NMR (126 MHz; CD_3OD): δ 132.53, 131.8, 131.1, 130.7, 130.46, 129.7, 127.2, 126.3, 80.9, 74.9, 66.0, 41.8. HRMS (ESI) *m/z* $[C_{13}H_{20}N]^+$ calculated 202.1590, found 202.1589.

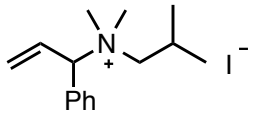

N-isobutyl-N,N-dimethyl-1-phenylprop-2-en-1-aminium iodide (**3e**)

General procedure for the alkylation of a secondary amine described previously yielded an off-white solid (74%). ^{1}H-NMR (500 MHz; CD_3OD): δ 7.68 (t, *J* = 3.6 Hz, 2H), 7.54 (t, *J* = 2.8 Hz, 3H), 6.72 (dt, *J* = 16.7, 10.2 Hz, 1H), 5.76 (d, *J* = 16.6 Hz, 1H), 5.70 (d, *J* = 10.2 Hz, 1H), 5.37 (d, *J* = 10.1 Hz, 1H), 3.23 (d, *J* = 4.9 Hz, 2H), 3.09 (s, 3H), 3.03 (s, 3H), 2.44-2.39 (m, 1H), 1.11 (d, *J* = 6.6 Hz, 6H). ^{13}C

NMR (126 MHz; CD_3OD): δ 132.9, 132.4, 131.9, 130.56, 130.47, 130.32, 129.8, 128.4, 127.2, 81.9, 71.5, 24.4, 23.4. HRMS (ESI) *m/z* $[C_{15}H_{24}N]^+$ calculated 218.1903, found 218.1902.

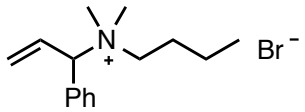

N,N-dimethyl-N-(1-phenylallyl)butan-1-aminium bromide (**3f**)

General procedure for the alkylation of a secondary amine described previously yielded a viscous oil (62%). ^{1}H-NMR (500 MHz; CD_3OD): δ 7.65-7.63 (m, 2H), 7.54 (dd, *J* = 5.0, 1.8 Hz, 3H), 6.71 (dt, *J* = 16.7, 10.2 Hz, 1H), 5.74 (d, *J* = 16.6 Hz, 1H), 5.69 (dd, *J* = 10.2, 0.8 Hz, 1H), 5.24 (d, *J* = 10.1 Hz, 1H), 3.29-3.23 (m, 2H), 3.04 (s, 3H), 2.98 (s, 3H), 1.84 (qt, *J* = 12.6, 6.2 Hz, 2H), 1.38 (sextet, *J* = 7.5 Hz, 2H), 1.00 (t, *J* = 7.4 Hz, 3H). ^{13}C NMR (126 MHz; CD_3OD): δ 132.8, 132.3, 131.9, 130.49, 130.39, 126.9, 80.7, 64.0, 25.4, 20.8, 13.9. HRMS (ESI) *m/z* $[C_{15}H_{24}N]^+$ calculated 218.1903, found 218.1902.

VI. NMR Spectra Alkylcinnamyl Ammonium Cations

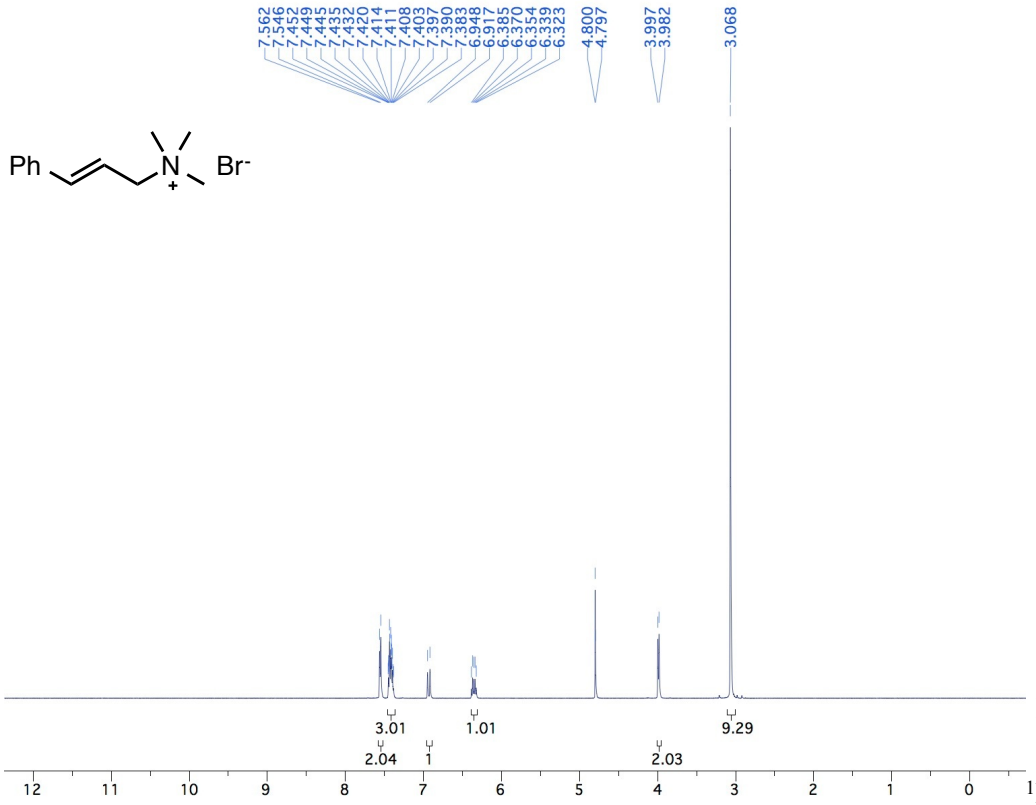

Figure S4. D_2O/ DMSO-D_6 ^{1}HNMR (**2b**)

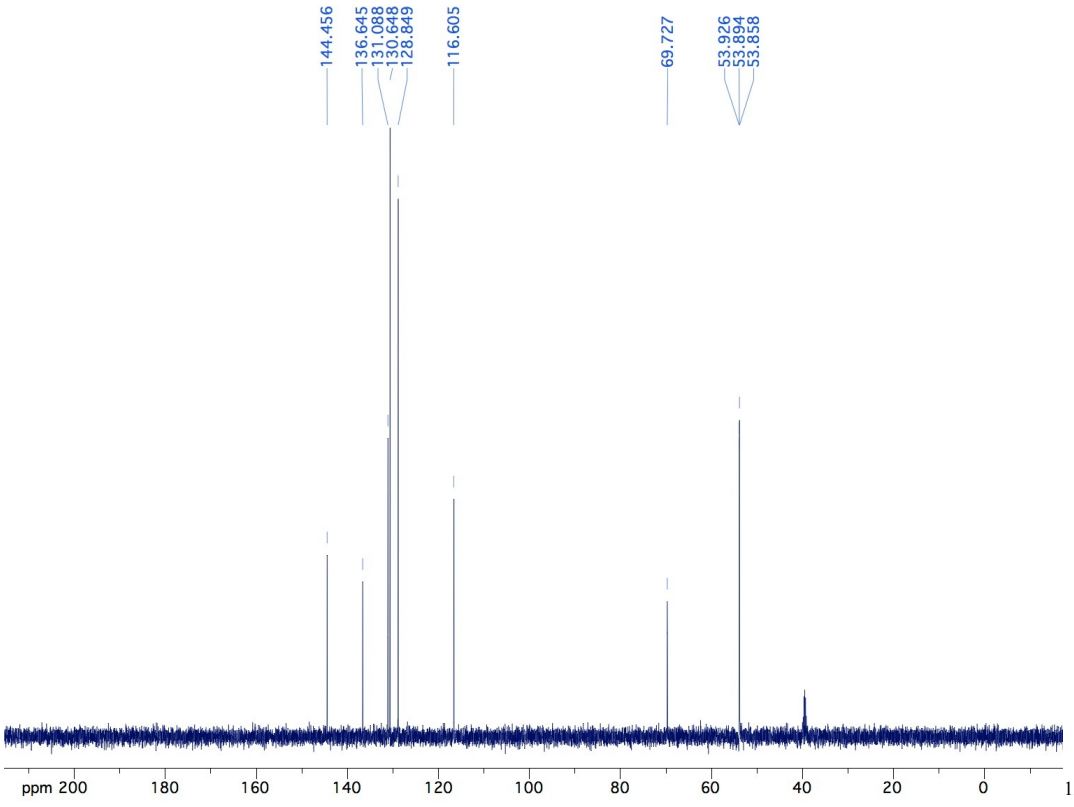

Figure S5. D_2O/ DMSO-D_6 ^{13}C NMR (**2b**)

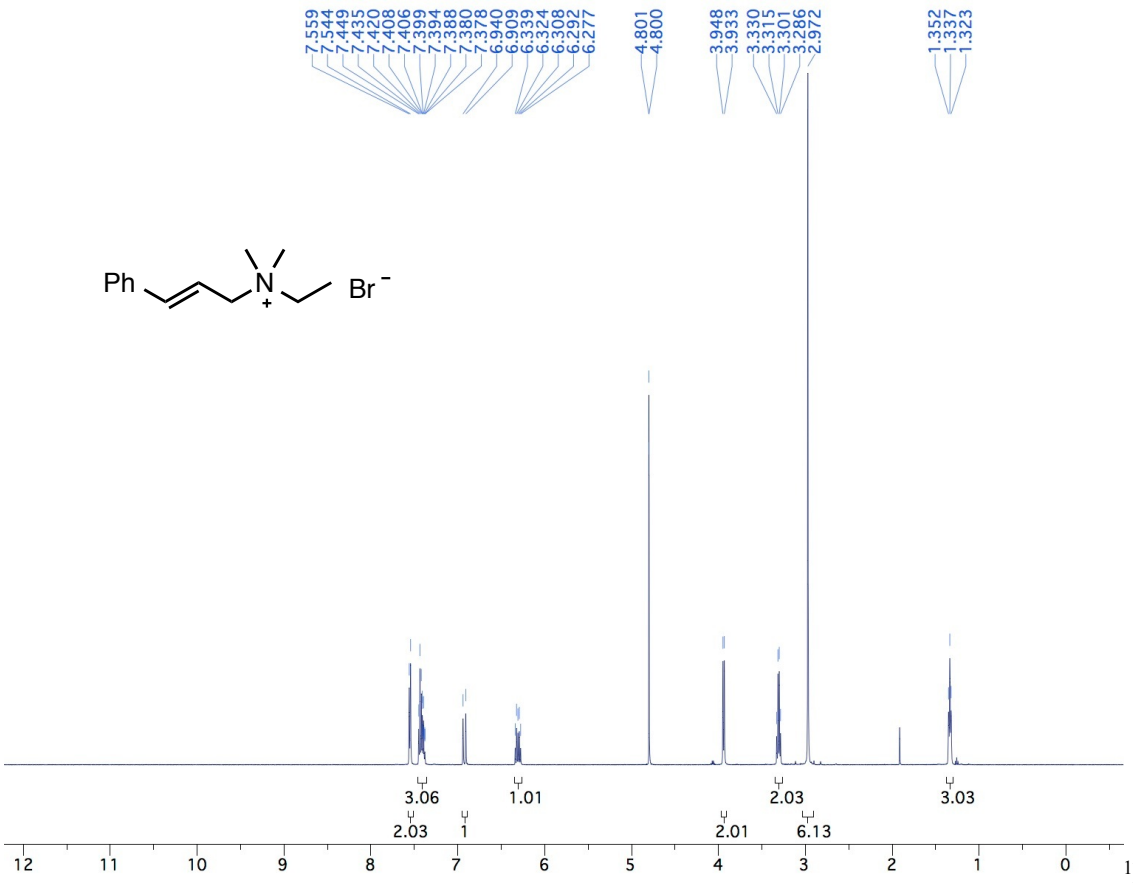

Figure S6. D_2O/ DMSO-D_6 ^1H NMR (**2c**)

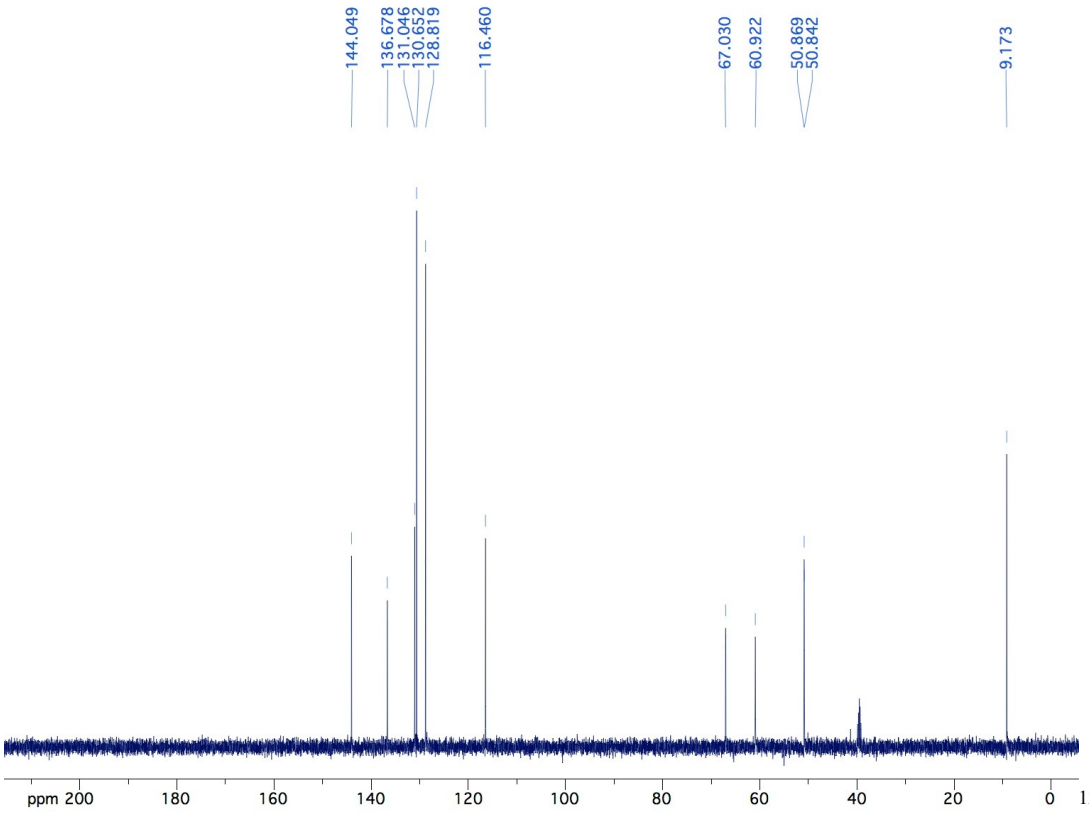

Figure S7. D_2O/ DMSO-D_6 ^{13}C NMR (**2c**)

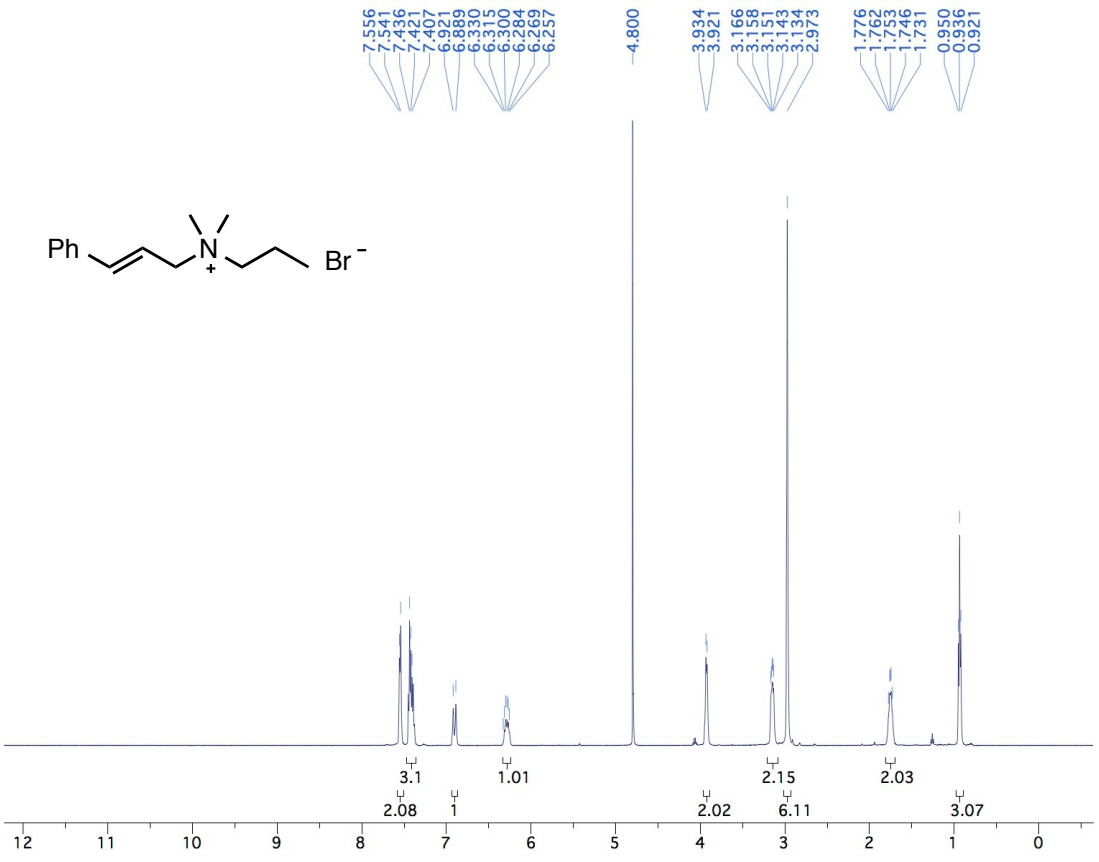

Figure S8. D_2O/ DMSO-D_6 ^1H NMR (**2d**)

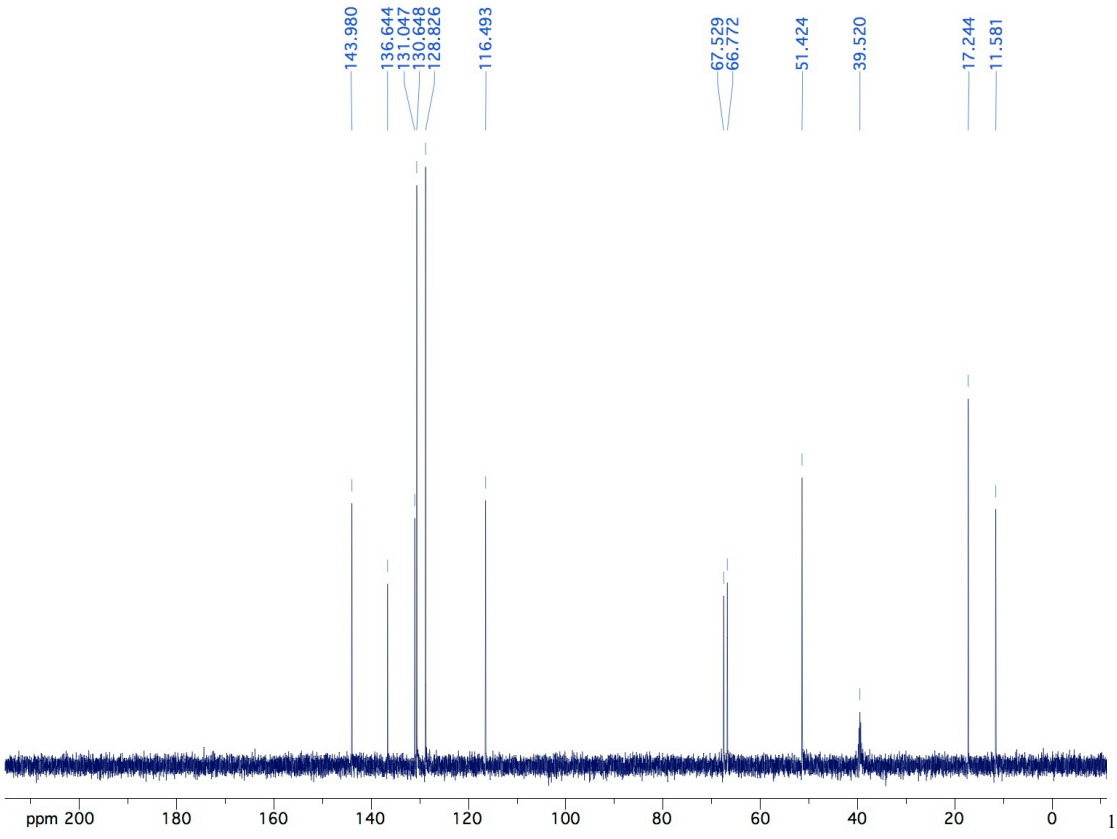

Figure S9. D_2O/ DMSO-D_6 ^{13}C NMR (**2d**)

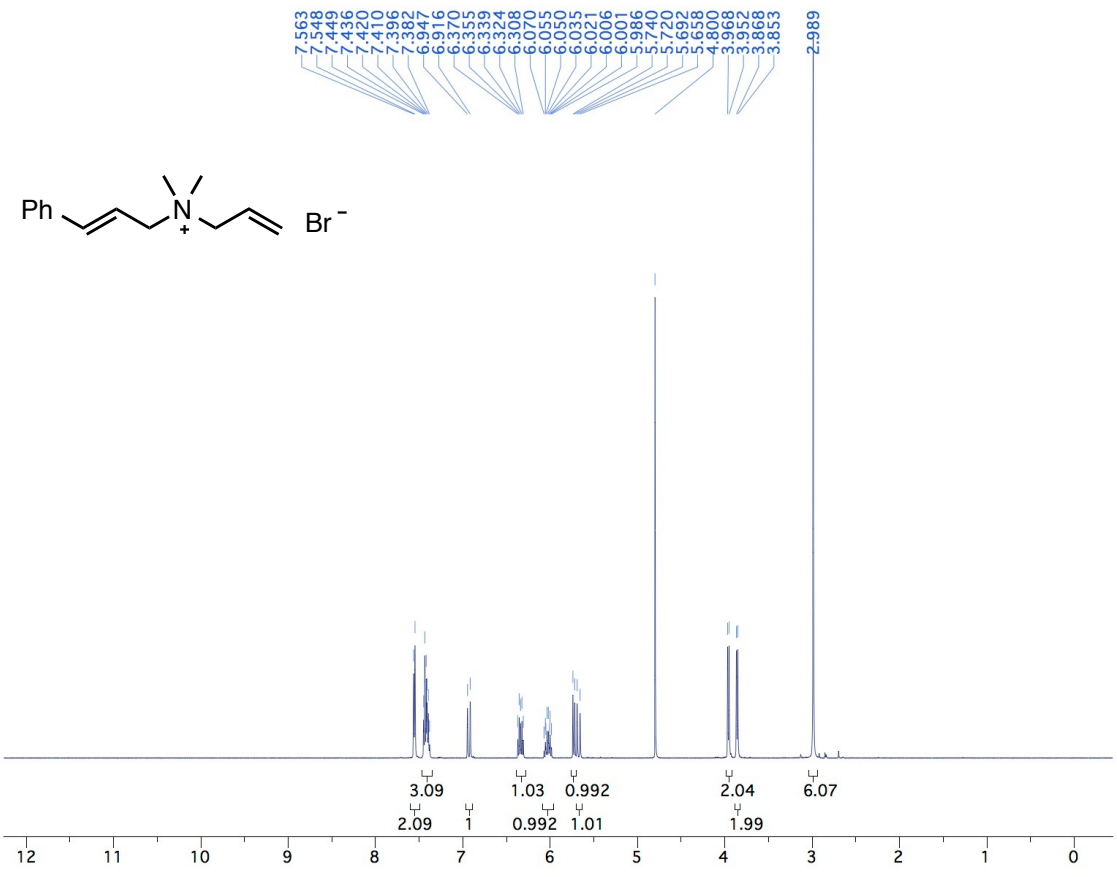

Figure S10. D_2O/DMSO-D_6 ^1H NMR (**2a**)

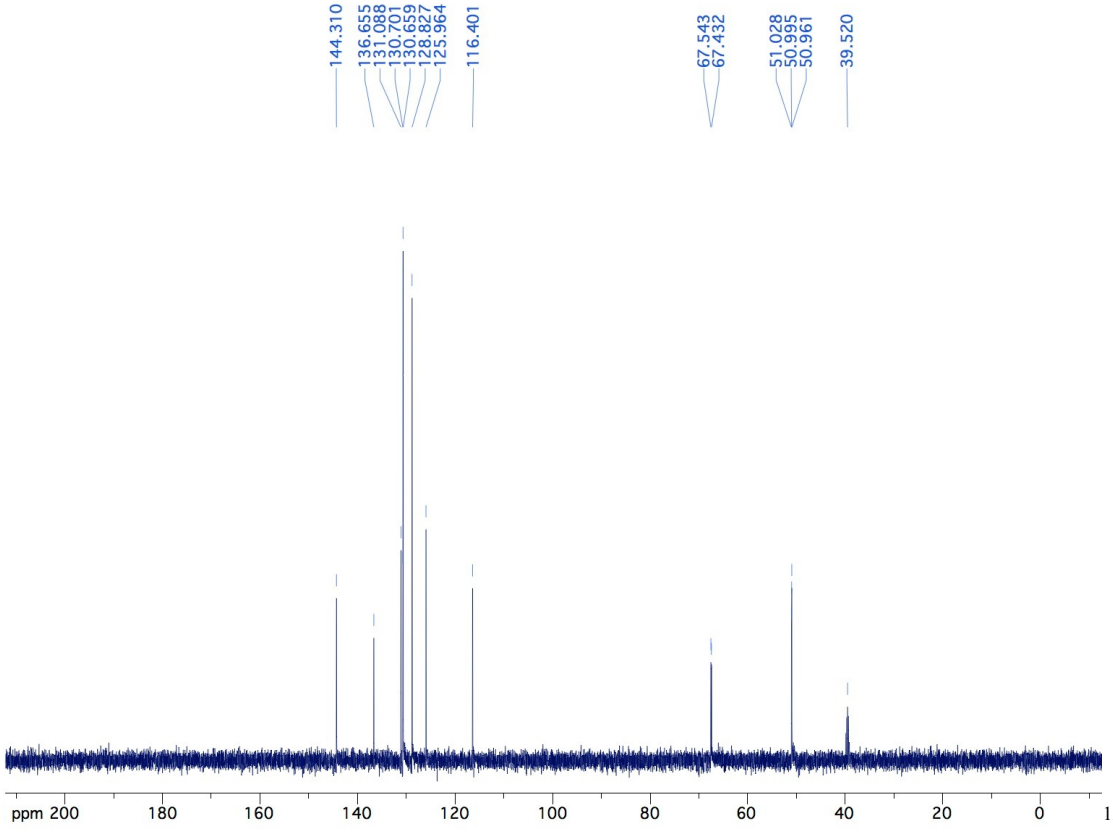

Figure S11. D_2O/DMSO-D_6 ^{13}C NMR (**2a**)

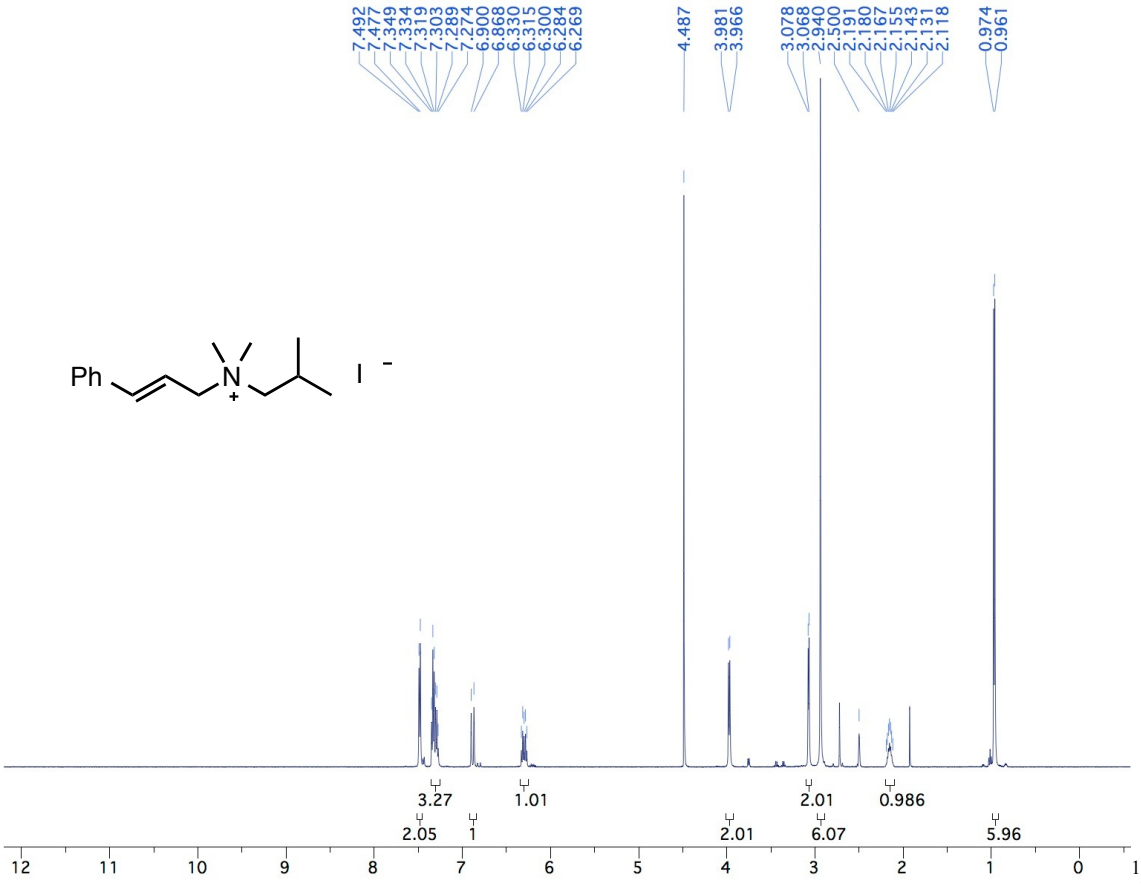

Figure S12. D_2O/DMSO-D_6 ^1H NMR (**2e**)

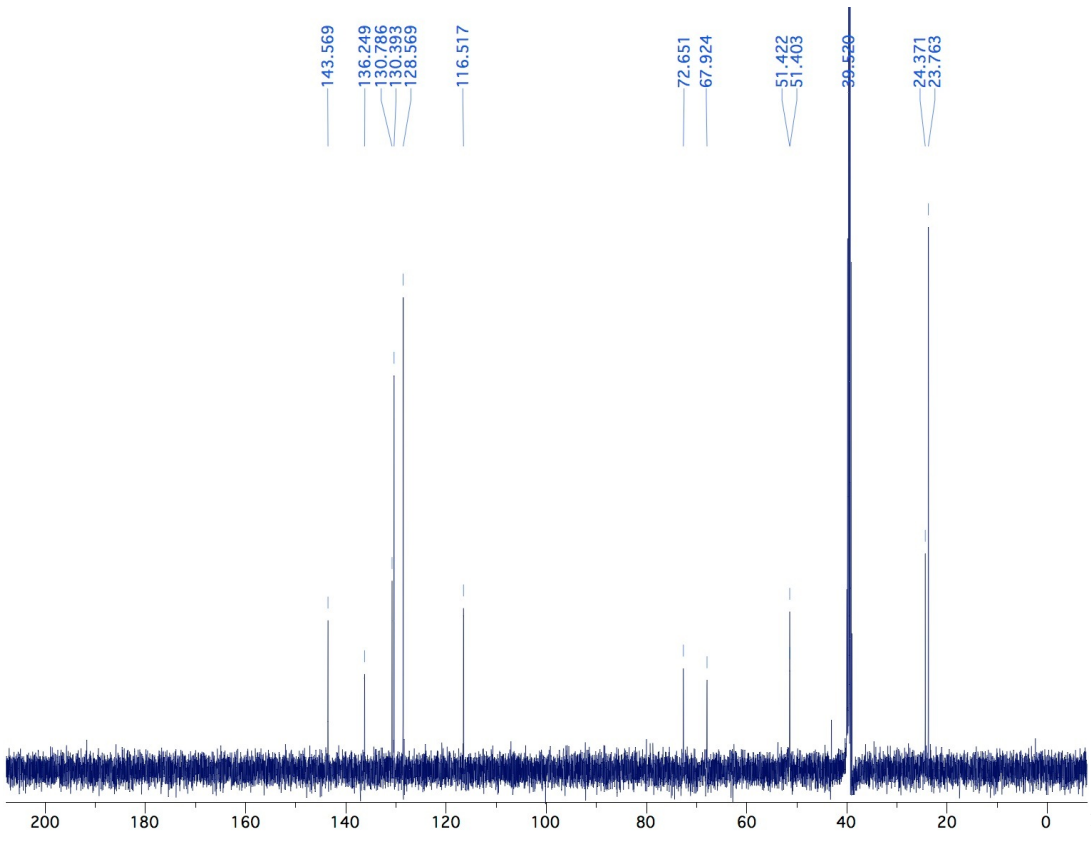

Figure S13. D_2O/DMSO-D_6 ^{13}C NMR (**2e**)

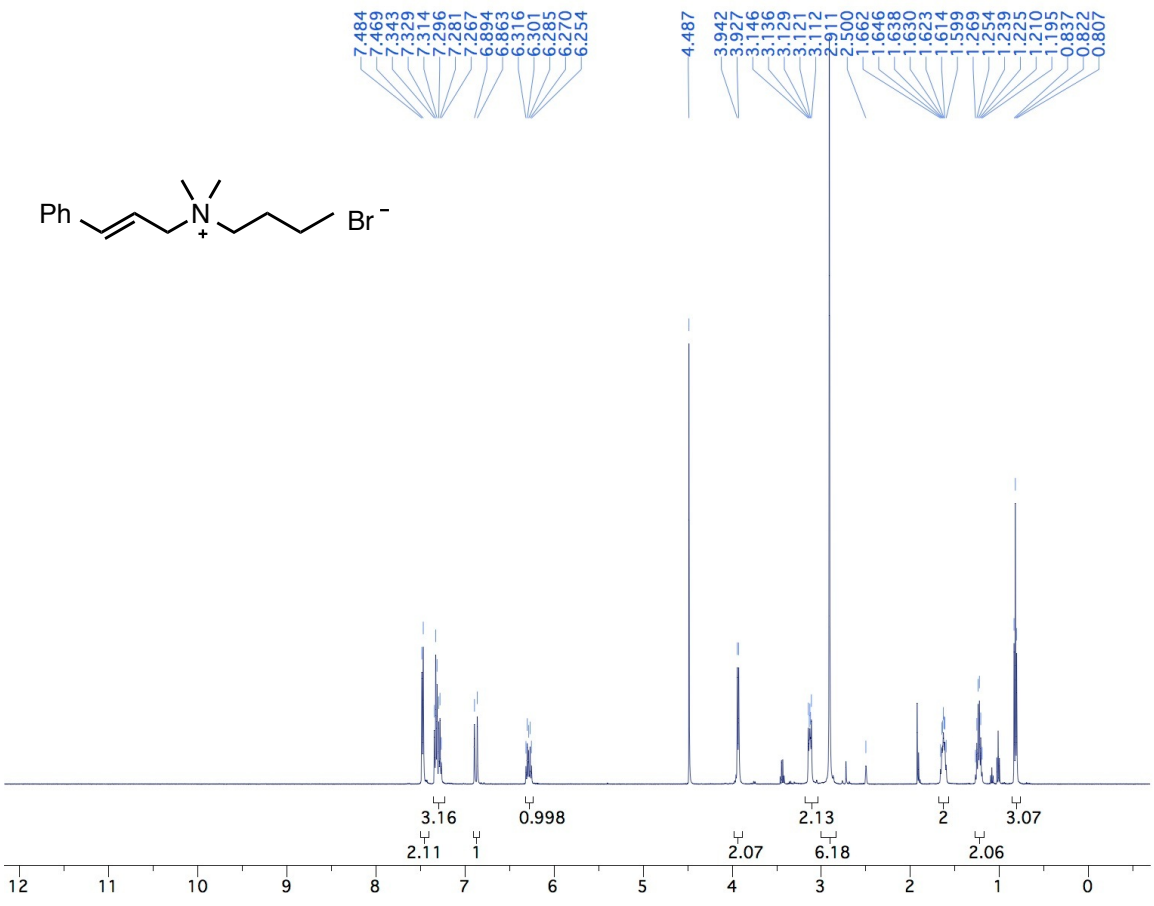

Figure S14. D_2O/DMSO-D_6 ^1H NMR (**2f**)

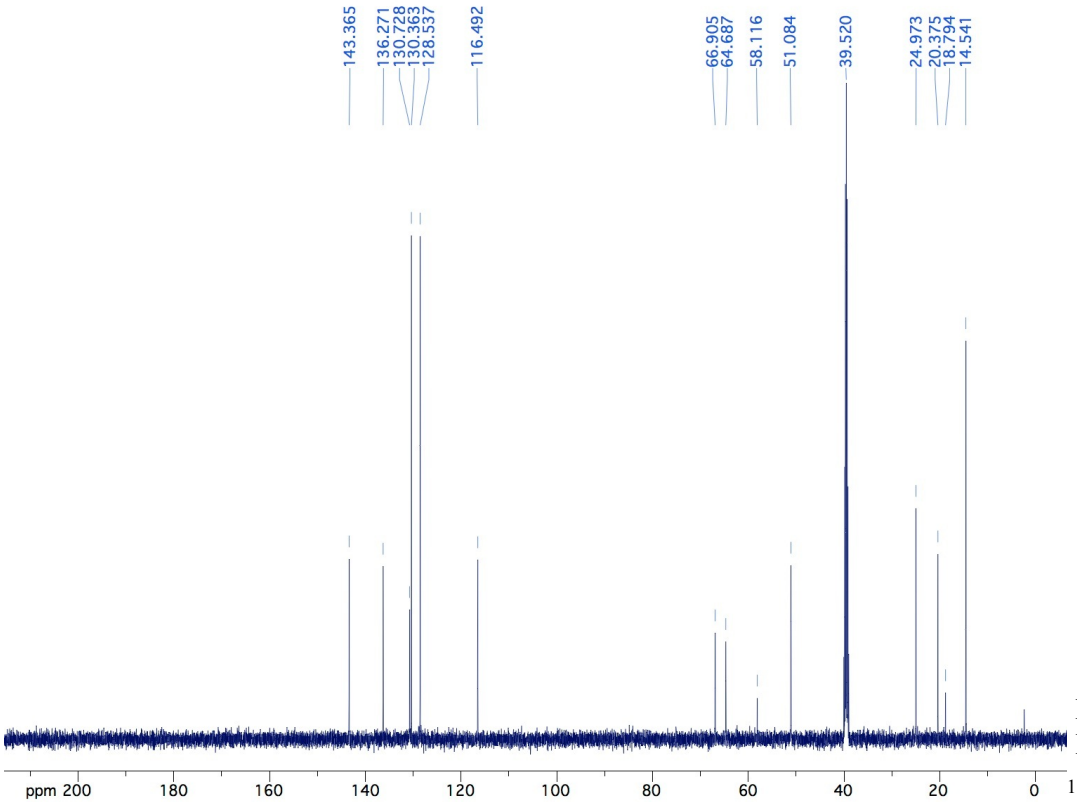

Figure S15. D_2O/DMSO-D_6 ^{13}C NMR (**2f**)

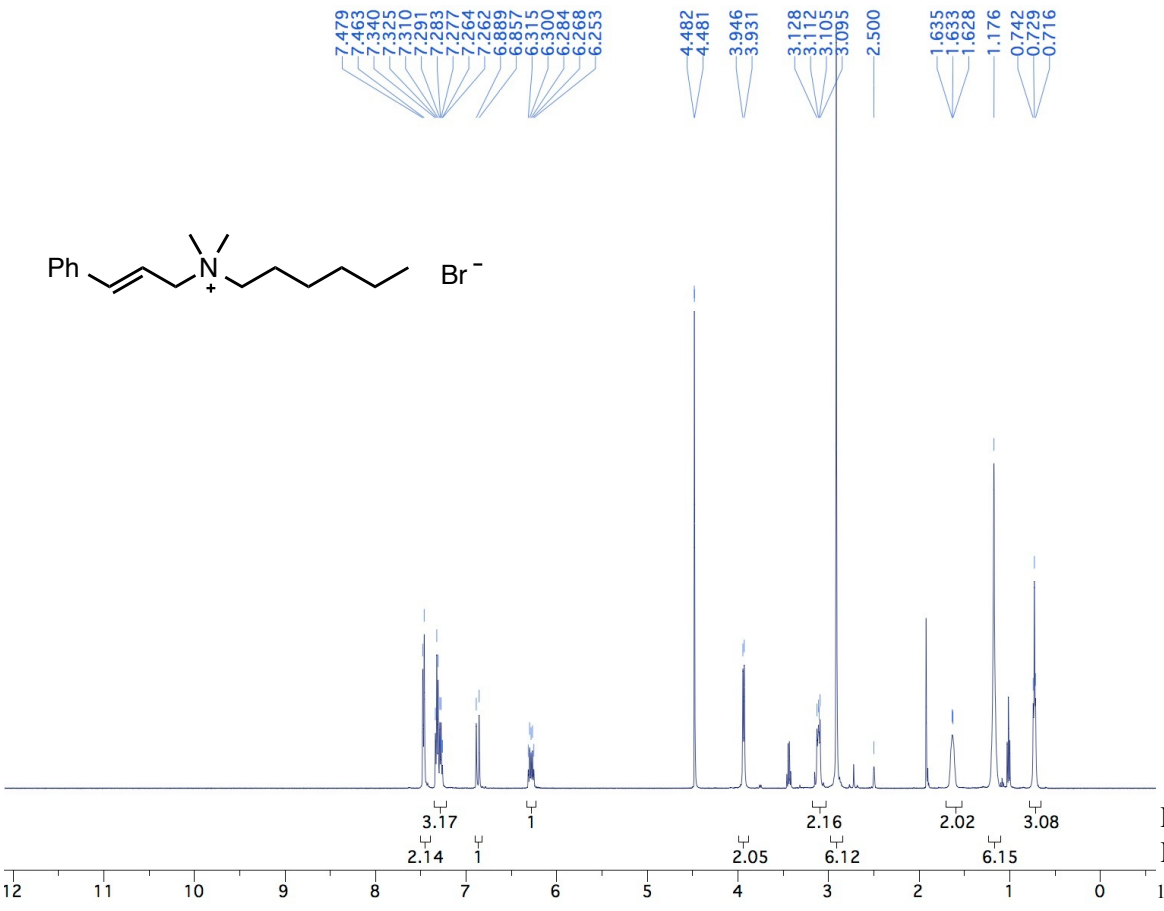

Figure S16. D_2O/DMSO-D_6 ^1H NMR (**2g**)

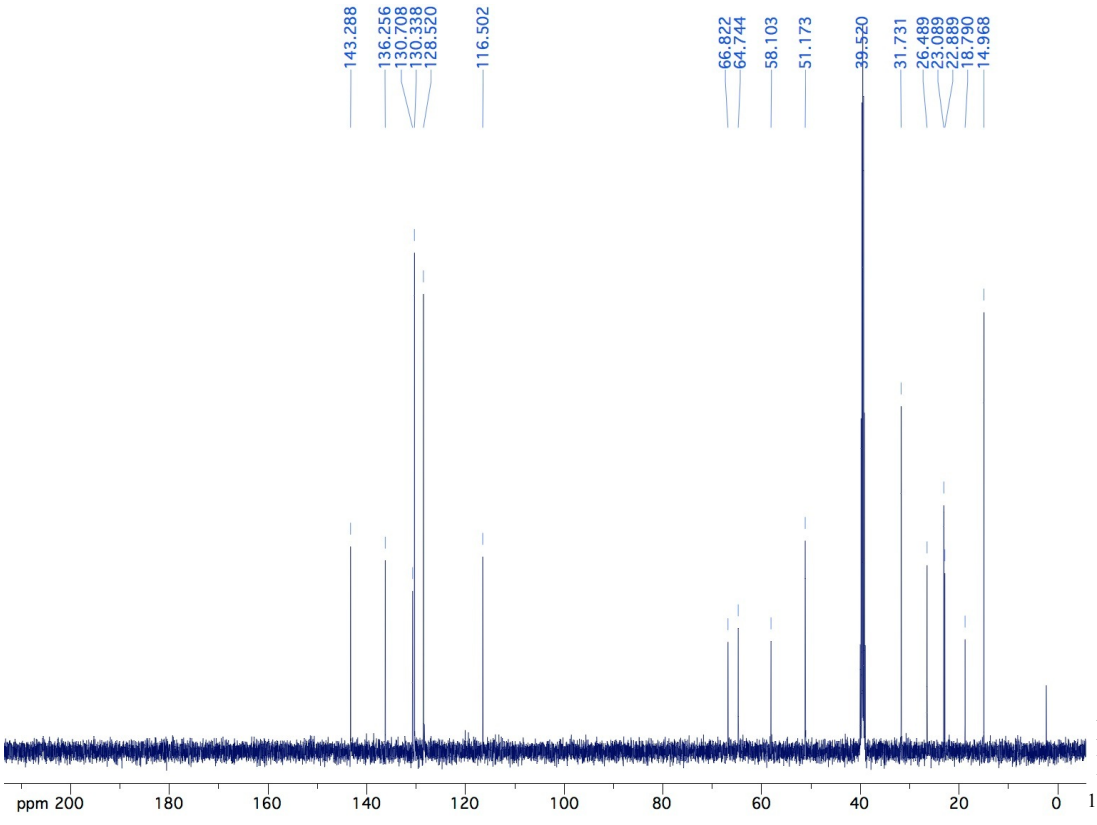

Figure S17. D_2O/DMSO-D_6 ^{13}C NMR (**2g**)

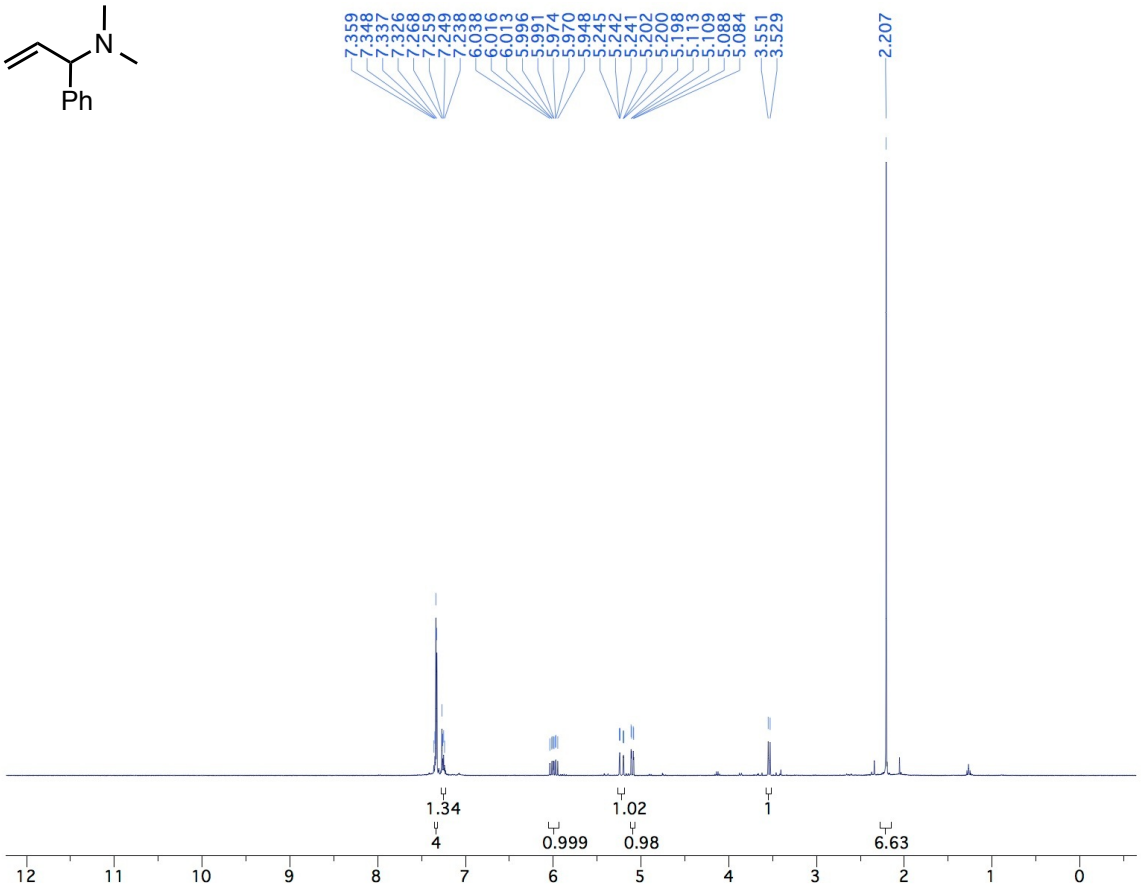

Figure S18. $CDCl_3$ ^1H NMR

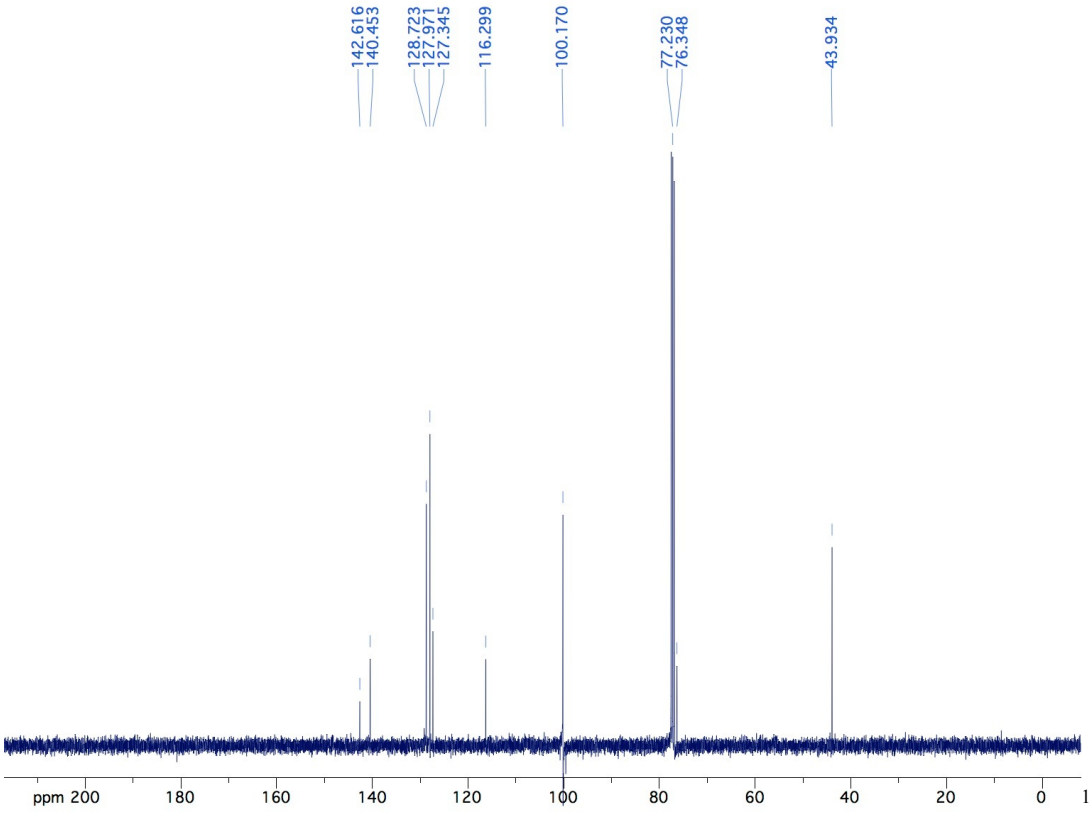

Figure S19. $CDCl_3$ ^{13}C NMR

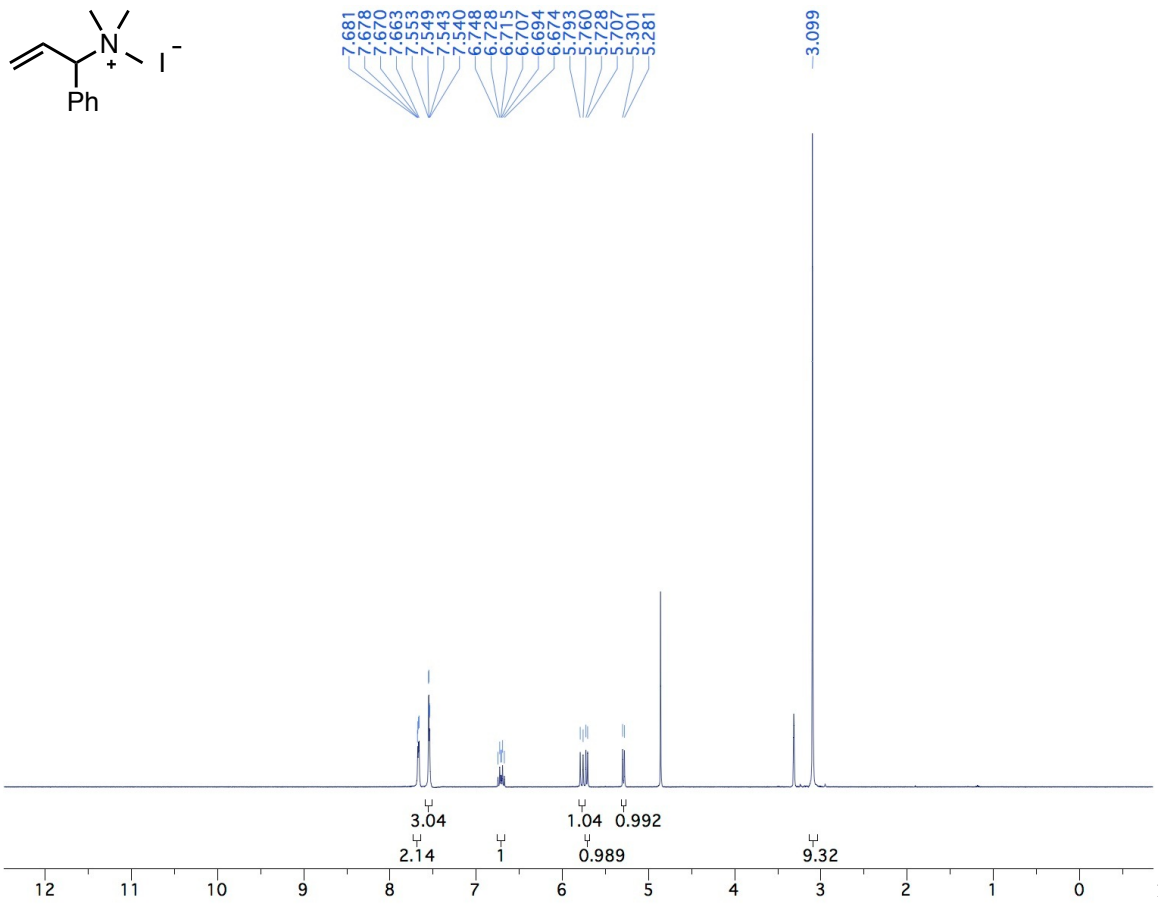

Figure S20. MeOD-D_4 ^{1}H NMR (**3b**)

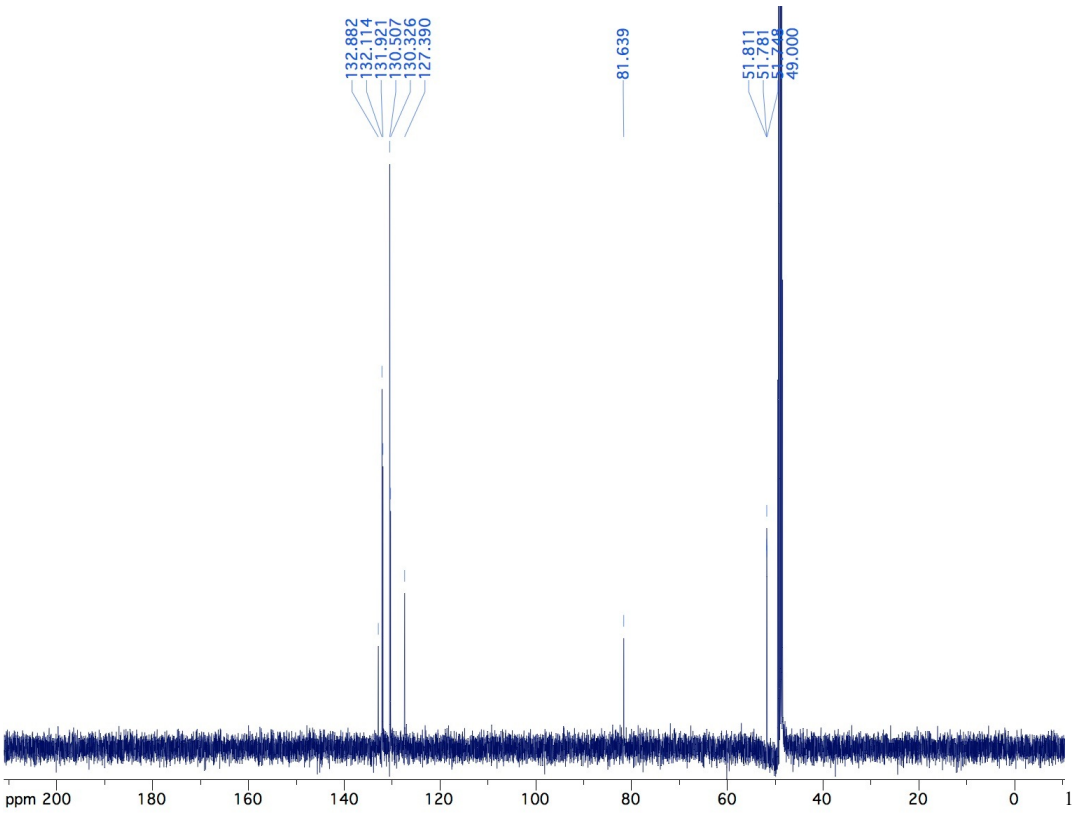

Figure S21. MeOD-D_4 ^{13}C NMR (**3b**)

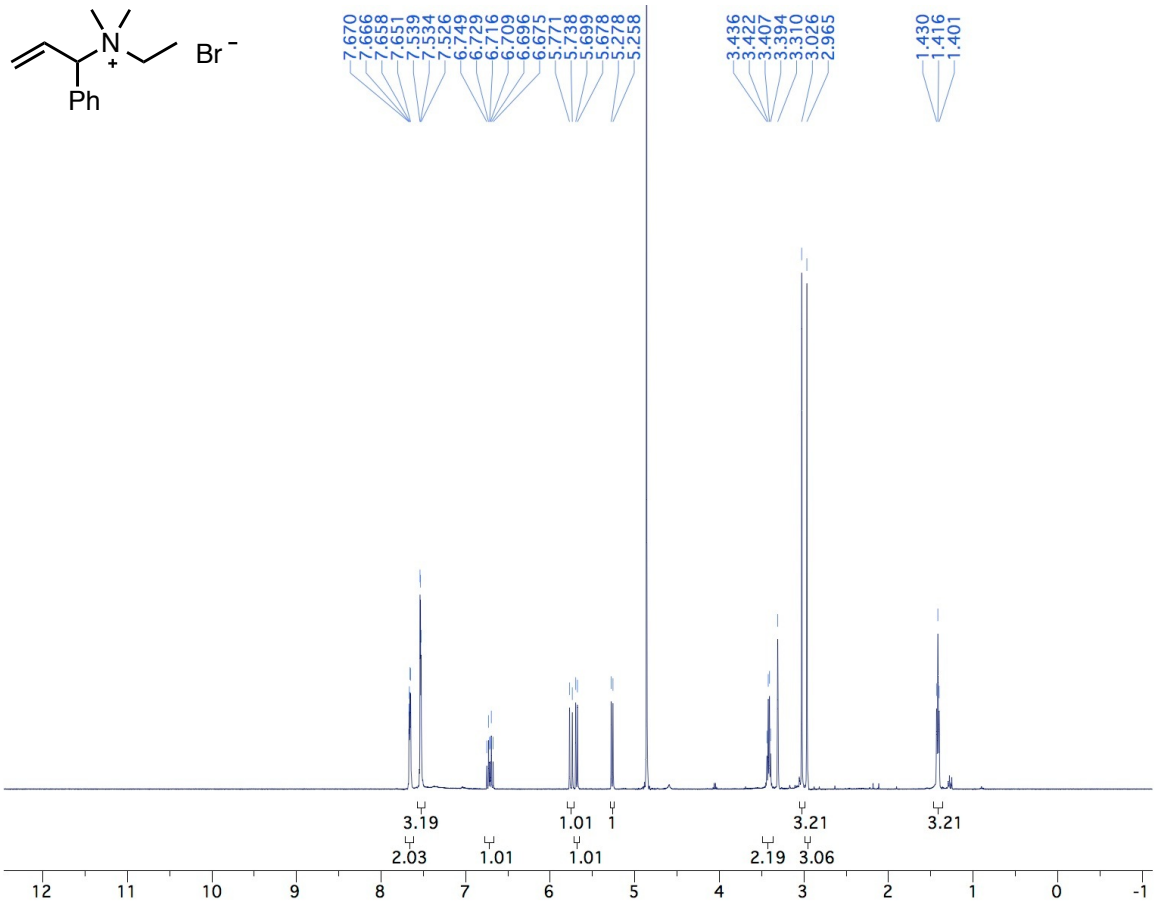

Figure S22. MeOD-D_4 ^{1}H NMR (**3c**)

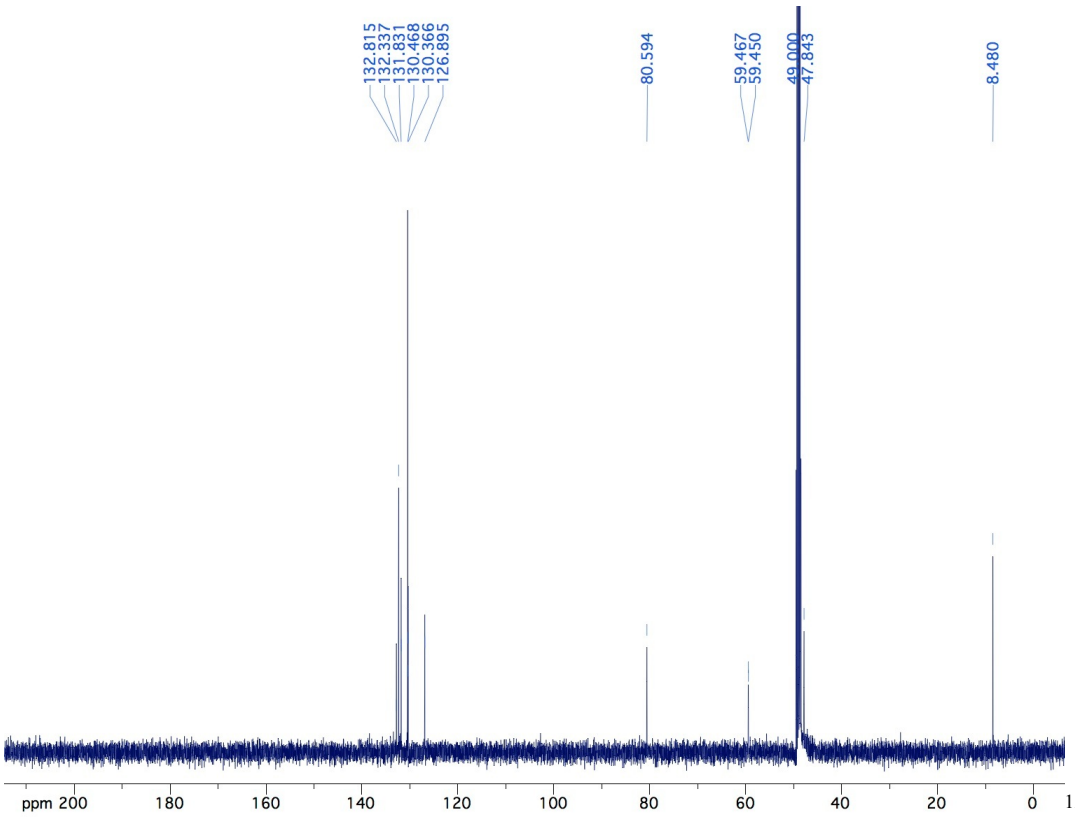

Figure S23. MeOD-D_4 ^{13}C NMR (**3c**)

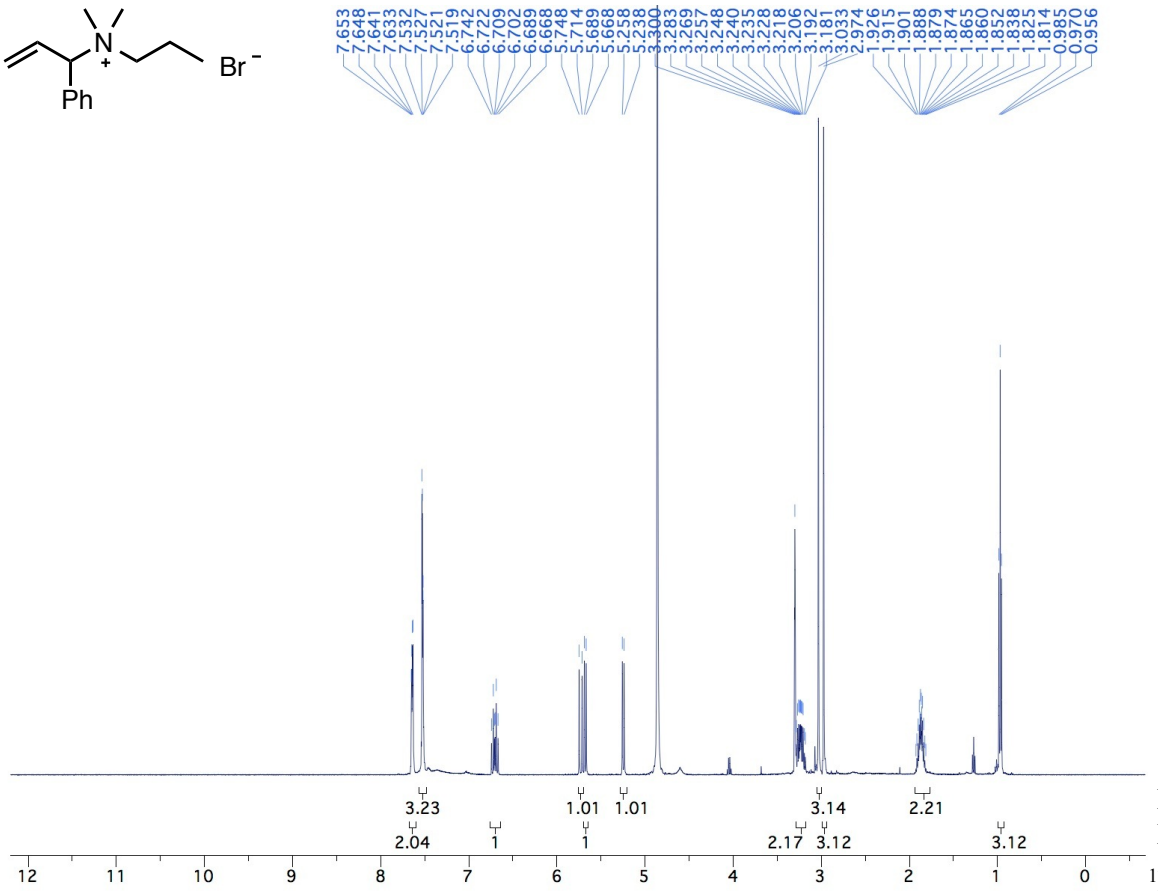

Figure S24. MeOD-D_4 ^{1}H NMR (**3d**)

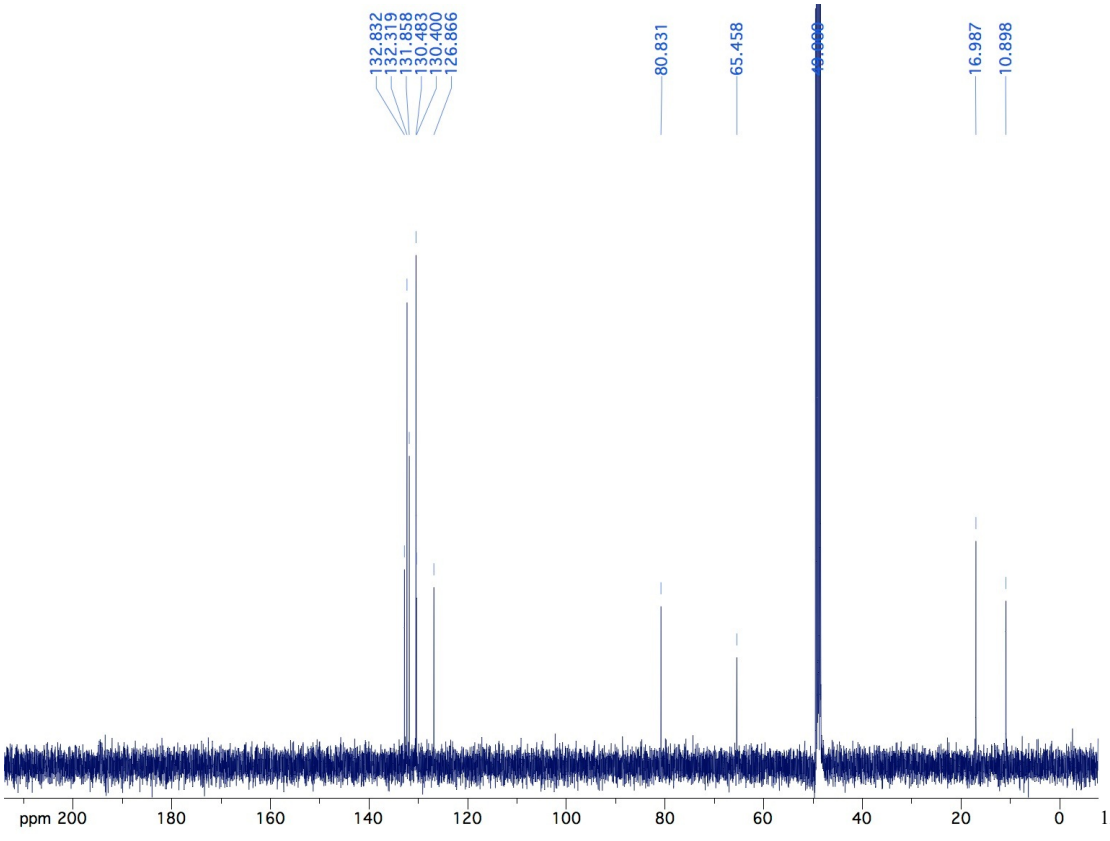

Figure S25. MeOD-D_4 ^{13}C NMR (**3d**)

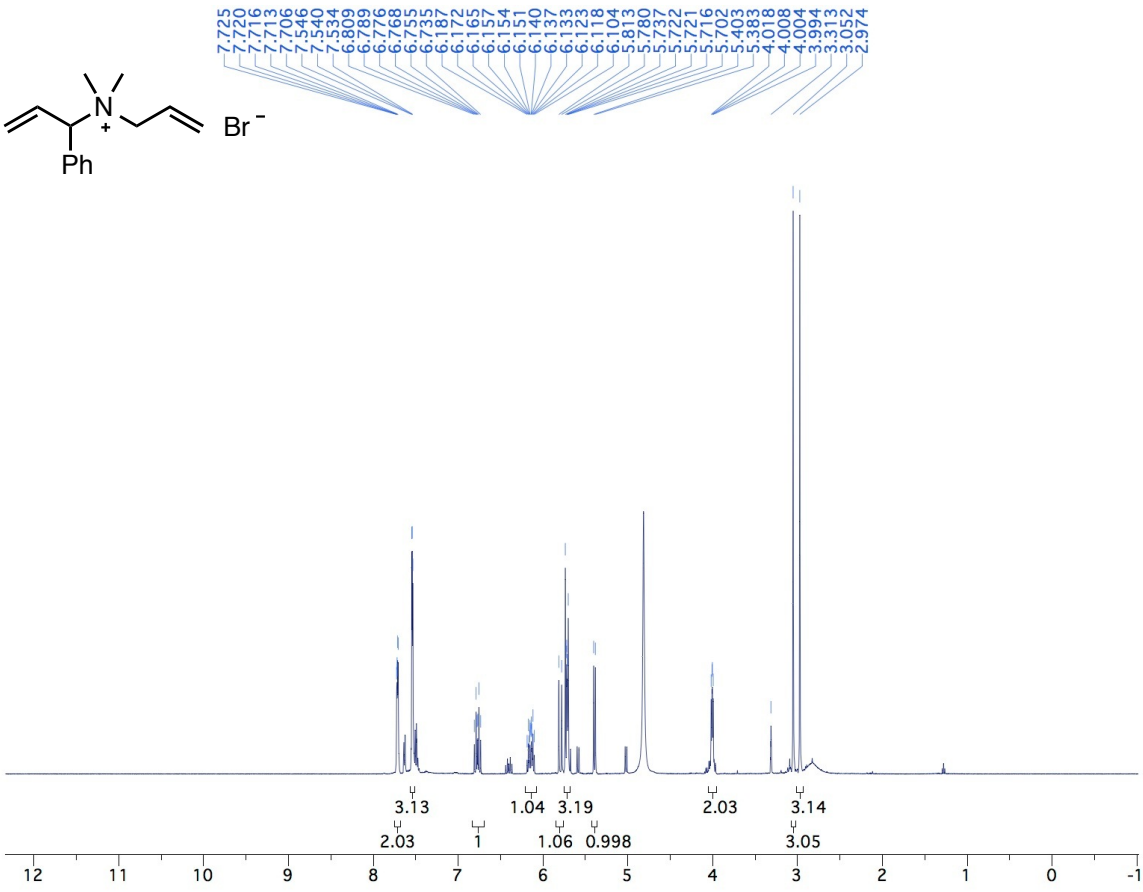

Figure S26. MeOD-D_4 ^{1}H NMR (**3a**)

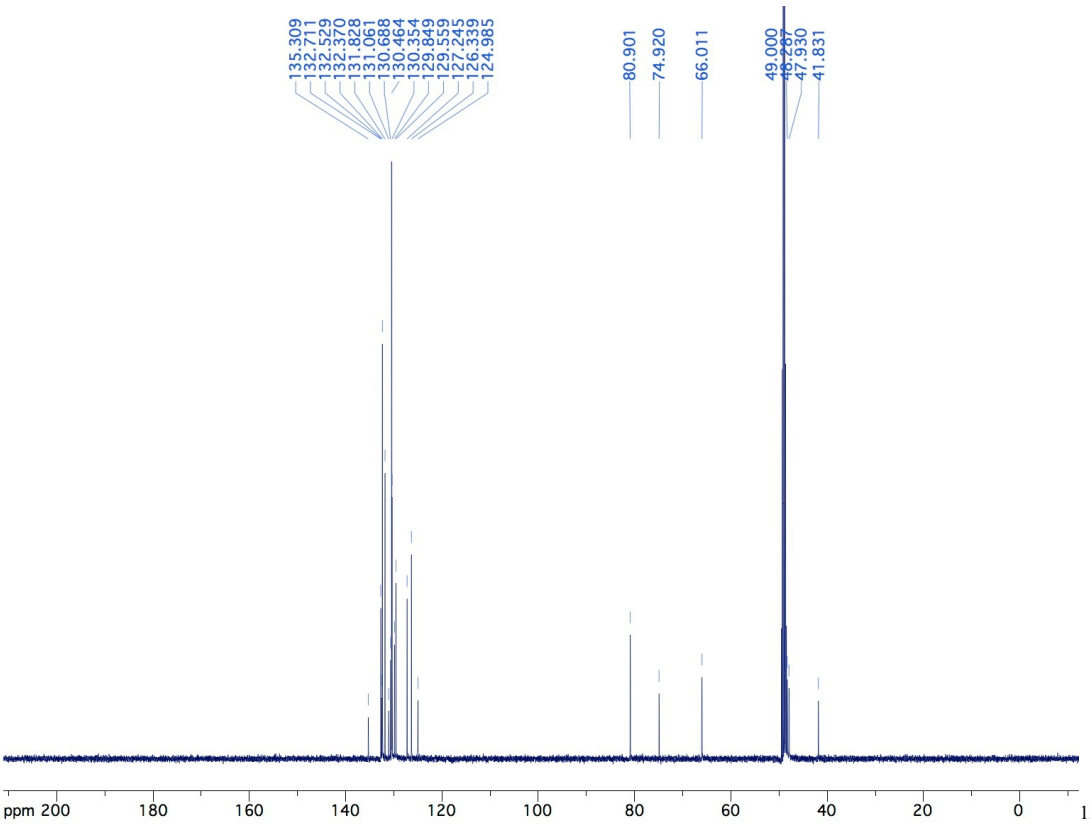

Figure S27. MeOD-D_4 ^{13}C NMR (**3a**)

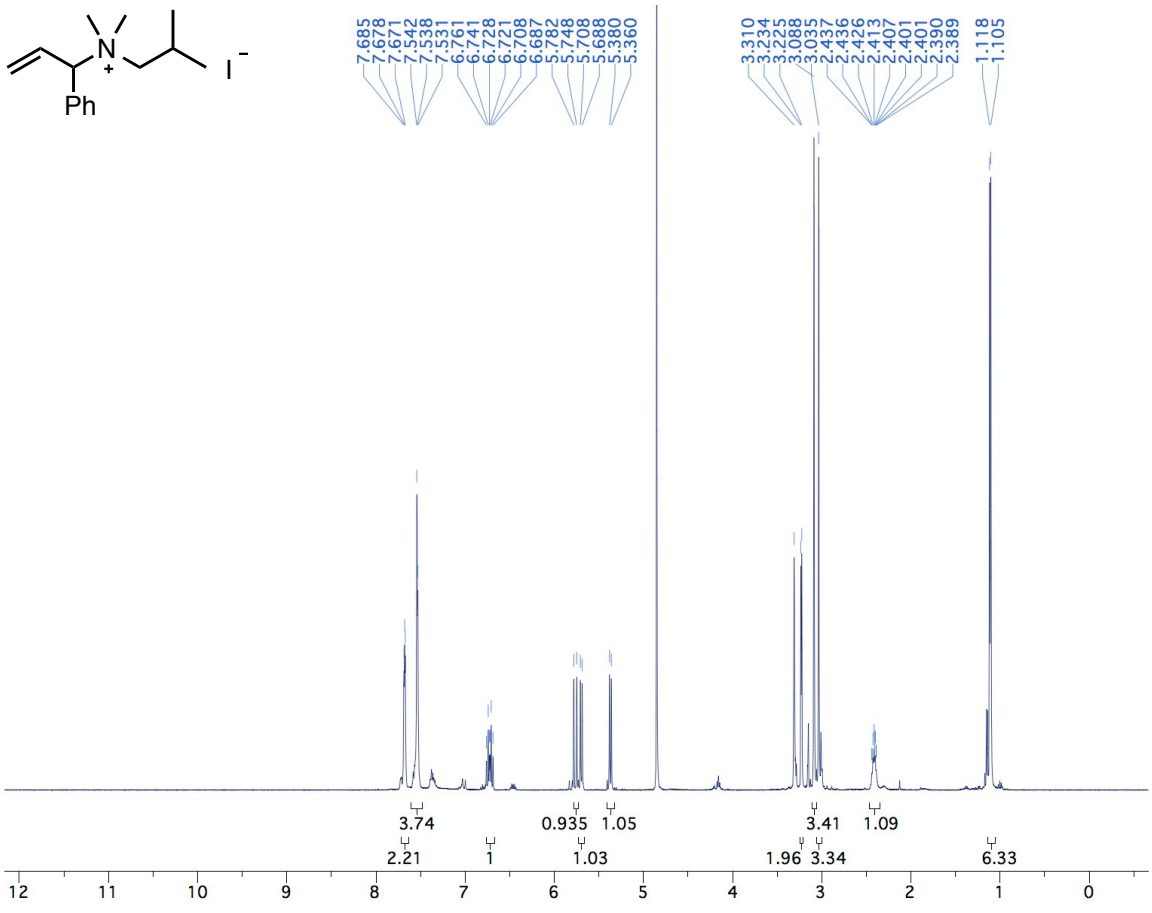

Figure S28. MeOD-D_4 ^{1}H NMR (**3e**)

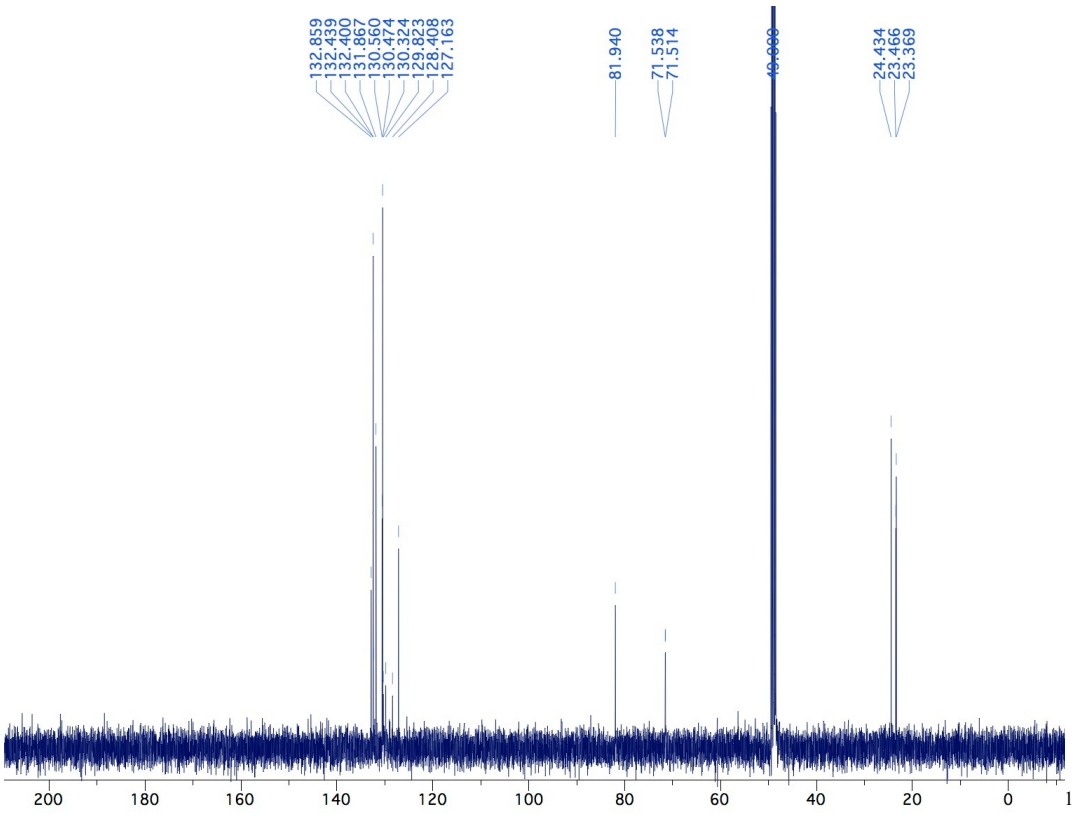

Figure S29. MeOD-D_4 ^{13}C NMR (**3e**)

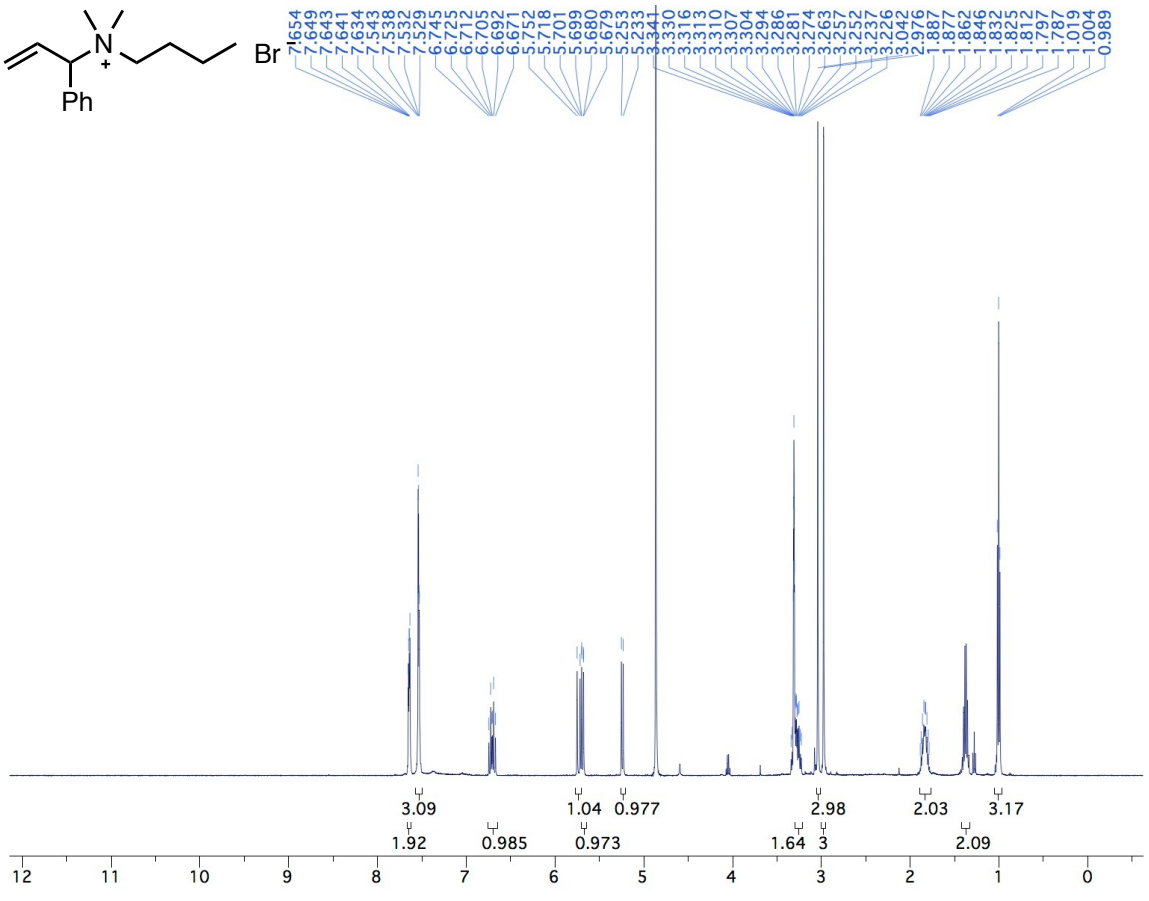

Figure S30. MeOD-D_4 ^{1}H NMR (**3f**)

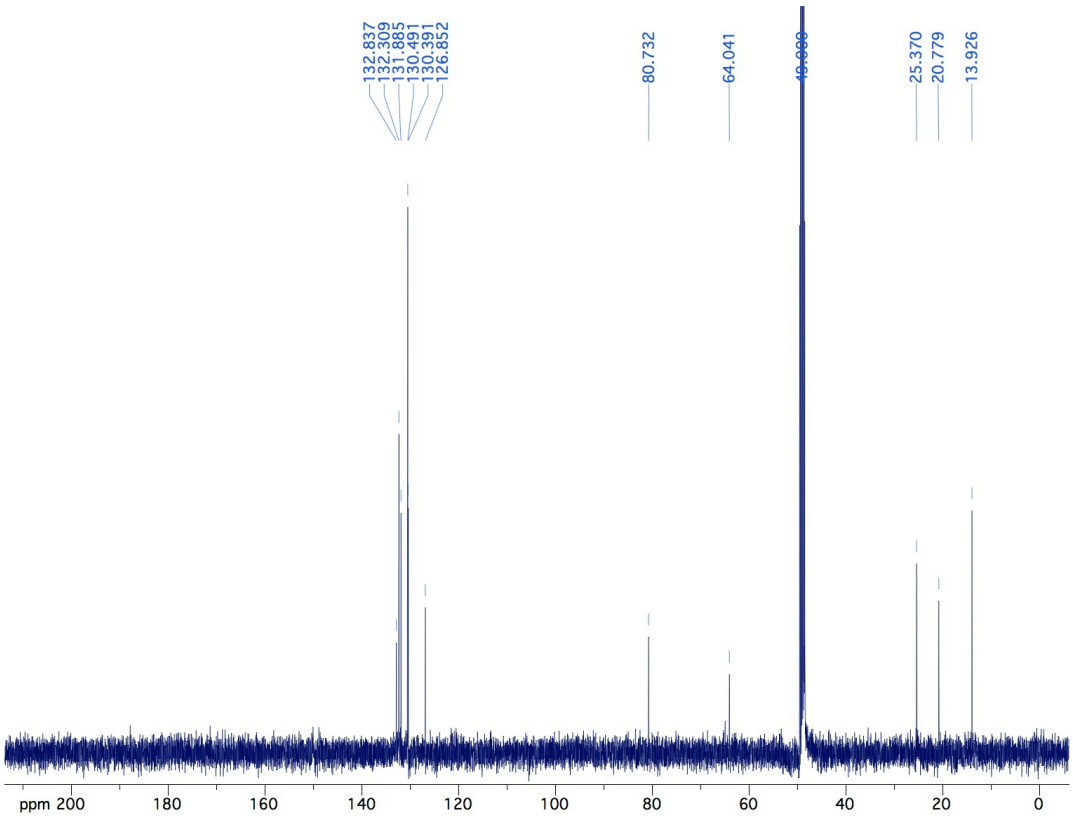

Figure S31. MeOD-D_4 ^{13}C NMR (**3f**)

VII. Photosensitized Rearrangement of Cinnamylammonium Ions

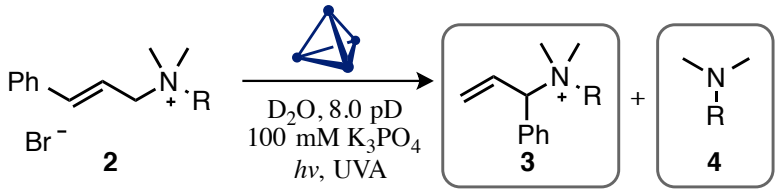

General procedure: In a N_2 atmosphere glovebox, *(E)-N,N,N*-trimethyl-3-phenylprop-2-en-1-aminium bromide (**2b**, 1 mg, 3.9 mmol) and $K_{12}Ga_4L_6$ (**1**, 15 mg, 4.2 mmol) were dissolved in degassed D_2O (700 µL, pD 8.0, 100 mM K_3PO_4) and mixed until a homogeneous yellow solution formed. Solution was then transferred to a pyrex reaction vessel (NMR tube or scintillation vial), capped and sealed with black electrical tape. Reaction vessel was irradiated with UVA light (6-8 UVA bulbs, 130 V, 8 W) in a Rayonet photoreactor for 12-24 h, unless otherwise specified. Reaction progress was monitored by ^{1}H NMR. The identity of reaction products was confirmed by independent synthesis of 1,3-rearrangement products, formation of host-guest complexes **3**⊂**1**, and evaluation by ^{1}H NMR.

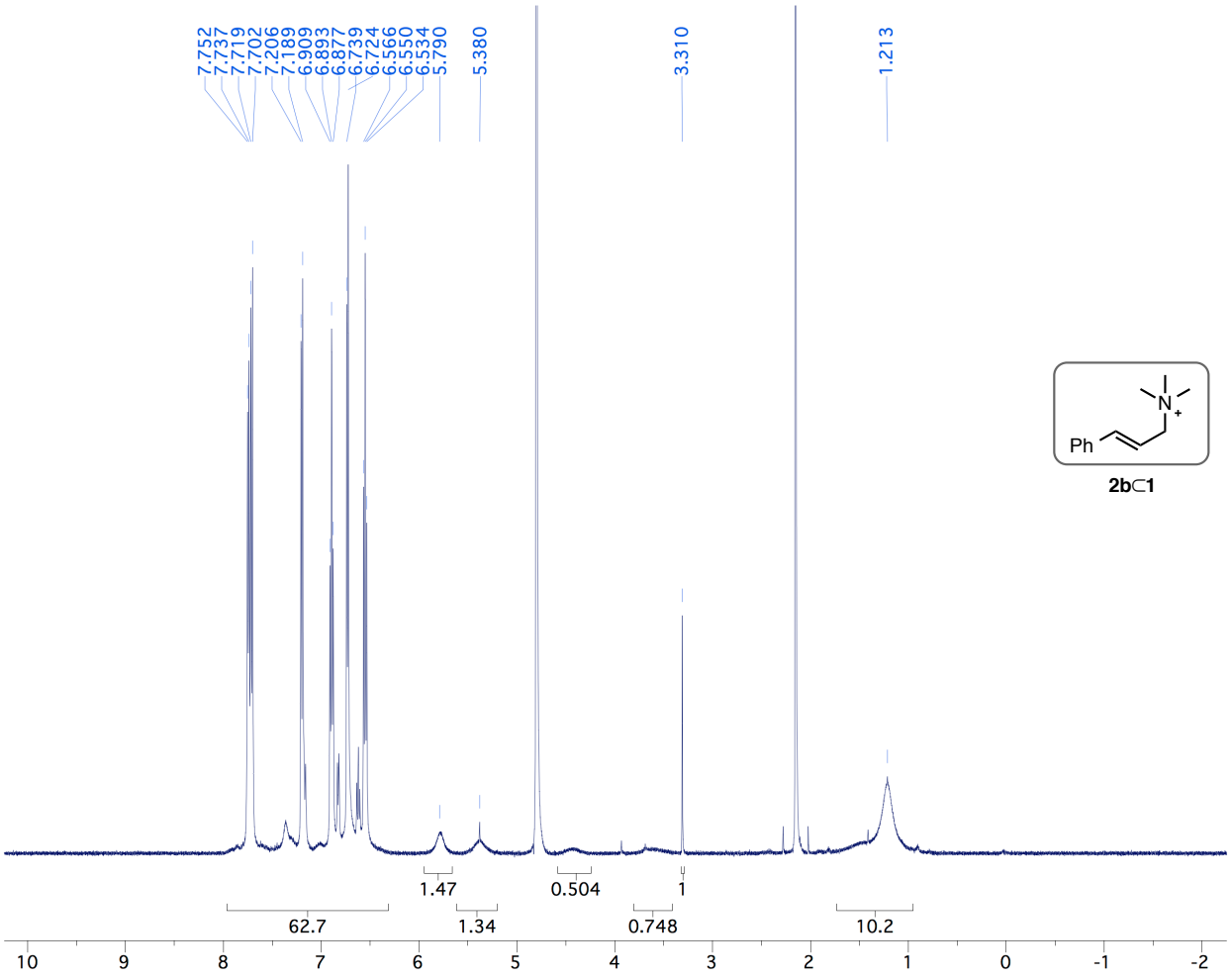

Figure S32. ^{1}H NMR of **2b** ⊂ **1** in D_2O 100 mM K_3PO_4 pD 8.0 (500 MHz).

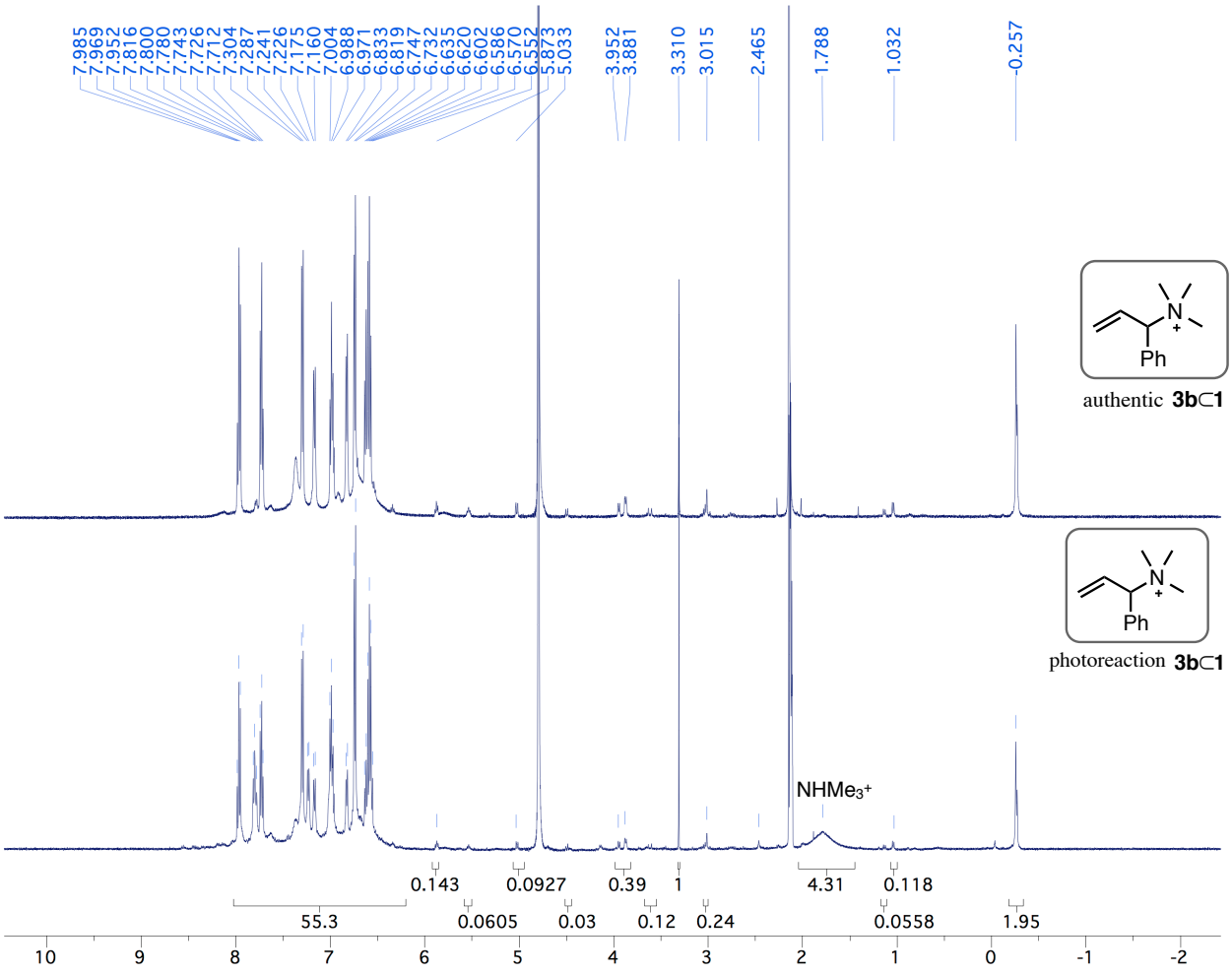

Figure S33. ^{1}H NMR of **3b** ⊂ **1** in D_2O 100 mM K_3PO_4 pD 8.0 after irradiation (below) 500 MHz. ^{1}H NMR of authentic **3b⊂1** above D_2O 100 mM K_3PO_4 pD 8.0 500 MHz (above).

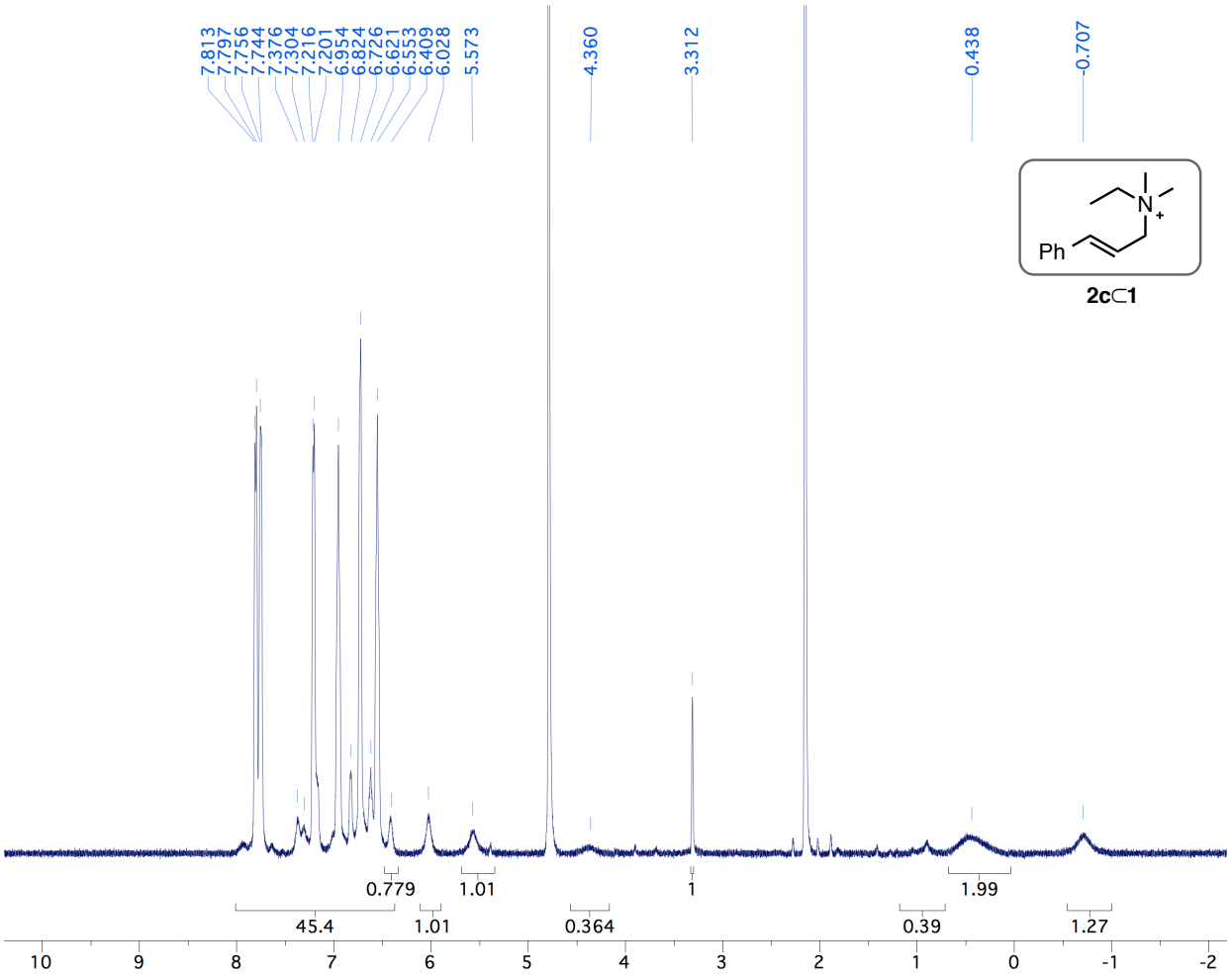

Figure S34. ^{1}H NMR of **2c** ⊂ **1** in D_2O 100 mM K_3PO_4 pD 8.0 (500 MHz).

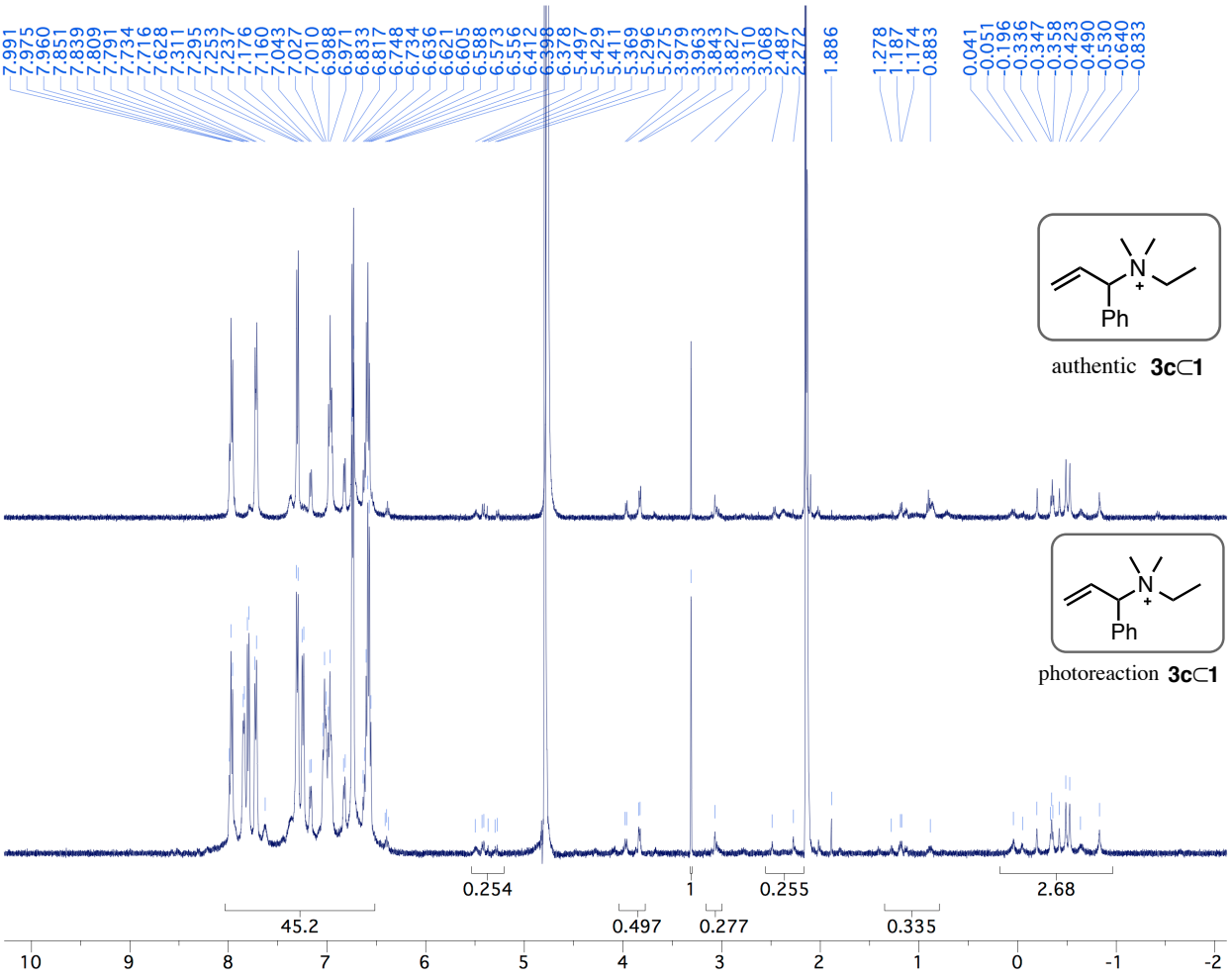

Figure S35. ^{1}H NMR of **3c** ⊂ **1** in D_2O 100 mM K_3PO_4 pD 8.0 after irradiation (below) 500 MHz. ^{1}H NMR of authentic **3c** ⊂ **1** above D_2O 100 mM K_3PO_4 pD 8.0 500 MHz (above).

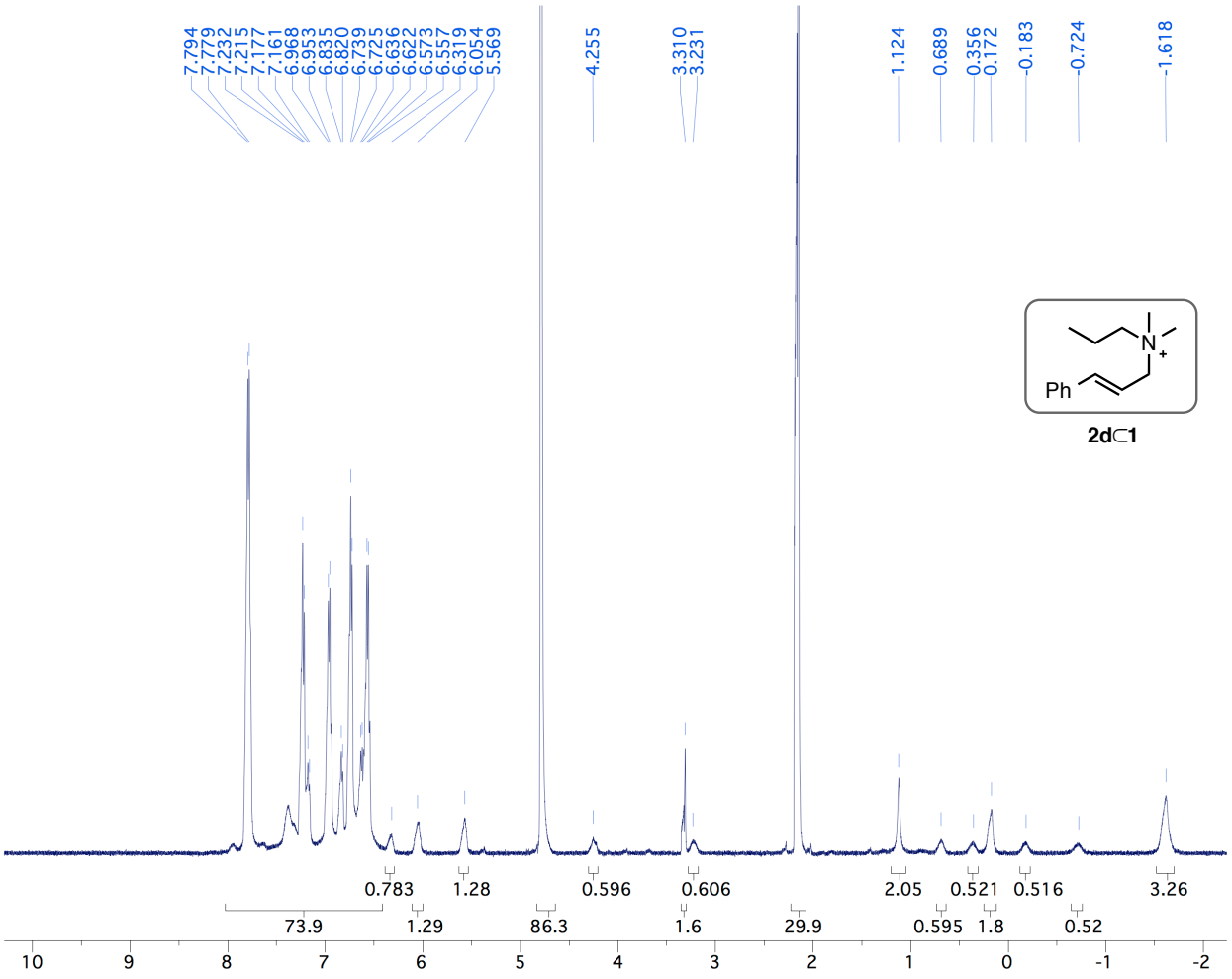

Figure S36. ^{1}H NMR of **2d** ⊂ **1** in D_2O 100 mM K_3PO_4 pD 8.0 (500 MHz)

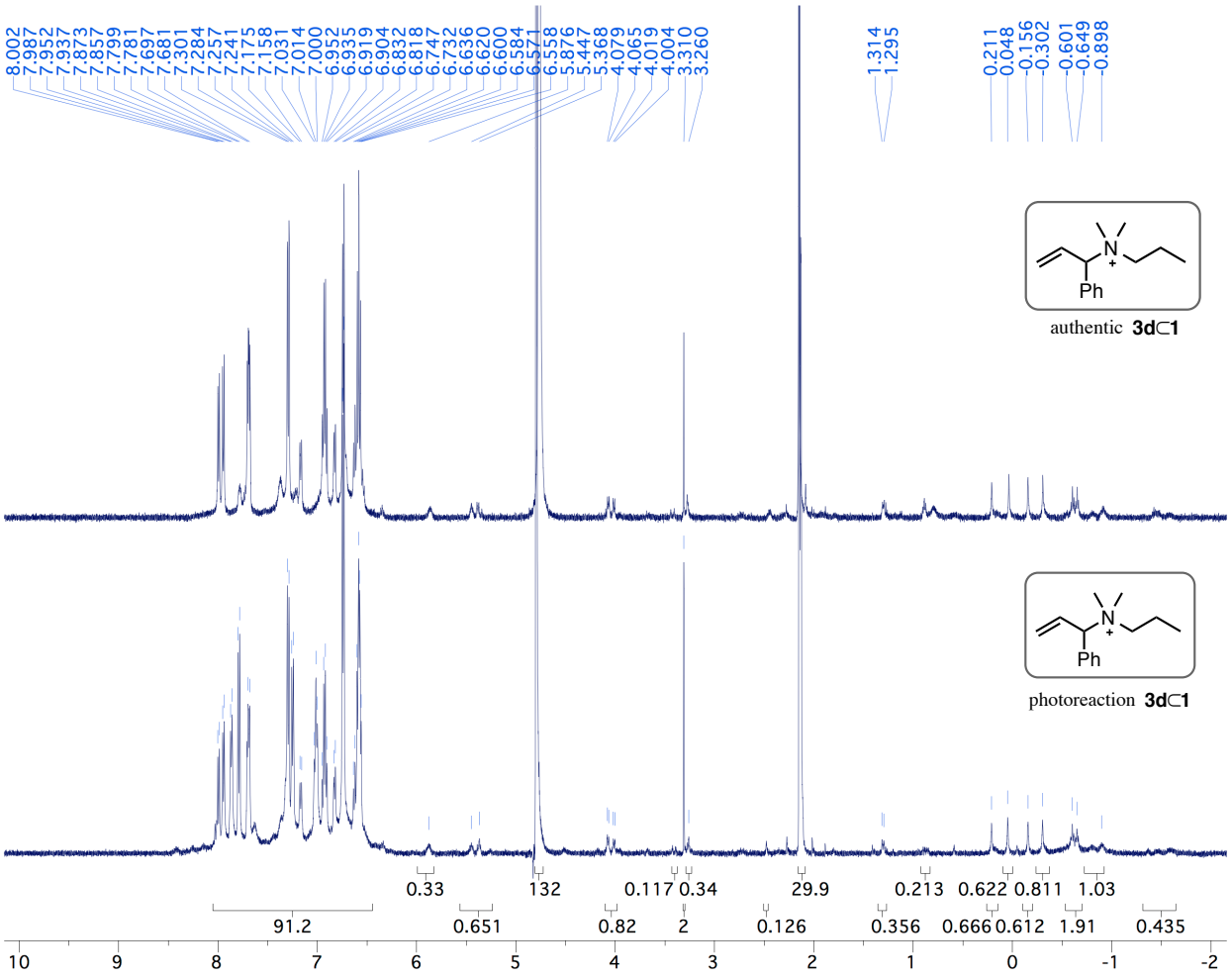

Figure S37. ^{1}H NMR of **3d** ⊂ **1** in D_2O 100 mM K_3PO_4 pD 8.0 after irradiation (below) 500 MHz. ^{1}H NMR of authentic **3d** ⊂ **1** above D_2O 100 mM K_3PO_4 pD 8.0 500 MHz (above).

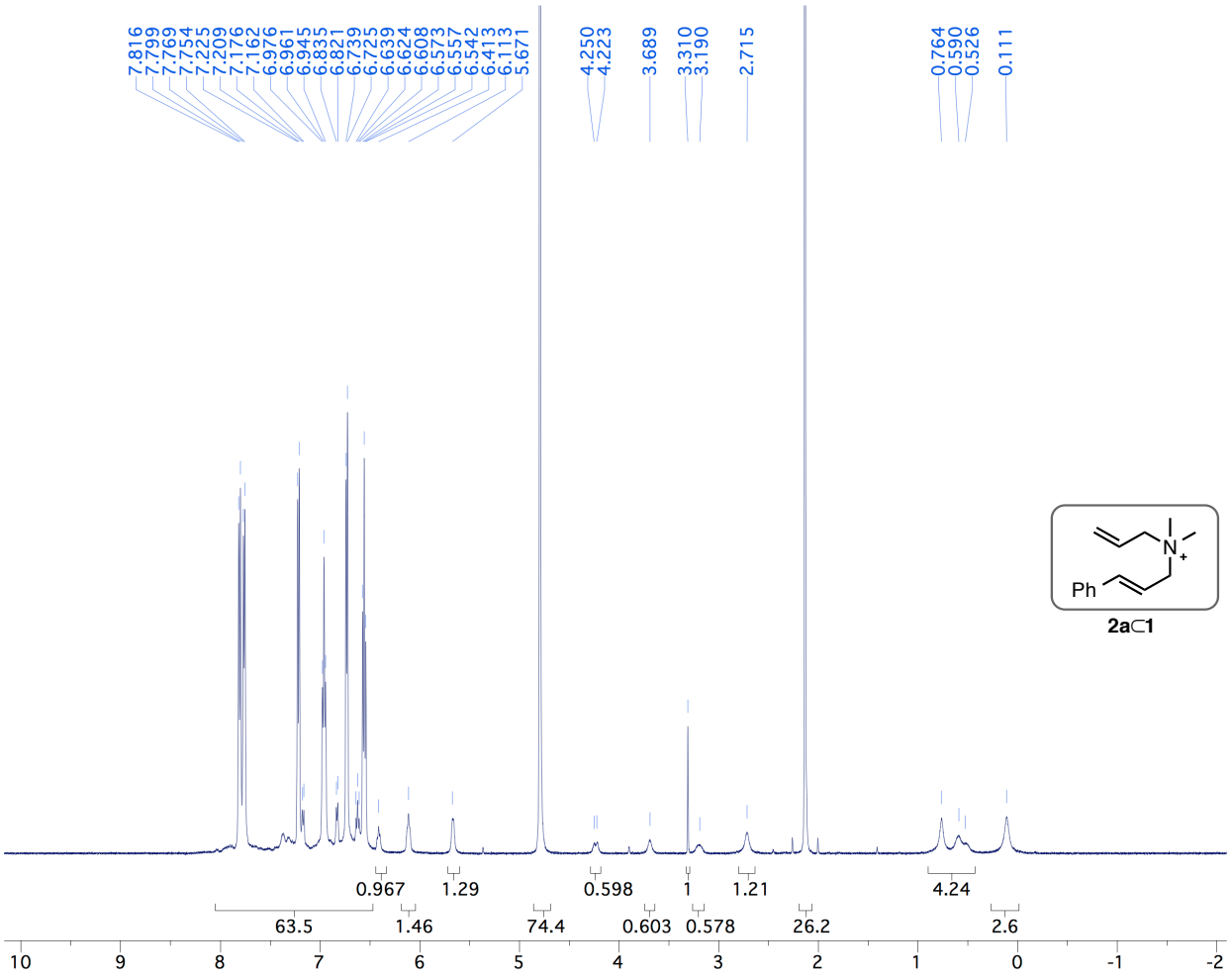

Figure S38. ^{1}H NMR of **2a** ⊂ **1** in D_2O 100 mM K_3PO_4 pD 8.0 (500 MHz)

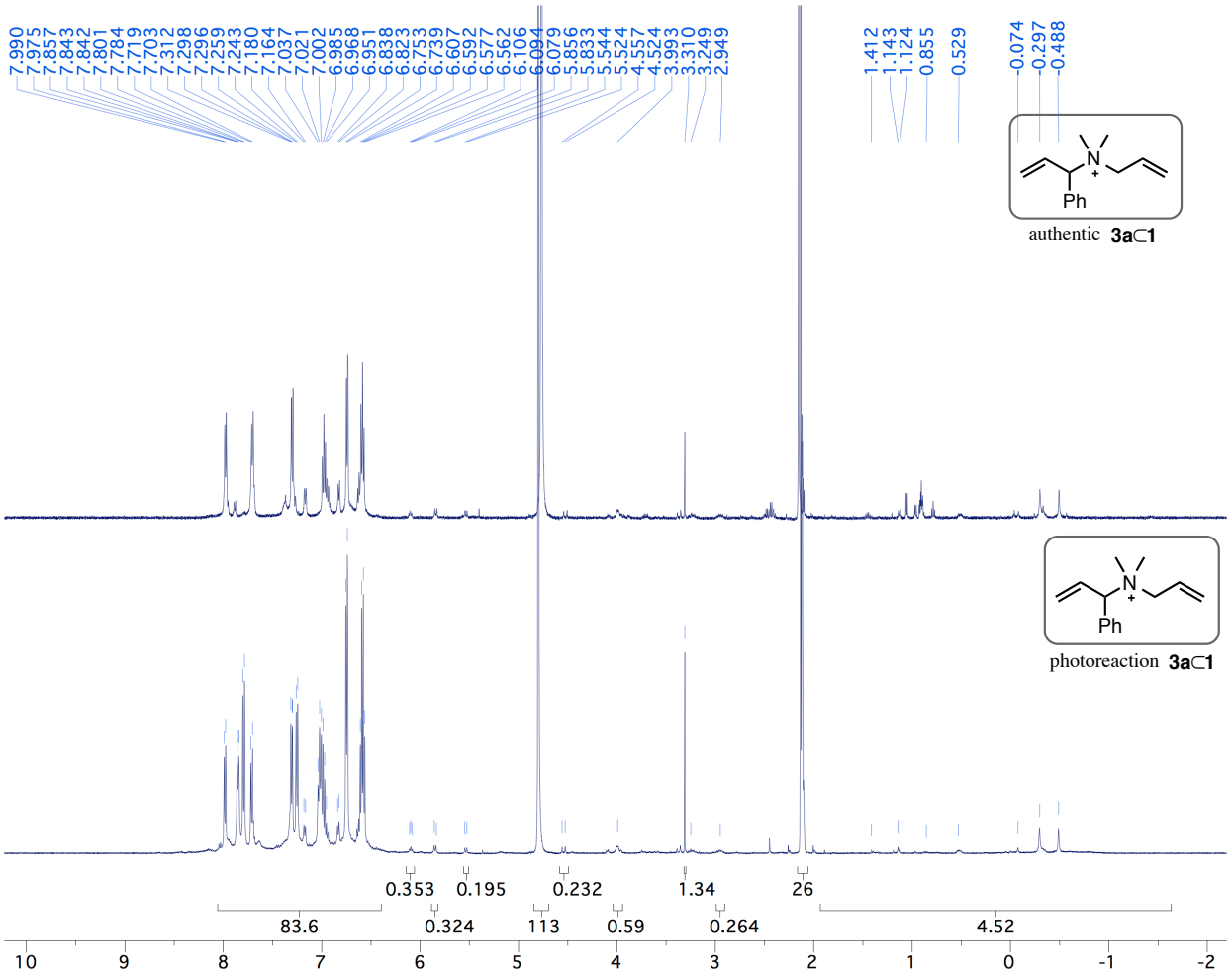

Figure S39. ^{1}H NMR of **3a** ⊂ **1** in D_2O 100 mM K_3PO_4 pD 8.0 after irradiation (below) 500 MHz. ^{1}H NMR of authentic **3a** ⊂ **1** above D_2O 100 mM K_3PO_4 pD 8.0 500 MHz (above).

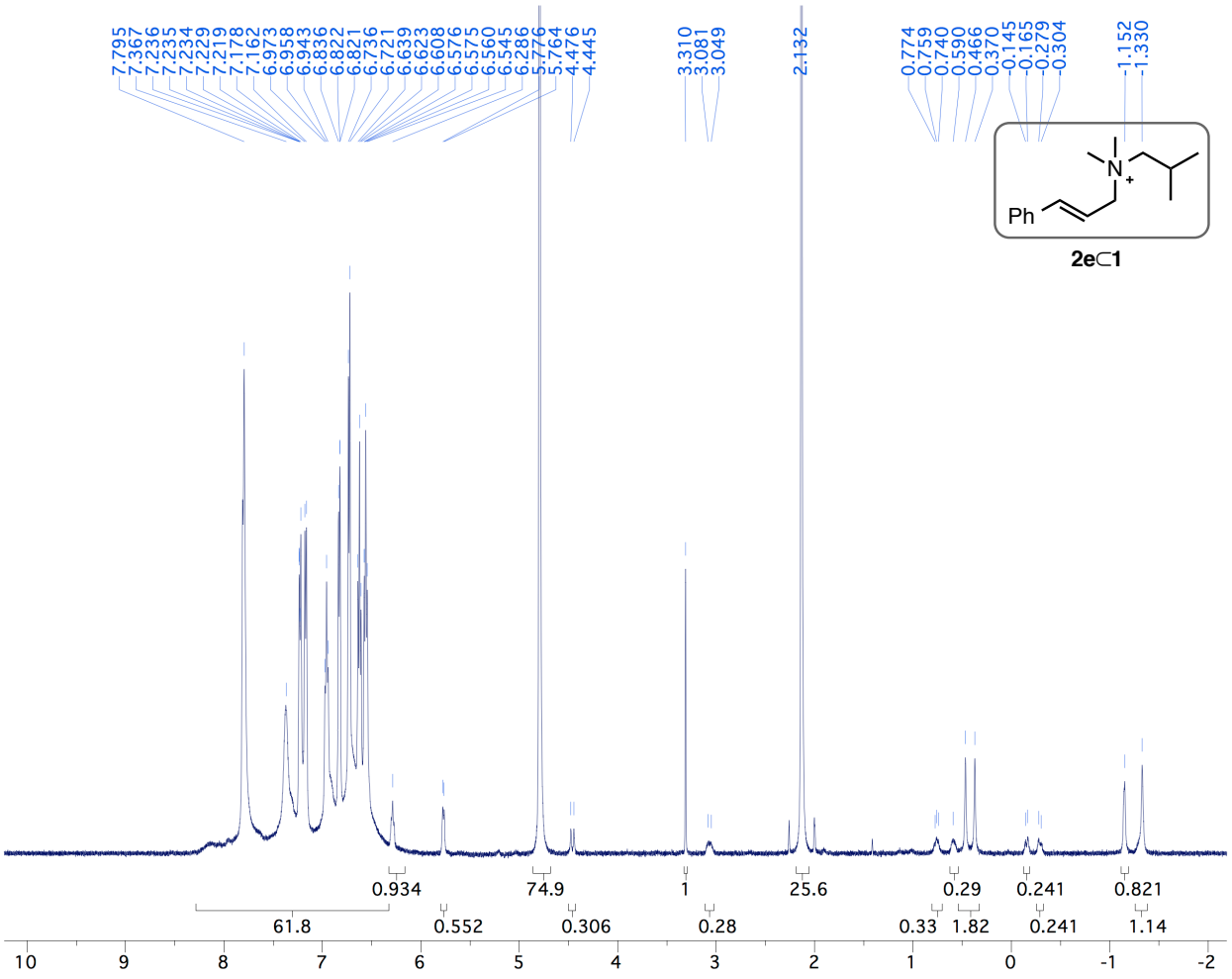

Figure S40. ^{1}H NMR of **2e** ⊂ **1** in D_2O 100 mM K_3PO_4 pD 8.0 (500 MHz).

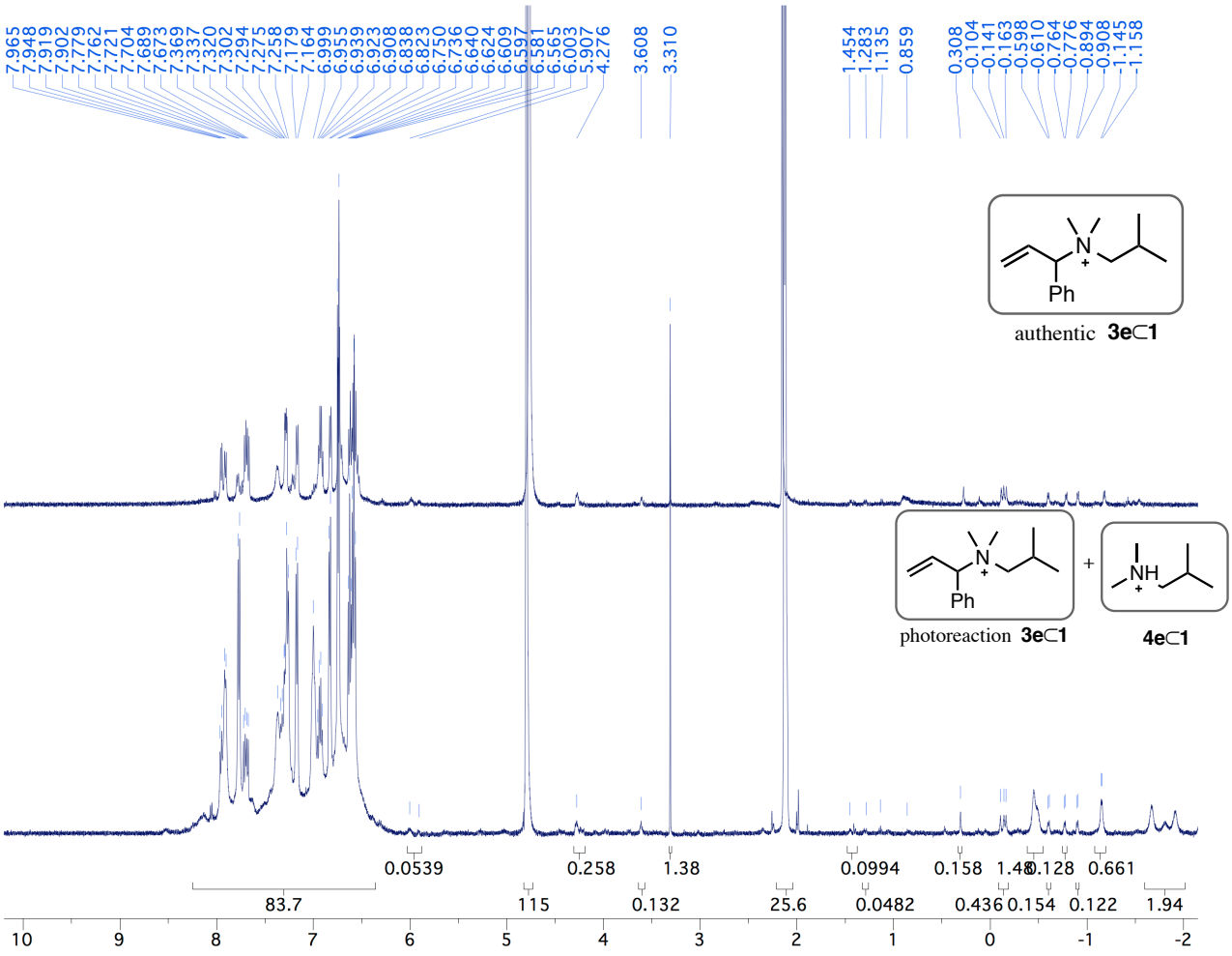

Figure S41. ^{1}H NMR of **3e** ⊂ **1** in D_2O 100 mM K_3PO_4 pD 8.0 after irradiation (below) 500 MHz. ^{1}H NMR of authentic **3e** ⊂ **1** above D_2O 100 mM K_3PO_4 pD 8.0 500 MHz (above).

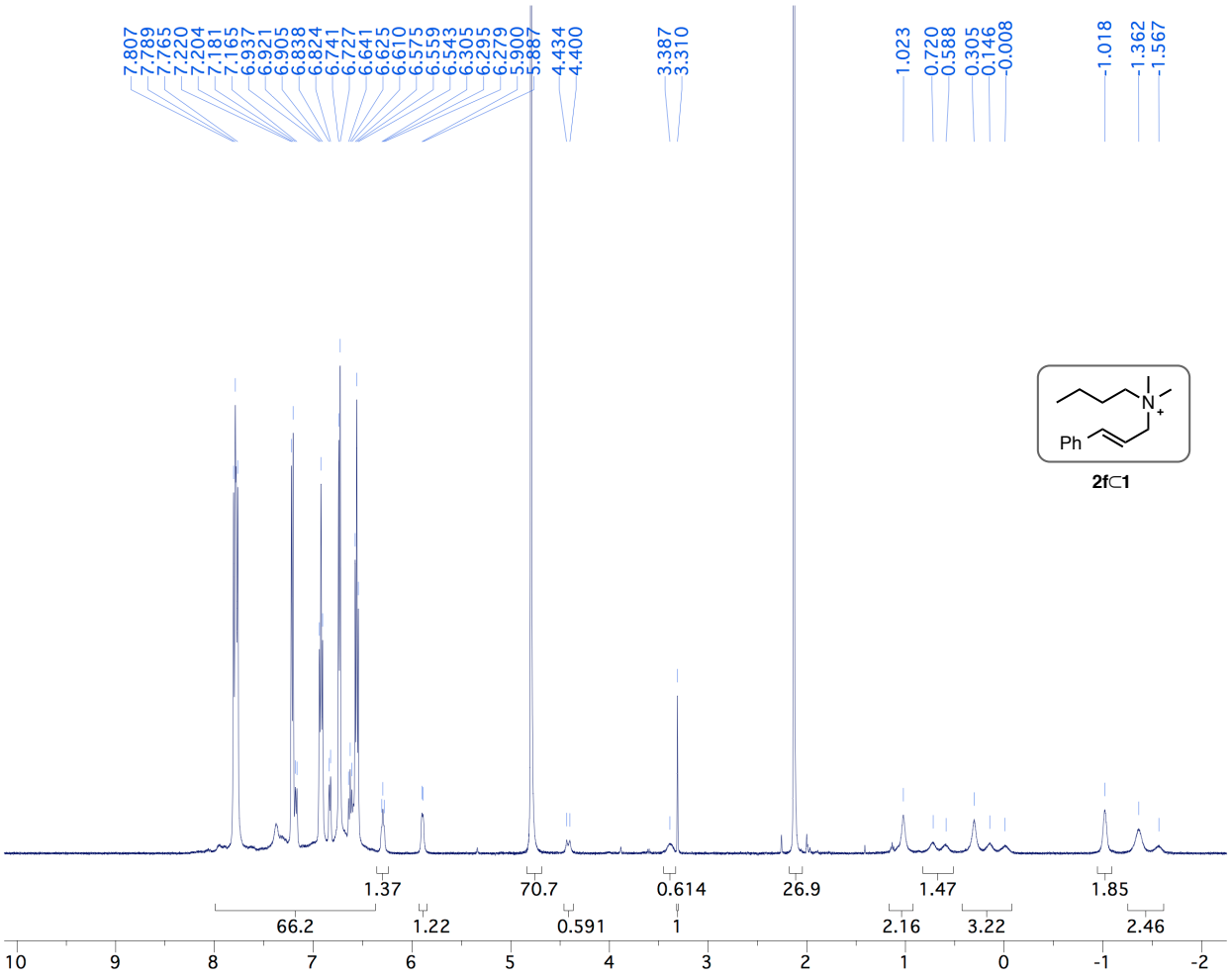

Figure S42. ^{1}H NMR of **2f** ⊂ **1** in D_2O 100 mM K_3PO_4 pD 8.0 (500 MHz).

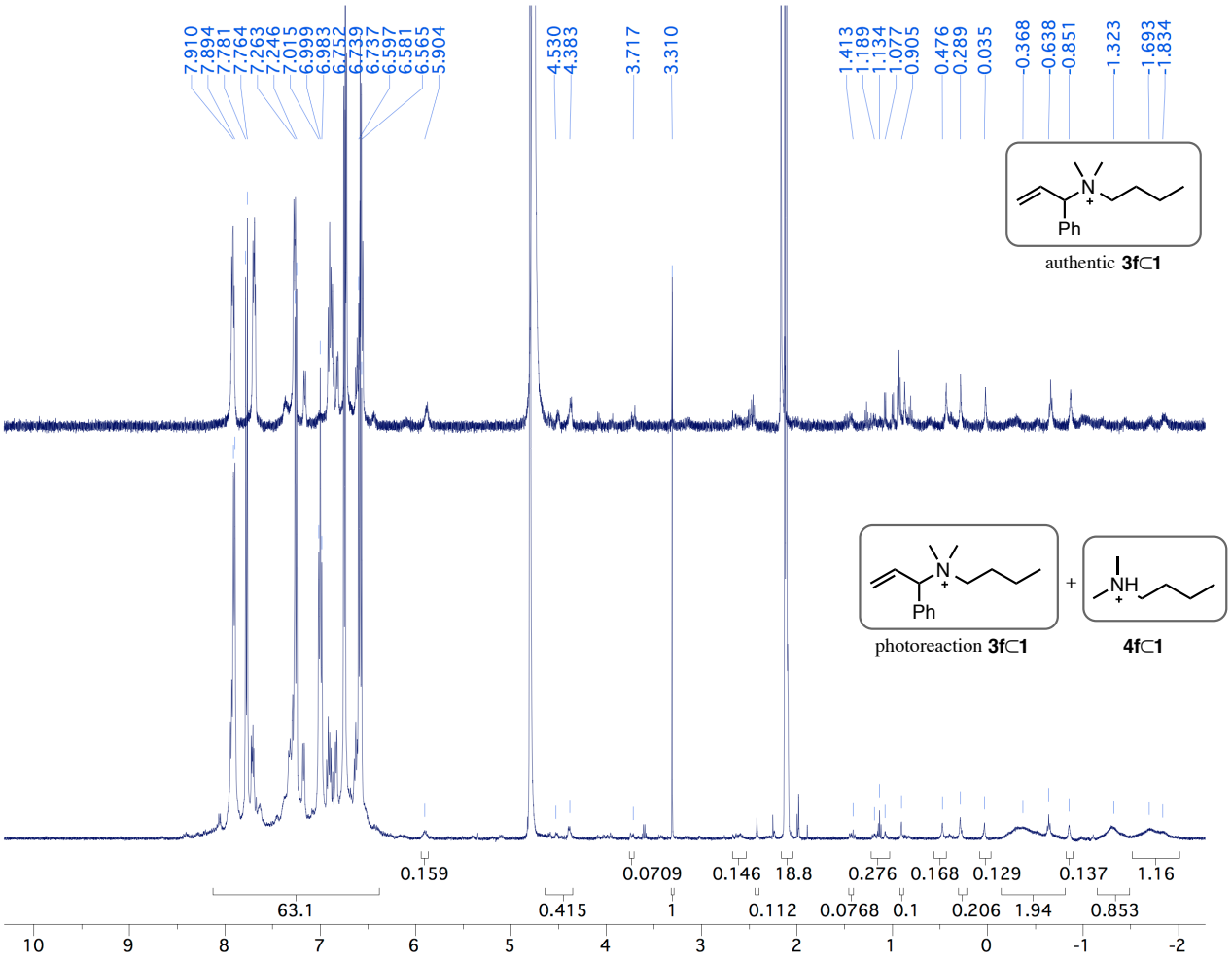

Figure S43. ^{1}H NMR of **3f** ⊂ **1** in D_2O 100 mM K_3PO_4 pD 8.0 after irradiation (below) 500 MHz. 1H NMR of authentic **3f** ⊂ **1** above D_2O 100 mM K_3PO_4 pD 8.0 500 MHz (above).

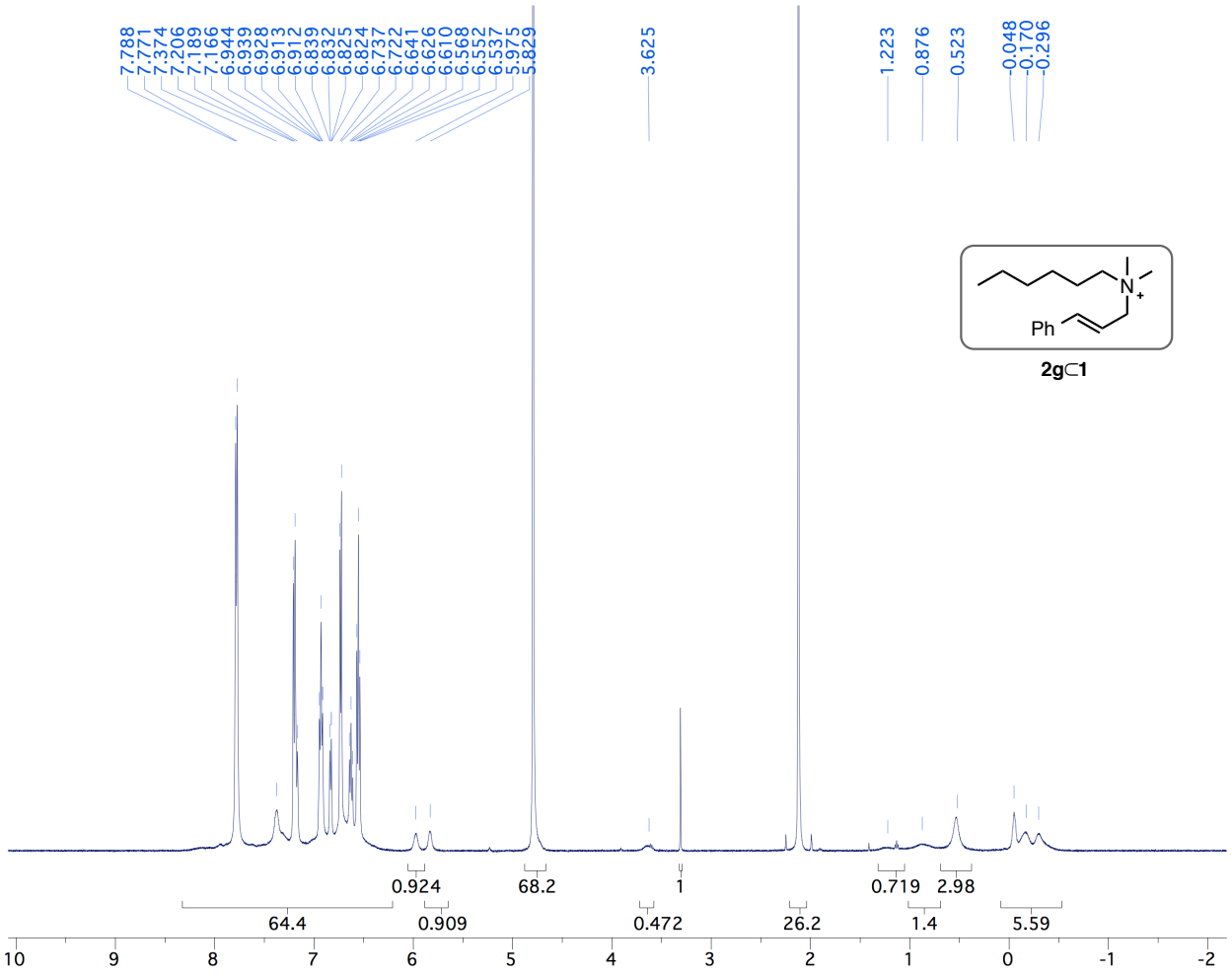

Figure S44. ^{1}H NMR of **2g** ⊂ **1** in D_2O 100 mM K_3PO_4 pD 8.0 (500 MHz).

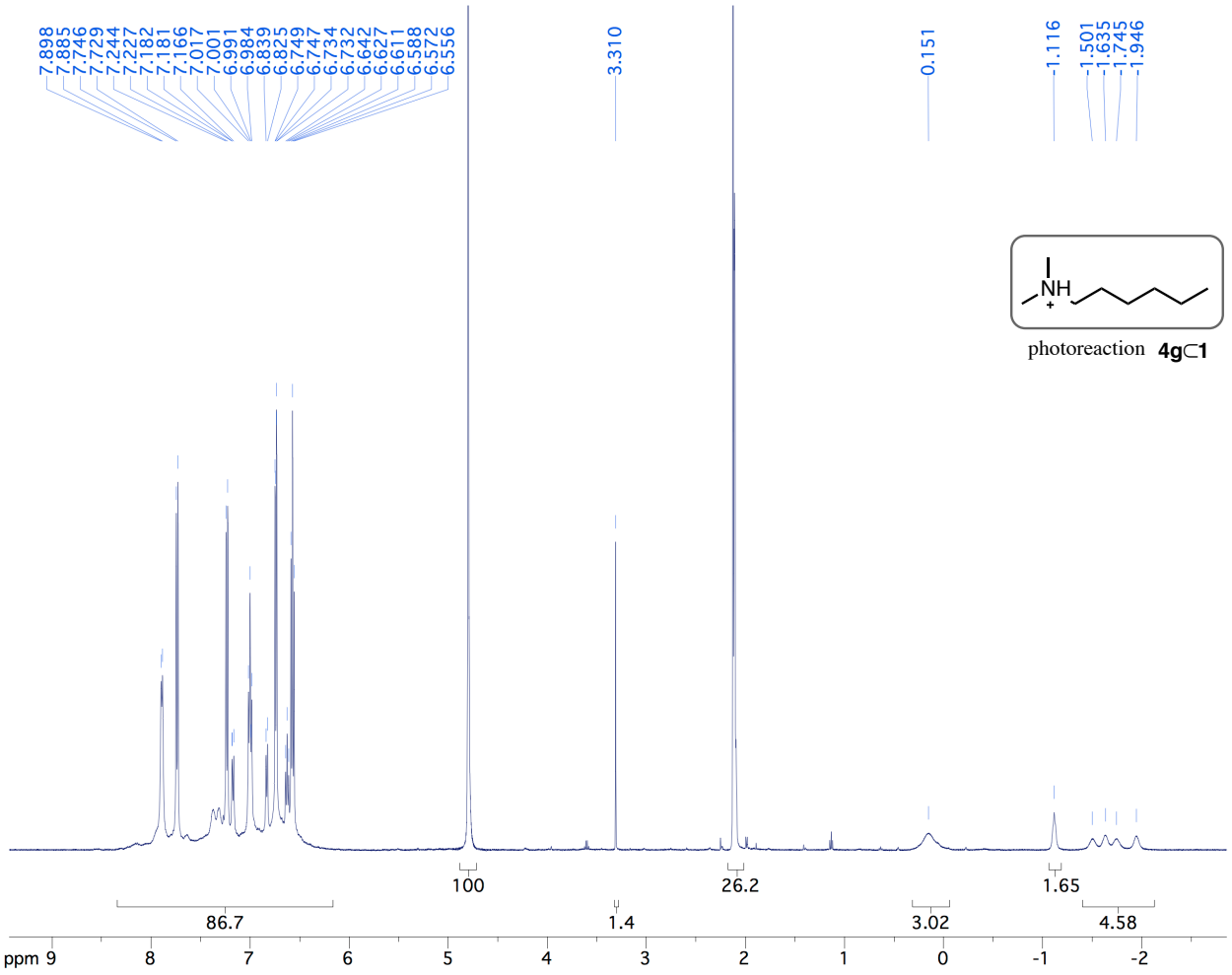

Figure S45. ^{1}H NMR of **3g** ⊂ **1** in D_2O 100 mM K_3PO_4 pD 8.0 after irradiation (below) 500 MHz. ^{1}H NMR of authentic **3g**⊂ **1** above D_2O 100 mM K_3PO_4 pD 8.0 500 MHz (above).

VIII. Control Reactions

In a N_2 atmosphere glovebox, *(E)-N,N,N*-trimethyl-3-phenylprop-2-en-1-aminium bromide (**2b**, 1 mg, 3.9 mmol) was dissolved in degassed D_2O (700 µL, pD 8.0, 100 mM K_3PO_4) and mixed until a homogeneous clear solution. Solution was then transferred to a pyrex reaction vessel (NMR tube or scintillation vial), capped and sealed with black electrical tape. Reaction vessel was irradiated with UVA light (6-8 bulbs, 130 V, 8 W) in a Rayonet photoreactor for 32h. Reaction progress was monitored by ^1H NMR. ^1H NMR does not indicate formation of the rearrangement product formation **3b**, but does show a minor amount of the cis isomer after prolonged irradiation times (green, Figure S46).

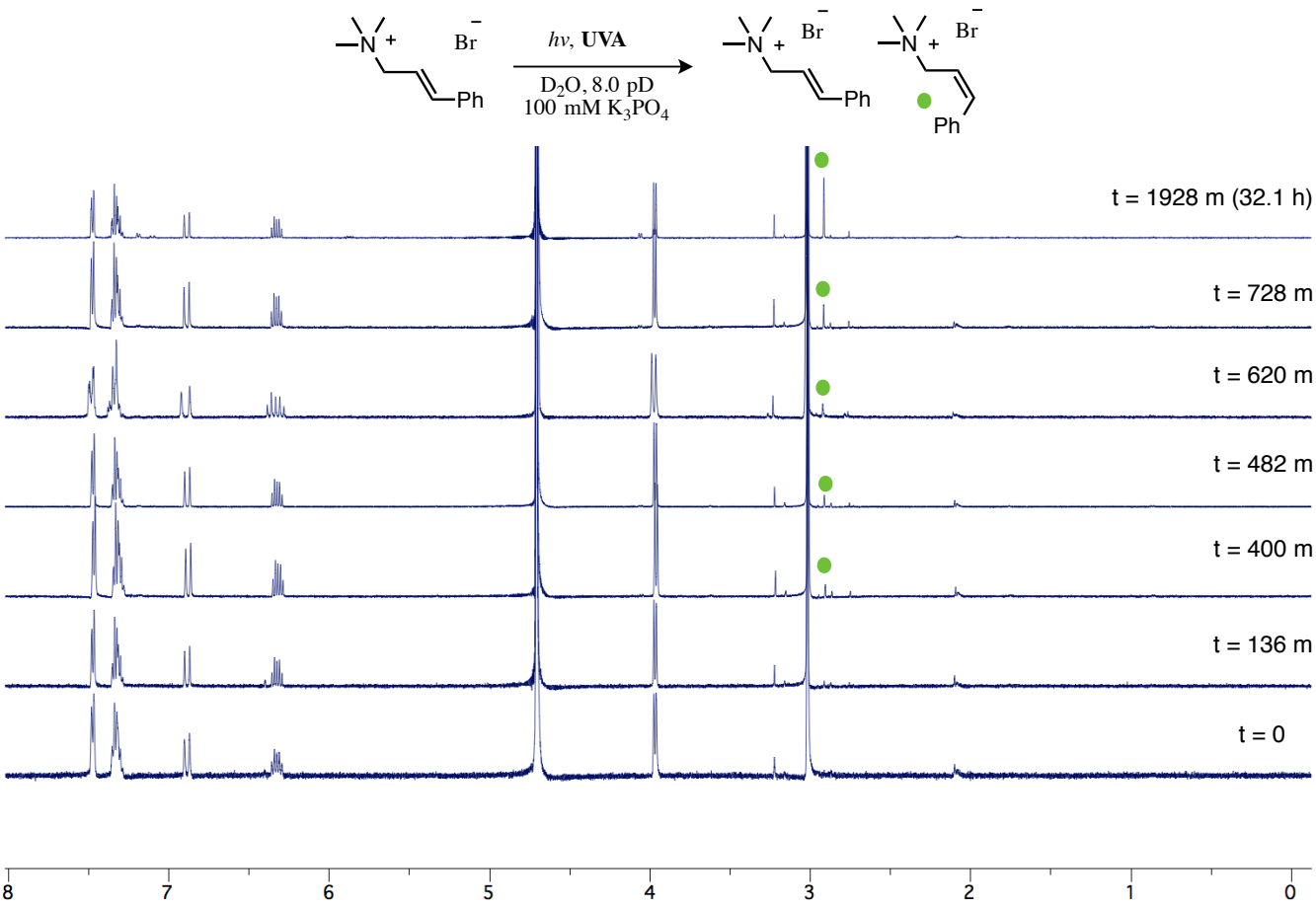

Figure S46. ^1H NMR spectra of **2b** in D_2O 100 mM K_3PO_4 pD 8.0 under UVA irradiation conditions over 32 h.

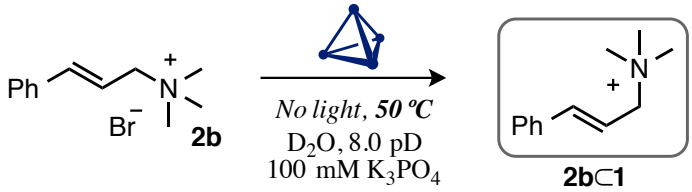

In a N_2 atmosphere glovebox, *(E)*-*N,N,N*-trimethyl-3-phenylprop-2-en-1-aminium bromide (**2b**, 1 mg, 3.9 mmol) and $K_{12}Ga_4L_6$ (**1**, 15 mg, 4.2 µmol) were dissolved in degassed D_2O (700 µL, pD 8.0, 100 mM K_3PO_4) and mixed until a homogeneous yellow solution. Solution was then transferred to a pyrex reaction vessel (NMR tube or scintillation vial), capped and sealed with black electrical tape. Reaction vessel was heated to 50 ºC for 16 h. Reaction progress was monitored by ^{1}H NMR. ^{1}H NMR spectra show no significant change to **2b** in that time.

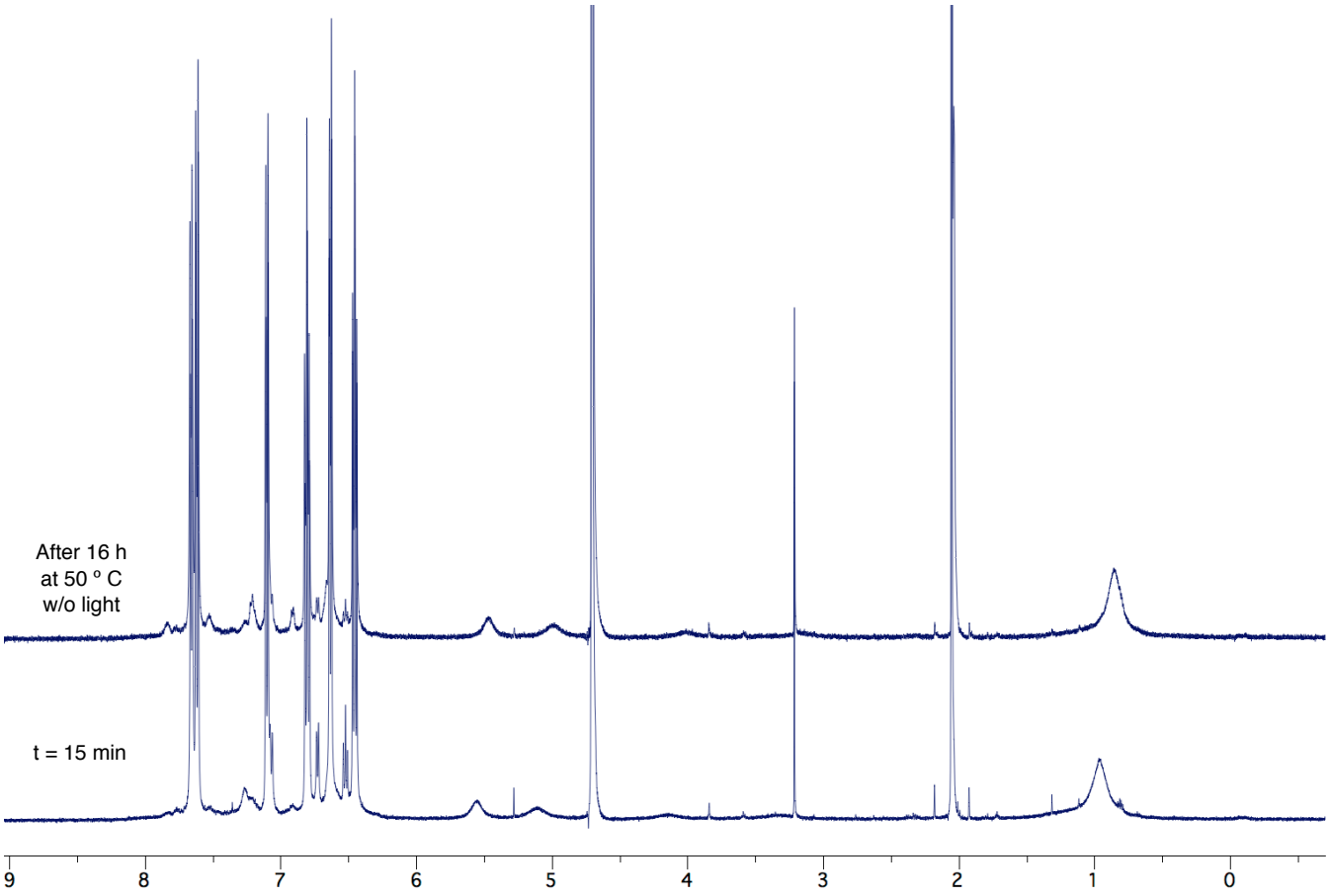

Figure S47. ^{1}H NMR of **2b⊂1** and **2b⊂1** after heating at 50 ºC for 16 h.

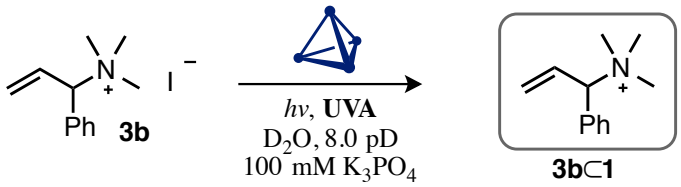

In a N_2 atmosphere glovebox, *N,N,N*-trimethyl-1-phenylprop-2-en-1-aminium iodide (**3b**, 1 mg, 3.9 mmol) and $K_{12}Ga_4L_6$ (**1**, 15 mg, 4.2 mmol) were dissolved in degassed D_2O (700 µL, pD 8.0, 100 mM K_3PO_4) and mixed until a homogeneous yellow solution and transferred to a pyrex reaction vessel (NMR tube or scintillation vial), capped and sealed with black electrical tape. Reaction vessel was irradiated with UVA light in a Rayonet photoreactor for 16 h. Reaction progress was monitored by ^{1}H NMR and does not show change to **3b** in that time nor formation of **4b**.

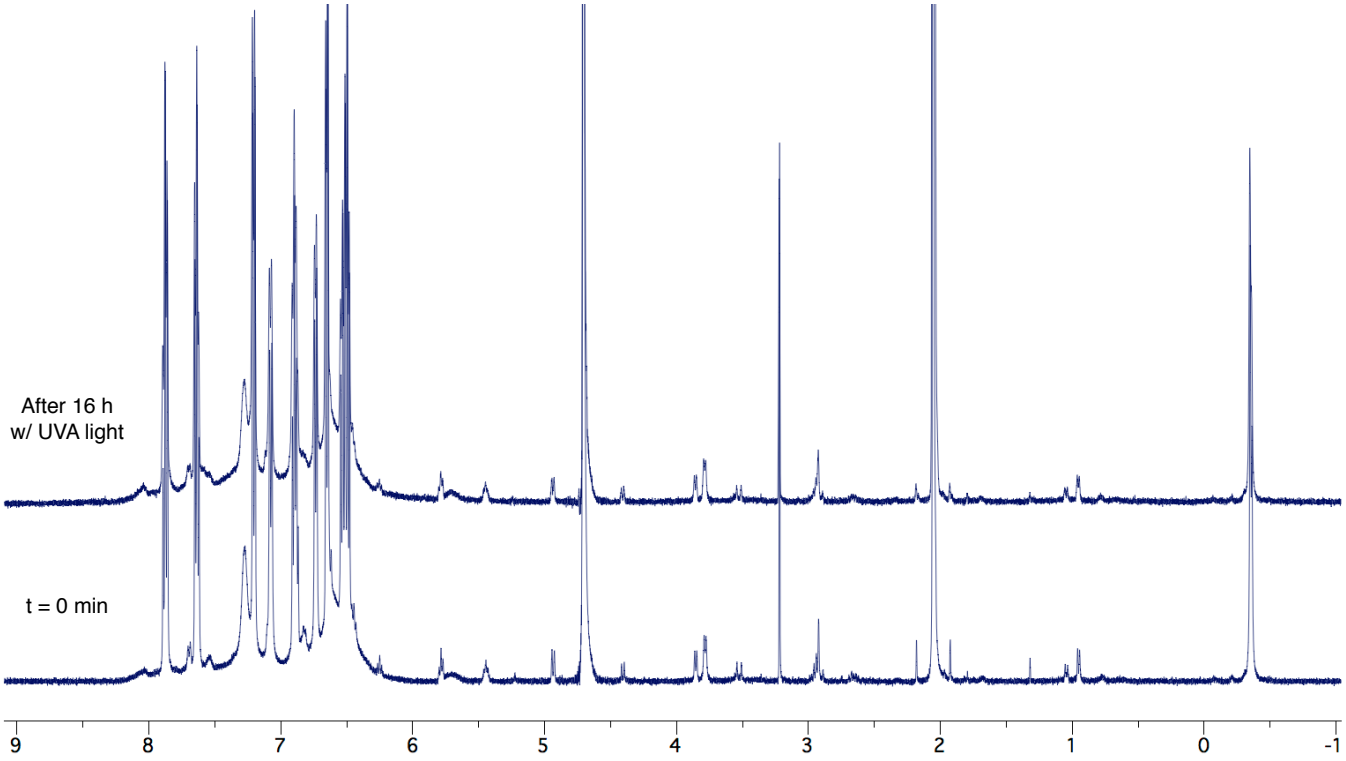

Figure S48. ^{1}H NMR of **3b⊂1** and **3b⊂1** after UVA irradiation for 16 h according to the general procedure.

Reaction of 2b with NEt4⊂1 in 100 mM K_3PO_4 pD 8.0 buffered D_2O

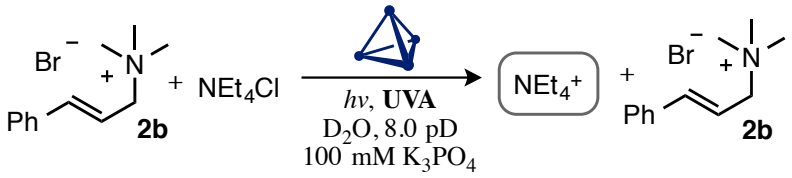

In a N_2 atmosphere glovebox, *(E)-N,N,N*-trimethyl-3-phenylprop-2-en-1-aminium bromide (**2b**, 1 mg, 3.9 mmol), $K_{12}Ga_4L_6$ (**1**, 15 mg, 4.2 mmol) and NEt_4Cl (4.2 mmol added as a solution in D_2O) were dissolved in degassed D_2O (700 µL, pD 8.0, 100 mM K_3PO_4) and mixed until a homogeneous yellow solution and transferred to a pyrex reaction vessel (NMR tube or scintillation vial), capped and sealed with black electrical tape. Reaction vessel was irradiated with UVA light in a Rayonet photoreactor for 16 h. Reaction progress was monitored by ^1H NMR and does not show change to **3b** in that time nor formation of **4b**.

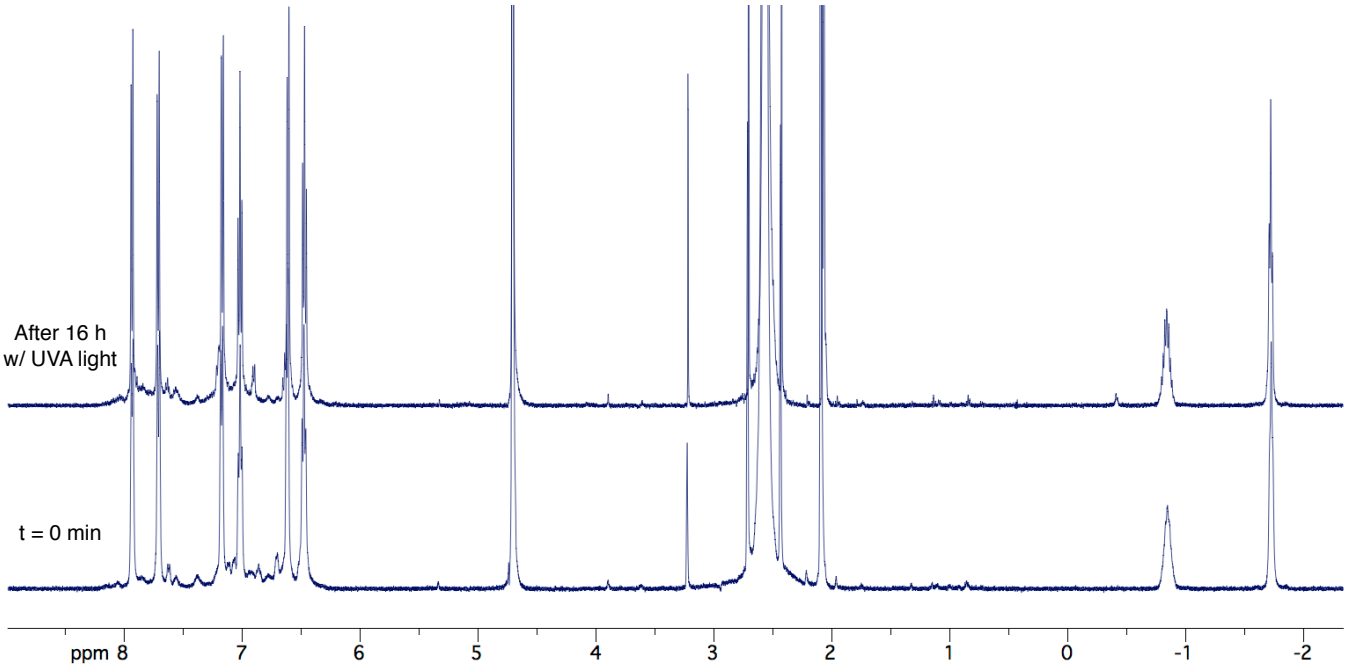

Figure S49. ^1H NMR spectra of a 100 µM K_3PO_4 D_2O solution of **2b**, **1** and NEt_4Cl before and after UVA irradiation for 16 h. The spectrum shows **NEt_4⊂1**.

IX. Quantum Yield Determination

Quantum yield experiments were conducted using a merry-go-round apparatus that has been described previously.[4] A 450 W Hanovia Hg lamp was used as the light source with borosilicate test tubes containing a 2 mM K_2CrO_4 in 1% K_2CO_3 aqueous solution as the filter. Reactions were monitored by ^1H NMR. All quantum yield experiments were conducted in triplicate and 95% confidence reported. The Norrish type II cleavage was conducted as previously described using C_6D_6 as solvent.[5]

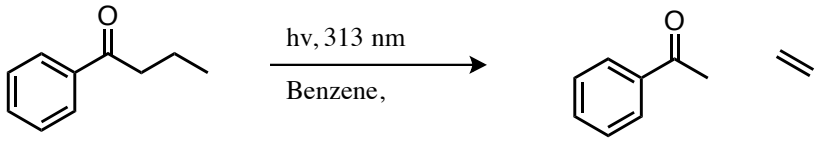

In an N_2 atmosphere glovebox, to a borosilicate NMR tube was added butyrophenone (0.0081 mmol) in degassed benzene-D_6 (0.9 ml, 0.009 M). The tube was capped and sealed with black electrical tape. NMR tubes were immersed in borosilicate test tubes with the previously mentioned chromate solution and irradiated for 14h. Reaction progressed was monitored by NMR.

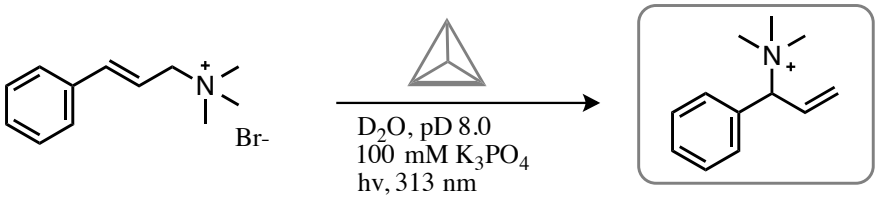

In a N_2 atmosphere glovebox, *(E)-N,N,N*-trimethyl-3-phenylprop-2-en-1-aminium bromide (**2b**, 2 mg, 0.0078 mmol) and $K_{12}Ga_4L_6$ (**1**, 15 mg, 4.2 mmol) were dissolved in degassed D_2O (700 μL, pD 8.0, 100 mM K_3PO_4) and mixed until a homogeneous yellow solution formed. Solution was then transferred to a NMR tube, capped and sealed with black electrical tape. NMR tubes were immersed in borosilicate test tubes with the previously mentioned chromate solution and irradiated for 14h. Reaction progressed was monitored by NMR.

X. Calculations

Using Gaussian 09 software package, geometry optimizations were performed using DFT-B3LYP methods and basis set 6-311 +G(d,p). Single point energy minima were determined in the gas phase using calculation method

[4] Winston, M. S.; Wolf, W. J.; Toste, F. D. *J. Am. Chem. Soc.* **2014**, *136*, 7777–7782.

[5] Wagner, P. J.; Kemppainen, A. E. *J. Am. Chem. Soc.* **1972**, *94*, 21, 7495.

RwB97XD and basis set 6-311+G(d,p) for a single positive charge and singlet spin state. Relative energy differences were determined for **2b** and **3b**.

XI. Electrochemical Methods

All electrochemical experiments were performed using a CH Instruments 660D potentiostat (Austin, TX) in a standard one-compartment, three-electrode electrochemical cell. Freshly polished glassy carbon (3 mm diameter, BASi; West Lafayette, IN) was used as the cathode in all experiments. Pt wire (electrochemical grade, purchased from Sigma Aldrich) was used as the anode in all experiments. Aqueous experiments were performed using a saturated Ag/AgCl reference purchased from BASi. Non-aqueous experiments were performed using Ag^0 wire as a quasi-reference, followed by addition of ferrocene as an internal standard at the conclusion of the experiment. Electrolytes were degassed by bubbling with Ar for 10 min. No iR compensation was applied.

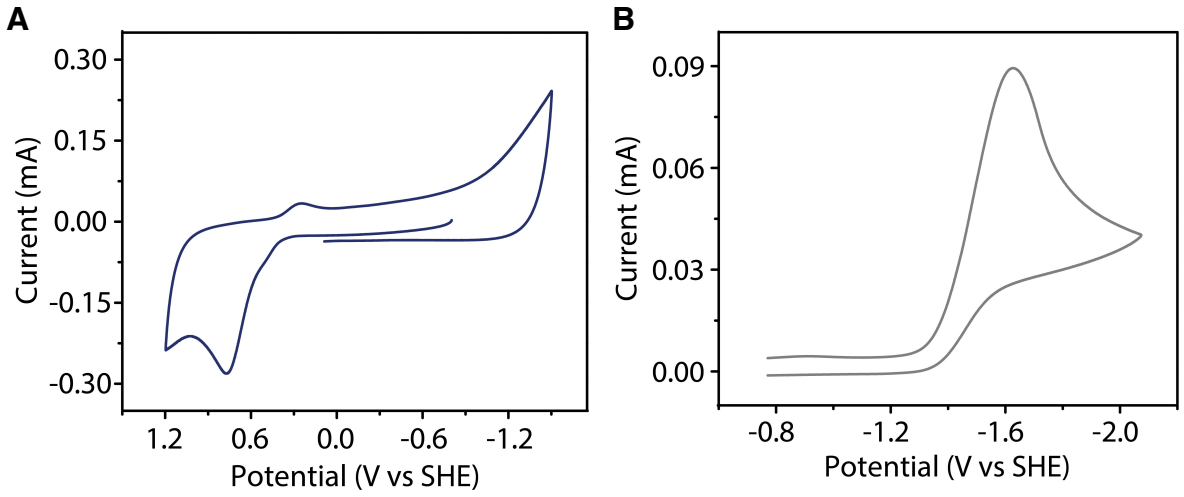

Figure S50. A) Cyclic voltammograms of $K_{12}Ga_4L_6$ (1mM) in H_2O with 100 mM K_3PO_4, pH 8.0, variable scan rates, sat. Ag/AgCl reference. B) Cyclic voltammogram of **2b** in DMF, 100 mM nBuN$_4$PF$_6$, Ferrocene reference, 100 mV/sec scan rate.

XII. Transient Absorption Spectroscopy

Materials and Methods.

Solutions of $K_{12}Ga_4L_6$ and $K_{12}Ga_4L_6$ with trimethylcinnamyl ammonium **2b** (**2b**⊂**1**) in water were filtered through a 40 μm Teflon filter to remove undissolved material. They were then diluted to an optical density of 0.6 at 400 nm and sealed inside a 2-mm path length cuvette with a

Teflon stopper while under nitrogen gas to prevent oxidation during optical measurements. Additionally a Teflon covered 2-mm iron stir bar was placed in the cuvette. During the 4-hour acquisitions, the samples were simultaneously stirred magnetically and translated perpendicular to the beam path to replenish the irradiated volume mitigating photoalteration effects.

The transient absorption data were acquired on a femtosecond stimulated Raman instrument with the Raman pump pulse blocked. This setup has been described previously[9,10]. Briefly, the fundamental from a femtosecond Ti:Sapphire oscillator amplifier is split into two beams. The actinic pump pulse (400 nm, 460 nJ, 165 fs FWHM) was generated through SHG in a 0.4 mm thick Type 1 BBO crystal. The bandwidth of the actinic pump pulse did not warrant further compression. The probe pulse (7 nJ, 50 fs FWHM) was generated through super-continuum generation in a 3-mm thick sapphire window and then compressed with a BK7 prism compressor. The temporal cross-correlation between the actinic pump and the probe pulses was measured to be Gaussian with a width of 172 fs using the optical Kerr effect in water (Figure S51). The two pulses were polarized parallel to one another and overlapped spatially and temporally in the sample. The transmitted probe was focused through the slit of a single spectrograph (Spex 500, 600 gr/mm, 500 nm blaze) and the dispersed second-order diffraction was read out at 1 kHz on a front-illuminated CCD (Princeton Instruments, Pixis 100F). The actinic pump was chopped at 250 kHz generating a transient absorption signal in the direction of the probe calculated as $-\log\left(\frac{Transmittance\ Probe,\ \ Actinic\ Pump\ On}{Transmittance\ Probe,\ \ Actinic\ Pump\ Off}\right)$.

[9] Shim, S.; Mathies, R. A. Development of a Tunable Femtosecond Stimulated Raman Apparatus and Its Application to B-Carotene. *J. Phys. Chem. B* **2008**, *112*, 4826–4832

[10] Creelman, M.; Kumauchi, M.; Hoff, W. D.; Mathies, R. A. Chromophore Dynamics in the PYP Photocycle from Femtosecond Stimulated Raman Spectroscopy. *J. Phys. Chem. B* **2014**, *118*, 659–667

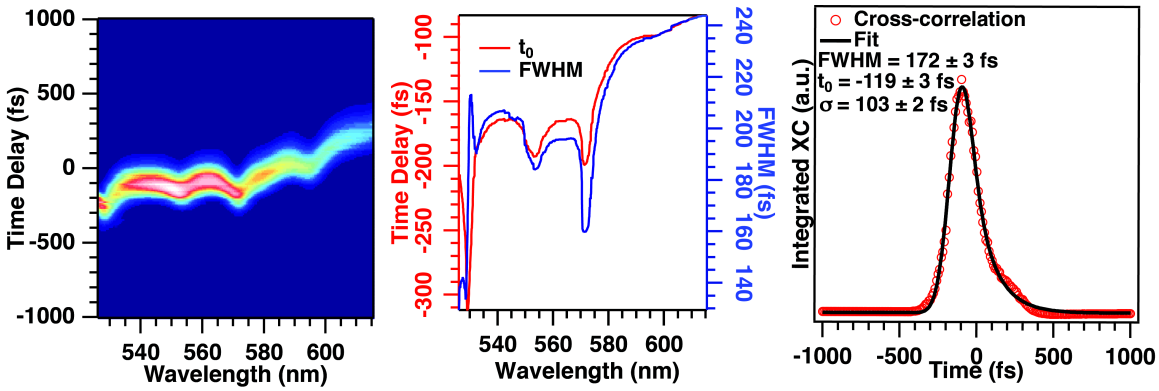

Figures S51. (Left) Frequency resolved cross-correlation of the probe. The probe signal was gated by the Kerr rotation of the probe interacting with the actinic pump in the aqueous sample. (Middle) Pixel-by-pixel fit parameters to the cross-correlation signal. (Right) Integrated cross-correlation signal over all pixels and Kerr fitting.

Data Analysis.

Transient absorption spectra of cage **1** in H_2O were collected pulsed excitation with 400 nm light source. The contour plots for the integrated transient absorption data of **1** and **1⊂2b** are shown in Figure S52 plotted as change in optical density (OD) versus wavelength over time. Absorption data were collected in 10 nm intervals (150 CCD pixels) and integrated numerically from 530-610 nm. This resulted in eight kinetic decay traces (Figure S52). The decay traces are also plotted individually as absorbance versus time. A global least-squares fitting was performed on all decay traces simultaneously. The fitting function was a triple exponential decay convolved numerically with a Gaussian instrument response function of width σ_{IRF} and center t_0.

$$S(t) = \left\{H(t-t_0)\left(A_0 Exp\left[-\frac{(t-t_0)}{\tau_1}\right] + A_1 Exp\left[-\frac{(t-t_0)}{\tau_2}\right] + A_2 Exp\left[-\frac{(t-t_0)}{\tau_3}\right]\right)\right\}$$

$$* \frac{1}{\sigma_{IRF}\sqrt{\pi}} Exp\left[-\frac{(t-t_0)^2}{2{\sigma_{IRF}}^2}\right]$$

$H(t\text{-}t_0)$ is a Heaviside step function. Parameters A_n are the initial amplitudes and τ_n are the time constants of the decays. The parameters t_0 and σ_{IRF} were held fixed to the values measured using the cross

correlation. Three time constants, τ_n, were globally fit to all wavelength intervals while the amplitudes, A_n, were fit independently at each wavelength because the signal was assumed to arise from a single excited state population involving dynamically correlated but spectrally unknown features.

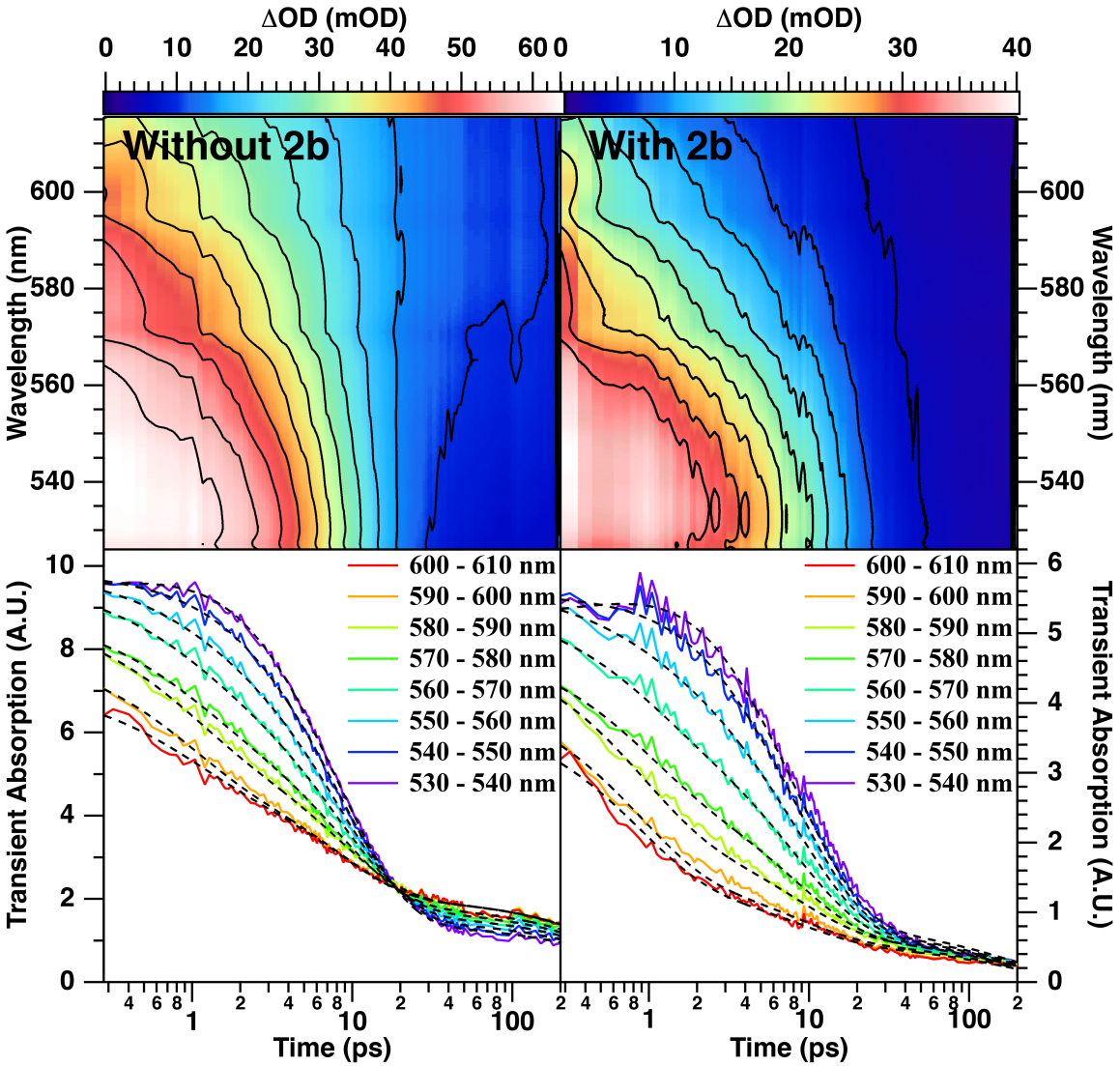

Figure S52. Comparison of transient absorption signal of $K_{12}Ga_4L_6$ with encapsulation of cinnamylammonium substrate **2b** (right) and without any substrate (left) over the first 200 ps after 400 nm actinic excitation. (bottom) Band integral over each 10-nm range in the TA and the global exponential fits.

The kinetics decays of the excited state absorption of **1⊂2b** were fit by holding the first two time constants (τ_1 & τ_2) fixed to values determined from solvent filled "empty" **1**. The assumption was that encapsulation of the substrate **2b** has a negligible impact on the early time dynamic processes but has a

substantial impact on weak coupling processes observed at later times. This assumption seems justified as a high quality fit was found using a minimum number of adjustable parameters (Figure S52).

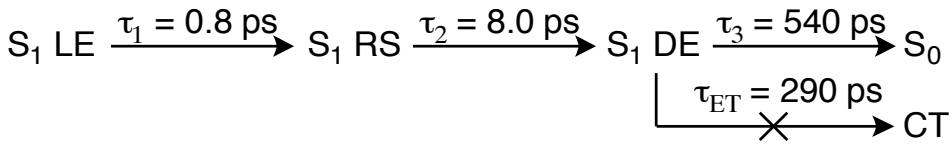

Scheme S1. Kinetic model for relaxation of $Ga_4L_6^{12-}$ after photoexcitation. S_1 LE is the first locally excited singlet state. RS indicates a relaxed solvent state. DE stands for a delocalized excitation state, S_0 is the ground electronic state. CT is a charge transfer state, which is only accessible when a cinnamylammonium substrate is encapsulated.

The rate of electron transfer from **1** to encapsulated **2b** was estimated by assuming a kinetic model with two competing pathways: electron transfer to a charge transfer state and internal conversion to the ground state (Scheme S1). The observed excited state decay rate with **2b** (k_{obs}) is the sum of the two decay rates (k_3 & k_{ET}). From the rates, the electron transfer quantum yield (Φ_{ET}) can be calculated.

$$k_{ET} = k_{obs} - k_3$$

$$\tau_{ET} = \frac{\tau_{obs}\tau_2}{\tau_3 - \tau_{obs}}$$

$$\phi_{ET} = \frac{k_{ET}}{k_{obs}} = \frac{\tau_{obs}}{\tau_{ET}}$$

The 95% confidence intervals for the parameters reported were calculated using the Igor Pro least squares fitting software package as described in Numerical Recipes in C.[11] To better determine the uncertainty of the final long time constant, τ_3, once it had been decoupled from the other fit parameters, the first two time constants were held fixed and the global-fitting error analysis was performed again. This resulted in a decrease in the confidence interval, $\delta\tau_3$, by an order of magnitude. The error was then propagated in the following manner.

[11] Press, W. H.; Teukolsky, S. A.; Vetterling, W. T. Numerical Recipes in C: The Art of Scientific Computing, 2; Cambridge University PressL Cambridge CB2 1TN, 2002; pp. 660-668.

$$\delta\tau_{ET} = \sqrt{\left(\frac{\partial\tau_{ET}}{\partial\tau_3}\right)^2(\delta\tau_3)^2 + \left(\frac{\partial\tau_{ET}}{\partial\tau_{obs}}\right)^2(\delta\tau_{obs})^2}$$

$$= \sqrt{\left(\frac{\tau_{obs}}{\tau_3 - \tau_{obs}} - \frac{\tau_{obs}\tau_3}{(\tau_3 - \tau_{obs})^2}\right)^2(\delta\tau_3)^2 + \left(\frac{\tau_3}{\tau_3 - \tau_{obs}} + \frac{\tau_{obs}\tau_3}{(\tau_3 - \tau_{obs})^2}\right)^2(\delta\tau_{obs})^2}$$

$$\delta\phi_{ET} = \sqrt{\left(\frac{\partial\phi_{ET}}{\partial\tau_{obs}}\right)^2(\delta\tau_{obs})^2 + \left(\frac{\partial\phi_{ET}}{\partial\tau_{ET}}\right)^2(\delta\tau_{ET})^2}$$

$$= \sqrt{\left(\frac{1}{\tau_{ET}}\right)^2(\delta\tau_{obs})^2 + \left(\frac{\tau_{obs}}{\tau_{ET}^2}\right)^2(\delta\tau_{ET})^2}$$

Transient Absorption Results and Discussion.

An excited state absorption by **1** and **1⊂2b** appears after excitation with 400 nm light. For both **1** and **1⊂2b** the excited state decays with three time constants as outlined in Scheme S1. The character of these dynamic excited state processes can be understood by examining the wavelength-separated amplitudes of the global multi-exponential fitting (Figure S53).

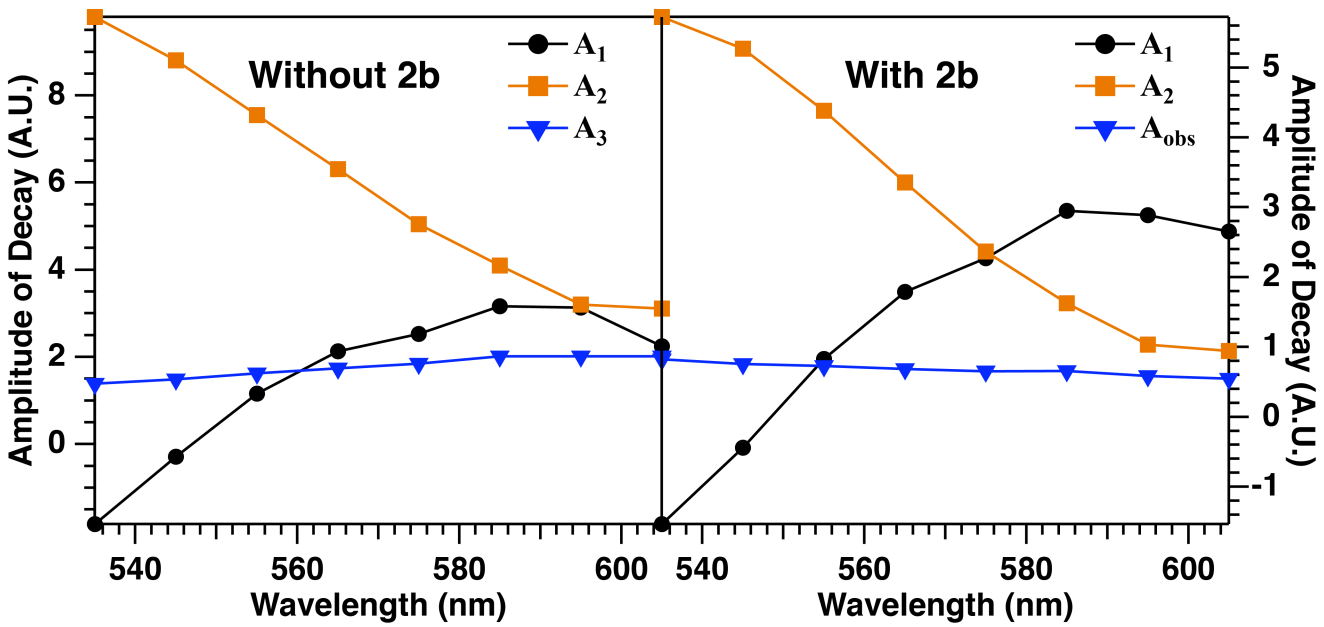

Figure S53. Amplitude fit parameters, A_n, corresponding to transient absorption decay processes τ_n.

As seen in Figure S53, an absorption feature that is decaying in intensity appears as a positive Gaussian while an absorption feature shifting in wavelength resembles a dispersive Gaussian (i.e. the first derivative of a Gaussian function). The first amplitude component A_1, corresponding to $\tau_1 = 0.8 \pm 0.3$ ps, appears as a dispersive Gaussian, with a negative amplitude in the region blue of 545 nm. This can be interpreted as a blue shift of the excited state absorption as the blue part of the spectrum is actually gaining intensity while the red part is losing intensity. This 0.8 ps blue shift is the result of an increase in the $S_1 \rightarrow S_n$ transition energy as the S_1 is stabilized by water solvation. The same stabilization process that causes an increase in the $S_1 \rightarrow S_n$ transition energy also results in a decrease in the $S_1 \rightarrow S_0$ transition energy; therefore, dipole correlation time constants have been most commonly measured as a red shift in time-resolved fluorescence up-conversion experiments. In Barbara *et al*. (1988), a red shift of the fluorescence band was observed with two time constants of 0.16 ps and 1.2 ps.[12] The authors note however that if a single time constant was used in the analysis they find a time constant of 0.86 ps for the redshift. It is reasonable to assume that in our transient absorption measurement there is a faster component to the blue shift that is not resolved by the 172 fs time resolution of the instrument response.

The second component of the transient absorption decay corresponding to $\tau_2 = 8.0 \pm 0.8$ ps appears as a large Gaussian feature with a maximum blue of the probe window. This decays in intensity is likely the result of rapid energy transfer between the six ligands of the tetrahedral cluster. Resonance energy transfer processes can occurs on time scales varying from less than 100 fs to greater than 1 ns. The rate of energy transfer depends on the molecular separation distance R_{DA}, the overlap integral of the absorption and fluorescence bands J_{DA}, the dot product of the transition dipoles $\varkappa$, the fluorescence quantum yield Φ_D, and the fluorescence emission lifetime τ_D.[13]

$$\frac{1}{\tau_{RET}} = \frac{9.76 \times 10^{-26}\, \kappa^2 J_{DA} \phi_D}{\tau_D |R_{DA}|^6}$$

[12] Jarzeba, W.; Walker, G. C.; Johnson, A. E.; Kahlow, M. A.; Barbara, P. F. Femtosecond Microscopic Solvation Dynamics of Aqueous Solutions. *J. Phys. Chem.* **1988**, *92*, 7039–7041

[13] Langhals, H.; Esterbauer, A. J.; Walter, A.; Riedle, E.; Pugliesi, I. Förster Resonant Energy Transfer in Orthogonally Arranged Chromophores. *J. Am. Chem. Soc.* **2010**, *132* (47), 16777-16782;

The actinic pump selectively excites to a superposition state where the selected ligands have their transition dipoles oriented in the direction of the pump electric field. Through resonance energy transfer (Förster) the excitation then migrates such that it is evenly distributed among the six ligands at which point the transition dipoles are nearly isotropically oriented with respect to the initial excitation.

To test this hypothesis we measured the fluorescence anisotropy of $K_{12}Ga_4L_6$ in water (λ_{EX} = 375 nm, λ_{EM} = 485 - 545 nm). If no rapid energy transfer occurs between the ligands, the anisotropy should decay with the rotational correlation time constant θ that can be approximated from a Stokes-Einstein radius calculation.[14]

$$\theta = \frac{\eta M V}{RT}$$

Where η is the viscosity. M is the molecular weight. V is the specific density. R is the gas constant and T is temperature. Taking the molecular weight of the cluster as 3300 g/mol and the specific volume to be 1 ml/g we find that the rotational correlation time constant is 1.2 ns. The steady state anisotropy, r, can then be calculated according to the following equation:

$$r = \frac{r_0}{1 + \tau_3/\theta}$$

Taking r_0 to be 0.4 and τ_3 to be 540 ps we find that the expected anisotropy to be $r \approx 0.28$. However, with 375 nm excitation we measured an anisotropy of less than 0.05 suggesting that the transition dipole reorients on a timescale much faster than molecular rotation due to fast intramolecular energy transfer.

In the final step of the excited state decay, a very broad absorption feature is observed to decay with a time-constant of τ_3 = 540 ± 40 ps. Although this process is not resolved fully within the time delay of the experiment, which is limited physically to 200 ps, a very clear slope is observed in the excited state decay both with and without inclusion of **2b**. This process reflects the final relaxation out of S_1 and the disappearance of the excited state absorption signal.

---

[14] Lakowicz, J. R.; Fluorescence Anisotropy. Principles of Fluorescence Spectroscopy, 2; Plenum Publishers: New York, NY, **1999**; pp 304-310.

The transient absorption signals with and without encapsulation of substrate **2b** are similar as is apparent in Figures S53 and S55. The greatest discrepancy between the two signals is apparent in the final relaxation step. In the presence of cinnamylammonium substrate **2b** the excited state is quenched with τ_{obs} = 190 ± 60 ps. This substantial increase in the rate of decays suggest that the S_1 state efficiently couples into a charge transfer state with a time constant of τ_{ET} = 290 ± 150 ps and a quantum yield of quantum yield of Φ_{ET} = 0.65 ± 0.34. A comparison of the estimated electron transfer quantum yield with the reaction quantum yield $\Phi_{R\text{-}2b}$ = 0.01± 0.007 suggests that once the charge transfer state has formed the rate of radical recombination significantly outpaces the rate of the 1,3-rearrangement resulting in a marked decrease in reactivity and stored energy.

XIV. Pre-resonance Raman Spectroscopy

Materials and Methods.

Solutions of 7 x10^{-4} M naphthalene biscatecholamide ligand were prepared under nitrogen in a solution of potassium methoxide and methanol to stabilize the tetra-anionic basic structure most relevant to the supramolecular cage assembly. Additionally, solutions of 7 x10^{-4} M $K_{12}Ga_4L_6$ and $K_{12}Ga_4L_6$ with **2b** were prepared in methanol with an optical density of 0.15 at 413.1 nm per pathlength. Solutions were flowed through a capillary tube (I.D. = 1.5 mm) at a rate of 2 m/s and kept under a positive pressure of nitrogen gas. Samples were irradiated with 70 mW of 413.1 nm light focused to a spot less than 0.5 mm diameter and the signal was collected in the standard 90° scattering geometry. Spectra were read out on a liquid-nitrogen-cooled CCD (Roper Scientific, LN/CCD 1100).

DFT Calculation.

The structure of the $K_{12}Ga_4L_6$ assembly with 1672 electrons is too large to be modeled adequately using DFT. Therefore we chose to model the geometry and vibrational spectra of a single naphthalene biscatcholamide tetra anion ligand with only 224 electrons. DFT geometry optimization and frequency

calculation were performed with the Gaussian 09 software package using unrestricted B3LYP functionals and the 6-311++G(D,P) basis set.

Pre-resonance Raman Results and Discussion.

To gain insight in to the vibrational and electronic structure of the $K_{12}Ga_4L_6$ cluster we investigated the pre-resonance Raman spectra of three important constituents to the cluster in solutions of methanol: the naphthalene biscatecholamide ligand alone uncomplexed to gallium, and the $K_{12}Ga_4L_6$ cluster with and without **2b**. The highly polarizable poly-anionic ligand and cluster afforded strong scattering intensity, which could easily be resolved over the weak fluorescence background.

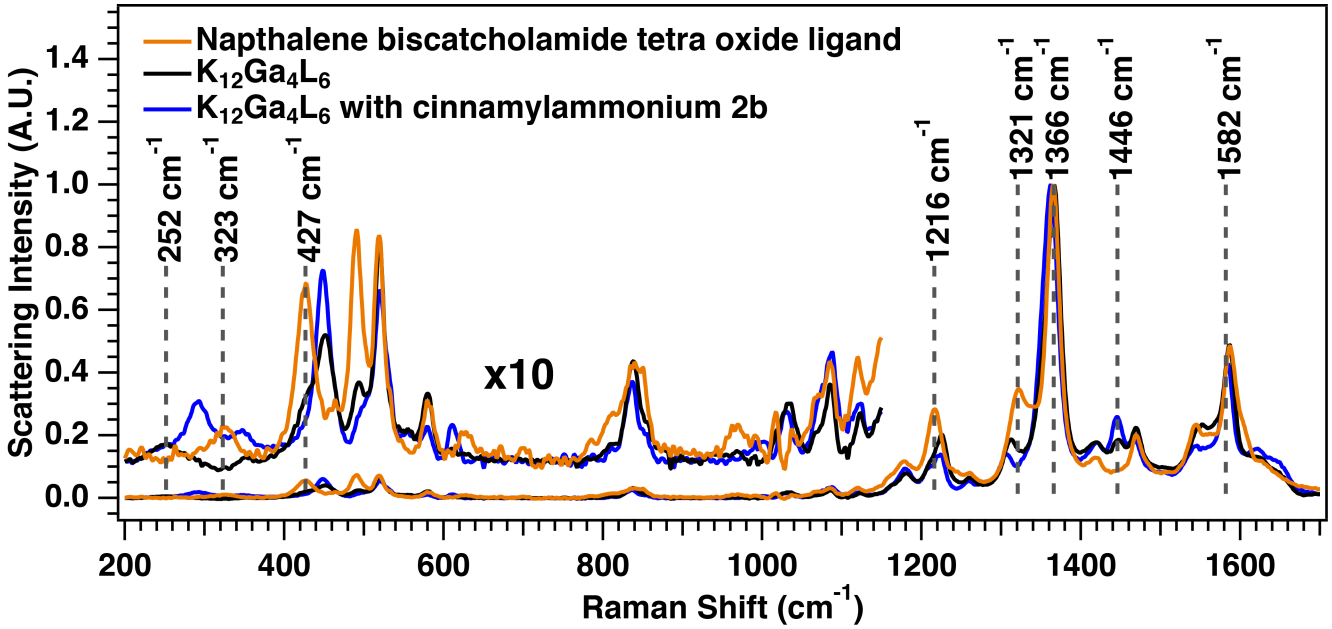

Figure S54. Comparison of three pre-resonance Raman spectra excited with 413.1 nm light. Yellow is the naphthalene biscatecholamide ligand stabilized as a tetranionic base in potassium methoxide. Black is the $K_{12}Ga_4L_6$ supramolecular cage in methanol. Blue is the $K_{12}Ga_4L_6$ assembly with cinnamylammonium **2b** in methanol. The low frequency region has been amplified by a factor of 10. The contribution of the methanol Raman scattering and the fluorescence baseline have been subtracted for clarity.

Figure S54 presents pre-resonance Raman spectra of the three constituents with 413.1 nm laser excitation at the red-edge of the lowest energy absorption band. The three spectra are very similar except for a few minor peak shift and changes in intensity. This similarity supports the idea that the tetra-anionic form of the naphthalene biscatecholamide ligand is the relevant structure in the cage.

Additionally, the similarity of the Raman spectra suggests that neither coordination with the gallium nor coupling between the ligand residues greatly perturbs the electronic or vibrational structure of ligand. Furthermore the similarity between spectra suggests weak electronic coupling between ligands and that the initial excitation has π-π* character localized on a single ligand residue and does involve a collective excitation of all six ligands.

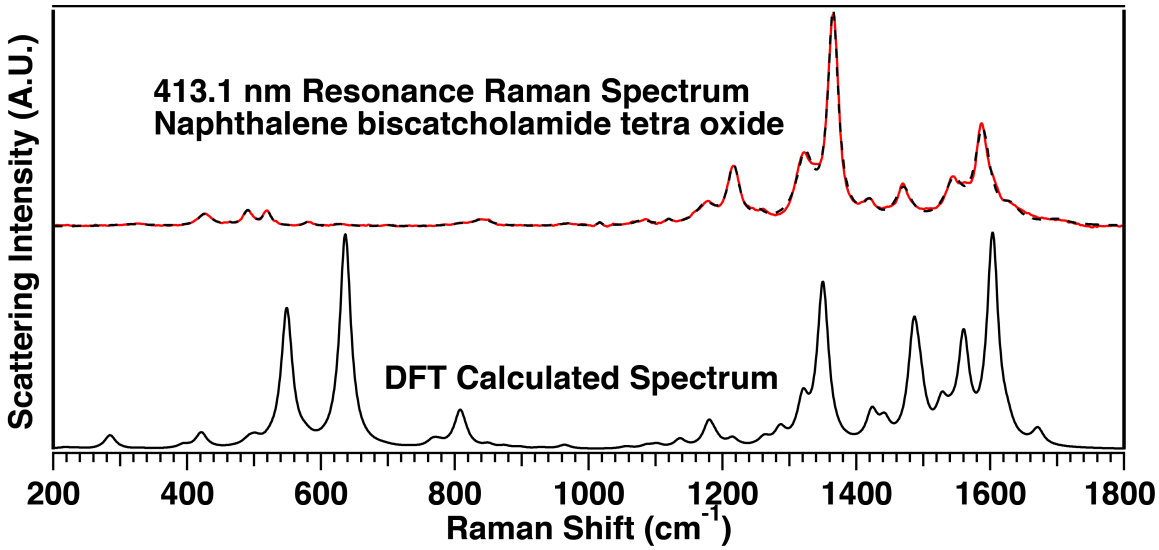

Figure S55. Comparison of measured resonance Raman spectrum of naphthalene biscatecholamide ligand with the spectrum calculated from theory. The black dashed line is a least squares fit result of 24 Lorentzian functions to the measured data (red). The calculated peaks are represented by Lorentzians with a full width half maximum of 20 cm^{-1} in agreement with the average peak width of the measured spectrum. The frequencies and intensities of the peaks reflect the calculated Raman shift and Raman activities, which have not been scaled.

Notable changes in peak frequencies and the appearance of new peaks indicate important structural changes, which accompany the formation of the cluster. The vibrational character of these frequencies can be assigned by comparison with the Raman spectrum of naphthalene biscatecholamide ligand calculated from theory. The comparison between theory and measured Raman spectra is presented in Figure S55. Most vibrations in the measured spectrum can be mapped onto Raman active vibrations with little ambiguity. The intensities of the calculated peaks reflect only off-resonance polarizability and therefore only show weak congruence with the measured intensities. The following analysis focuses on the most robust changes in the spectroscopic signals to gain a heuristic insight into

the solution phase structure of the cluster.

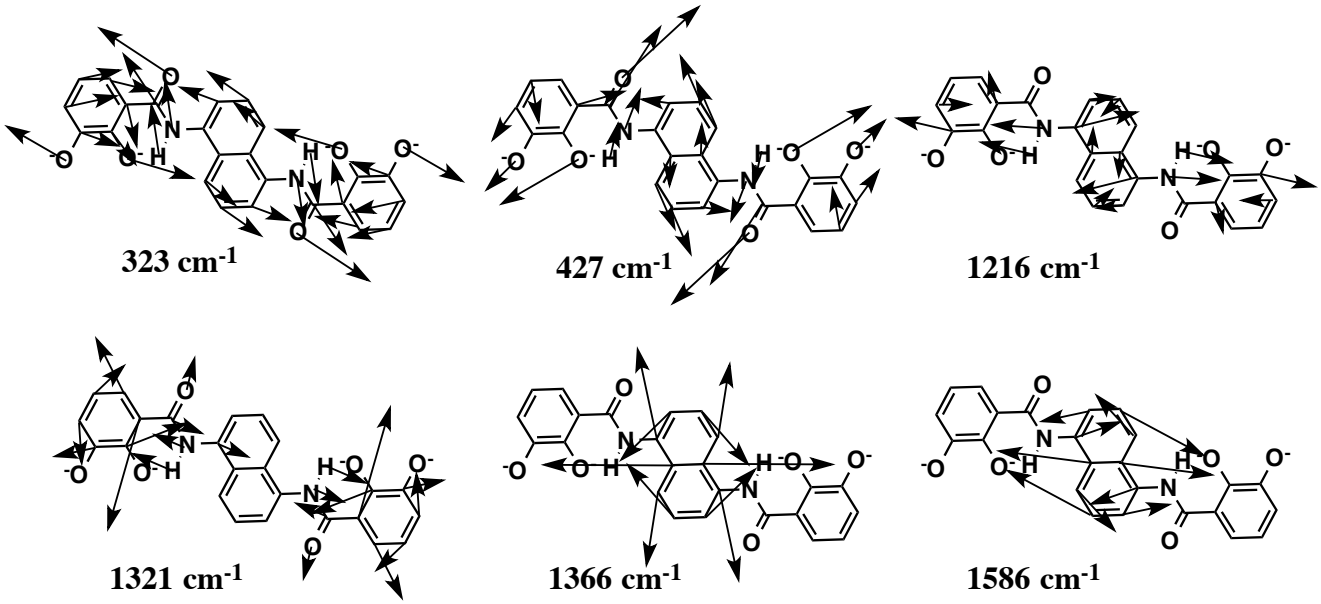

Figure S56. Approximate mode character of six Raman active modes discussed in the text.

When the ligand coordinates with the gallium forming the $K_{12}Ga_4L_6$ cluster, the following spectroscopic changes occur: A new peak at 252 cm^{-1} appears which presumably involves Ga-O stretching character (Figure S56). The peak at 323 cm^{-1} corresponding to in-plane bending of the catecholate oxygens blue shifts to 352 cm^{-1} as restoring force of this motion is strengthened by complexation with the gallium. The peak at 427 cm^{-1} corresponding to in plane distortion along the (O=CC)-(C-O^-) angle blue shifts to 452 cm^{-1}. The peak at 1216 cm^{-1} corresponding to OC-NH stretching blue shifts to 1225 cm^{-1}. The peak at 1321 cm^{-1} corresponding to aromatic distortion on the catecholate redshifts to 1312 cm^{-1}. Finally a new peak appears at 1446 cm^{-1} which we propose may be an asymmetric C=O stretch which becomes Raman active as the ligand vibrations couple in the higher dimensional tetrahedral symmetry. These results are consistent with a breaking of aromaticity as the molecule distorts along the OC-C-CO dihedral angle of the catechol groups.

The Raman scattering from the cinnamylammonium substrate **2b** was too weak to be observed at the concentration employed because the excitation wavelength is far removed from its resonance. Thus the spectra presented above reflect only spectroscopic changes in $K_{12}Ga_4L_6$ indirectly induced by

encapsulation of **2b** and not signals from **2b** itself. Assignment of vibrational mode character is made difficult because the $K_{12}Ga_4L_6$ cluster is too large to be modeled from density functional theory, however; a qualitative understanding of the vibrational character can be deduced by comparison with the ligand spectrum. Encapsulation of **2b** is accompanied a red shift of three pronounced peaks at 1317, 1366, and 1586 cm^{-1} to resultant frequencies of 1312, 1364 and 1582 cm^{-1} respectively. The vibrational character of these three modes is dominated by stretching of the catecholate and naphthalene rings. Additionally a new peak at 293 cm^{-1} is observed with unknown character. These results are consistent with a weakening the pi-bond strength as the ligands donate electron density to the lowest unoccupied molecular orbital of substrate **2b**.